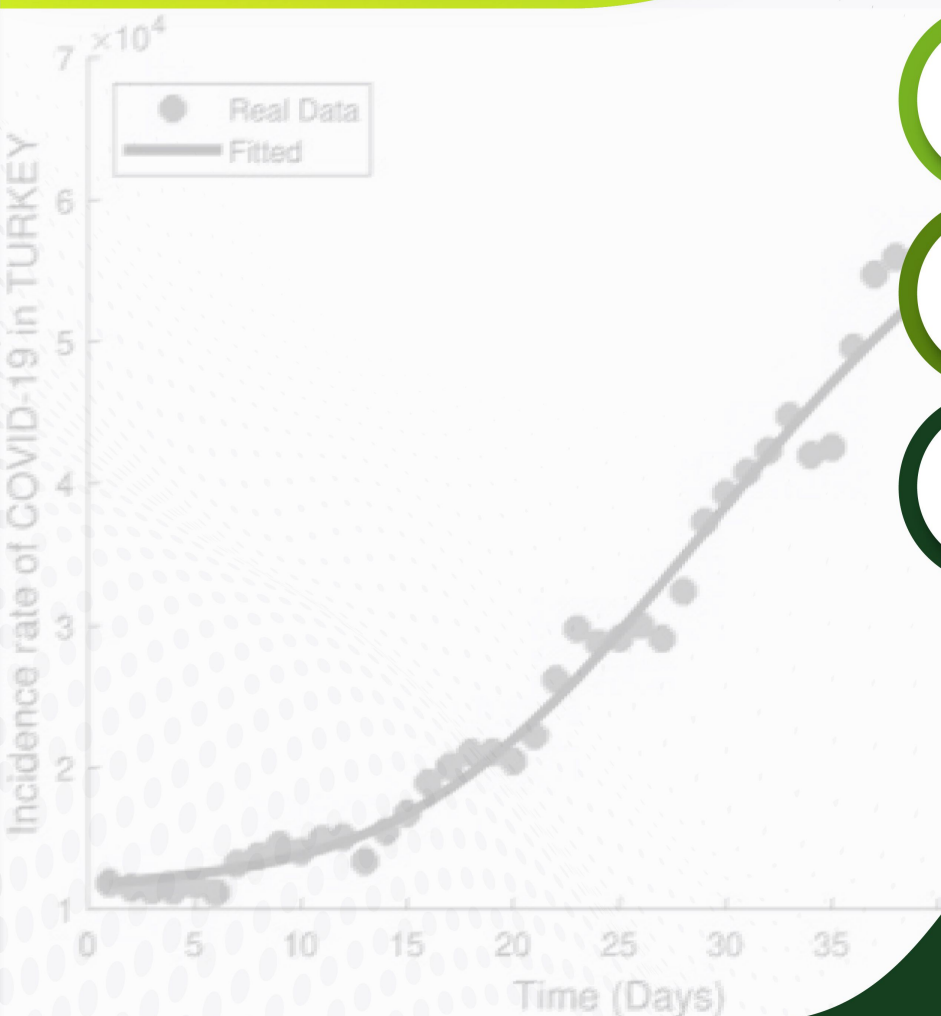


ISSN ONLINE  
2980-1869



BULLETIN OF  
BIOMATHEMATICS



2023

YEAR

1

VOLUME

1

ISSUE

Editor-in-Chief  
Mehmet Yavuz, PhD



[www.bulletinbiomath.org](http://www.bulletinbiomath.org)

VOLUME: 1    ISSUE: 1  
ISSN ONLINE: 2980-1869

April 2023  
<https://bulletinbiomath.org>



B U L L E T I N   O F  
**BIOMATHEMATICS**

**BULLETIN OF BIOMATHEMATICS**

---

## Editor-in-Chief

---

Mehmet Yavuz  
Department of Mathematics and Computer Sciences,  
Faculty of Science, Necmettin Erbakan University,  
Meram Yenyol, 42090 Meram, Konya / TÜRKİYE  
mehmetyavuz@erbakan.edu.tr

---

## Publisher

---

Firat Evirgen  
Department of Mathematics,  
Faculty of Science and Arts, Balıkesir University,  
Çağış Campus, 10145 Çağış, Balıkesir / TÜRKİYE  
fevirgen@balikesir.edu.tr

---

## Editorial Board

---

Abdeljawad, Thabet  
Prince Sultan University  
*Saudi Arabia*

Agarwal, Praveen  
Anand International College of Engineering  
*India*

Aguilar, José Francisco Gómez  
CONACyT- National Center for Technological Research  
and Development  
*Mexico*

Ahmad, Hijaz  
International Telematic University Uninettuno  
*Italy*

Arqub, Omar Abu  
Al-Balqa Applied University  
*Jordan*

Asjad, Muhammad Imran  
University of Management and Technology  
*Pakistan*

Atangana, Abdon  
University of the Free State  
*South Africa*

Baleanu, Dumitru  
Cankaya University, *Türkiye*;  
Institute of Space Sciences, Bucharest, *Romania*

Başkonuş, Hacı Mehmet  
Harran University  
*Türkiye*

Biswas, Md. Haider Ali  
Khulna University  
*Bangladesh*

Bonyah, Ebenezer  
Department of Mathematics Education  
*Ghana*

Bulai, Iulia Martina  
University of Basilicata  
*Italy*

Cabada, Alberto  
University of Santiago de Compostela  
*Spain*

Dassios, Ioannis  
University College Dublin  
*Ireland*

Eskandari, Zohreh  
Shahrekord University  
*Iran*

Flaut, Cristina  
Ovidius University of Constanta  
*Romania*

González, Francisco Martínez  
Universidad Politécnica de Cartagena  
*Spain*

Gürbüz, Burcu  
Johannes Gutenberg-University Mainz, Institute of  
Mathematics, *Germany*

Hammouch, Zakia  
ENS Moulay Ismail University Morocco;  
Thu Dau Mot University Vietnam and China Medical  
University, *Taiwan*

Hristov, Jordan  
University of Chemical Technology and Metallurgy  
*Bulgaria*

Jafari, Hossein  
University of Mazandaran, *Iran*;  
University of South Africa, *South Africa*

Jajarmi, Amin  
University of Bojnord  
*Iran*

Lupulescu, Vasile  
Constantin Brâncuși University of Târgu-Jiu  
*Romania*

Naik, Parvaiz Ahmad  
Department of Mathematics and Computer Science,  
Youjiang Medical University for Nationalities, *China*

Owolabi, Kolade  
Federal University of Technology  
*Nigeria*

Otero-Espinar, Maria Victoria  
University of Santiago de Compostela  
*Spain*

Özdemir, Necati  
Balıkesir University  
*Türkiye*

Pinto, Carla M.A.  
ISEP, *Portugal*

Povstenko, Yuriy  
Jan Długosz University in Czestochowa  
*Poland*

Qureshi, Sania  
Mehran University of Engineering and Technology  
*Pakistan*

Sabatier, Jocelyn  
Bordeaux University  
*France*

Safaei, Mohammad Reza  
Florida International University  
*USA*

Salahshour, Soheil  
Bahçeşehir University  
*Türkiye*

Sarı, Murat  
Yıldız Technical University  
*Türkiye*

Sarris, Ioannis E.  
University of West Attica  
*Greece*

Sene, Ndolane  
Cheikh Anta Diop University  
*Senegal*

Stamova, Ivanka  
University of Texas at San Antonio  
*USA*

Torres, Delfim F. M.  
University of Aveiro  
*Portugal*

Townley, Stuart  
University of Exeter  
*United Kingdom*

Valdés, Juan Eduardo Nápoles  
Universidad Nacional del Nordeste  
*Argentina*

Yang, Xiao-Jun  
China University of Mining and Technology  
*China*

Yuan, Sanling  
University of Shanghai for Science and Technology  
*China*

---

## Technical Editor

---

Kerim Sarıgöl  
Research Information System, Gazi University,  
Ankara / TÜRKİYE  
kerimsarigul@gazi.edu.tr

---

---

## English Editor

---

Abdulkadir Ünal  
School of Foreign Languages, Foreign Languages, Alanya  
Alaaddin Keykubat University, Antalya / TÜRKİYE  
abdulkadir.unal@alanya.edu.tr

---

---

## Editorial Secretariat

---

Fatma Özlem Coşar  
Department of Mathematics and Computer Sciences,  
Faculty of Science, Necmettin Erbakan University,  
Meram Yenyol, 42090 Meram, Konya / TÜRKİYE

Müzeyyen Akman  
Department of Mathematics and Computer Sciences,  
Faculty of Science, Necmettin Erbakan University,  
Meram Yenyol, 42090 Meram, Konya / TÜRKİYE

# Contents

## *Research Articles*

- 1 Piecewise fractional analysis of the migration effect in plant-pathogen-herbivore interactions  
*Mati ur Rahman, Muhammad Arfan, Dumitru Baleanu* 1-23
- 2 Analysis of the disturbance effect in intracellular calcium dynamic on fibroblast cells with an exponential kernel law  
*Hardik Joshi, Mehmet Yavuz, Ivanka Stamova* 24-39
- 3 Numerical investigations and simulation of calcium distribution in the alpha-cell  
*Tejaswi Singh, Vaishali, Neeru Adlakha* 40-57
- 4 Asymptotic extinction and persistence of a perturbed epidemic model with different intervention measures and standard Lévy jumps  
*Yassine Sabbar* 58-77
- 5 A fractional order vaccination model for COVID-19 incorporating environmental transmission: a case study using Nigerian data  
*Anne Ojoma Atede, Andrew Omame, Simeon Chioma Inyama* 78-110



RESEARCH PAPER

## Piecewise fractional analysis of the migration effect in plant-pathogen-herbivore interactions

Mati ur Rahman <sup>1,2,\*,\dagger</sup>, Muhammad Arfan <sup>3,\dagger</sup> and Dumitru Baleanu <sup>4,\dagger</sup>

<sup>1</sup>School of Mathematical Sciences, Shanghai Jiao Tong University, 800 Dongchuan Road Shanghai, PR China, <sup>2</sup>Department of Computer Science and Mathematics, Lebanese American University, Beirut, Lebanon, <sup>3</sup>Department of Mathematics, University of Malakand, Dir(L), Khyber Pakhtunkhwa, Pakistan, <sup>4</sup>Department of Mathematics, Cankaya University, 06530 Balgat, Ankara, Türkiye

\* Corresponding Author

\dagger [matior.rahman@lau.edu.lb](mailto:matior.rahman@lau.edu.lb) (Mati ur Rahman); [arfan\\_uom@yahoo.com](mailto:arfan_uom@yahoo.com) (Muhammad Arfan); [dumitru@cankaya.edu.tr](mailto:dumitru@cankaya.edu.tr) (Dumitru Baleanu)

### Abstract

This study introduces several updated results for the piecewise plant-pathogen-herbivore interactions model with singular-type and nonsingular fractional-order derivatives. A piecewise fractional model has developed to describe the interactions between plants, disease, (insect) herbivores, and their natural enemies. We derive essential findings for the aforementioned problem, specifically regarding the existence and uniqueness of the solution, as well as various forms of Ulam Hyers (U-H) type stability. The necessary results were obtained by utilizing fixed-point theorems established by Schauder and Banach. Additionally, the U-H stabilities were determined based on fundamental principles of nonlinear analysis. To implement the model as an approximate piecewise solution, the Newton Polynomial approximate solution technique is employed. The applicability of the model was validated through numerical simulations both in fractional as well as piecewise fractional format. The motivation of our article is that we have converted the integer order problem to a global piecewise and fractional order model in the sense of Caputo and Atangana-Baleanu operators and investigate it for existence, uniqueness of solution, Stability of solution and approximate solution along with numerical simulation for the validity of our obtained scheme.

**Keywords:** Crossover behavior; piecewise global fractional derivatives; Newton interpolation formula; equicontinuous mapping; Schauder's fixed point theorem

**AMS 2020 Classification:** 34A34; 34A36; 92B05

## 1 Introduction

The interactions between plants, herbivores, and pathogens in nature are complex and multifaceted. According to a reference [1], approximately 50% of the estimated 6 million species of insects are

herbivorous. On the other hand, plant pathogenic microbes pose significant threats to plants [2], but their total number has not been accurately estimated. Plants have evolved sophisticated defense mechanisms to detect and respond to multiple attacks by herbivores and pathogens [3]. These mechanisms can be broadly classified into two types: physical and chemical defenses. Regarding chemical defense, plants have the ability to release volatile organic compounds (VOCs) that can attract natural enemies of herbivores. This process can ultimately help to decrease herbivore pressure [4, 5]. Predatory mites and parasitic wasps are among the natural enemies of herbivores that are attracted by volatile organic compounds (VOCs) released by plants [6].

A good example of this is when lima bean and apple plants are attacked by spider mites. In response to this damage, the plants release volatile compounds that can attract predatory mites to help control the spider mite population. Similarly, several plant species, including cucumber, corn, and cotton, release herbivore-induced plant volatiles (HIPVs) when attacked by herbivores. The use of HIPVs can help control pests and potentially reduce the need for artificial pesticides. Plants have the ability to release HIPVs, which are lipophilic liquids with high vapor pressures that can be emitted from various parts of a plant, such as its leaves, flowers, and fruits [7]. Through the release of HIPVs, plants may help protect forestry and agriculture by potentially attracting predatory arthropods or repelling herbivores, ultimately promoting plant fitness [8–10]. In addition, the release of volatile compounds can also help damaged plants by attracting natural enemies of herbivores [11]. Studies focusing on the interactions between plants and herbivores, as well as plants and pathogens, have been extensively researched. The influence of VOCs in mediating tri-trophic interactions, which occur when plants are attacked by both herbivores and pathogens, has yet to be fully understood. In a recent study by Liu et al. [12], they examined a model that involved plants, herbivores, and natural enemies of herbivores in the context of tri-trophic interactions, but did not take into account the potential pathogenic effects on the plant population. The study indicated that an increase in the strength of plant-induced volatile attraction to natural enemies resulted in a greater fluctuation amplitude of plant biomass and herbivore population.

Previous studies have primarily investigated the interactions between plants and either herbivores or pathogens. However, the extent to which VOCs mediate tri-trophic interactions when plants are attacked by both herbivores and pathogens remains uncertain. In a recent study by Liu et al. [12], they investigated tri-trophic interactions involving plants, herbivores, and natural enemies of herbivores without considering the pathogenic effects on plant populations. They found that an increase in the attraction strength of plant-induced volatiles to natural enemies leads to high fluctuation amplitudes of plant biomass and herbivore populations. Based on the study by Fergola and Wang [13], when the attack strength of natural enemies reaches a certain level, the fluctuation amplitude of plant biomass and herbivore population decreases, and the plant biomass tends to approach its environmental carrying capacity. They enhanced Liu et al.'s model [12] by considering the impact of time delay. Their research indicated that for Volterra-type interactions, chemical attractions do not affect the threshold value for the persistence of herbivore and carnivore populations. In addition, their observations showed that the presence of carnivores could lead to a decrease in herbivore density while increasing plant density. Moreover, the model demonstrated a fold bifurcation when the predation process follows Leslie-type interactions.

Based on the literature discussed above, we investigated a model for plants [14] using the framework of piecewise derivative and integral operators. The model consists of four compartments, including the susceptible plant compartment (S), the infected plant compartment (I), and the herbivore (Y) and natural enemy (Z) populations. The system of ordinary differential equations

can be expressed as follows:

$$\begin{aligned}
 \frac{dS}{dt} &= S \left[ r \left( 1 - \frac{S}{k} \right) - \frac{\beta I}{1 + \alpha S} - p_1 Y \right], \\
 \frac{dI}{dt} &= I \left( \frac{\beta S}{1 + \alpha S} - \omega \right), \\
 \frac{dY}{dt} &= Y \left( -d_1 + C_1 p_1 S - p_2 Z \right), \\
 \frac{dZ}{dt} &= -Y_2 Z + C_2 p_2 Y Z + \mu.
 \end{aligned}
 \tag{1}$$

The parameters used in the above system with details are presented in Table 1.

**Table 1.** Details of the used parameters in model (1).

Notations	Details
$r$	The growth rate of plant
$k$	The rate of environmental carrying capacity
$\beta$	The rate of transmission of the disease
$\alpha$	Rate of the inhibition effect
$\omega$	Death rate of the infected plants
$d_1$	Herbivore death rate
$c_1, c_2$	The rates of conversion
$\mu$	The rate herbivore natural enemy
$p_1, p_2$	The rates of predation for plants

Fractional derivatives are known for their ability to incorporate memory and genetic effects, making them essential for studying various real-world dynamic problems. The application of fractional-order derivatives in mathematical models of infectious disease spread makes the situation more realistic and plausible. The conventional fractional calculus method involves long memory effects, which can lead to complications when dealing with long-term calculation problems. Moreover, power-law long memory is represented using classical fractional calculus mathematical tools, which consist of fractional order derivatives and integrals. Several researchers have presented different fractional operators and investigated mathematical modeling of linear and nonlinear problems to discuss real-world phenomena [15–18]. It is worth noting that when modeling different memory phenomena, the memory process is generally split into two stages. The memory process is typically divided into two stages, one involving short-term memory with permanent retention, while the other is governed by a simple fractional derivative model [19]. To tackle the issue of short-term memory, it is necessary to employ equations with piecewise fractional-order derivatives. This approach can enhance performance and efficiency, enabling clearer explanations of physical phenomena (see [20] for further information). Moreover, the idea of using piecewise derivatives of fractional orders has recently been explored in several studies. The concept of piecewise fractional differential equations has been employed by researchers in recent studies, after Atangana and Araz presented in [21], to explore various dynamical systems [22–24]. Such operators have proven useful in solving problems that exhibit crossover behavior and are gaining popularity among researchers. For instance, in [25], the CAT-T cells-SARS-2 disease model was investigated using the concept of piecewise fractional differential equations. Similarly, a Covid-19 model was studied using this approach in [26]. Additionally, authors in [27] examined the third wave of the Covid-19 outbreak in Türkiye, Spain, and Czechia by

employing piecewise differential and integral operators in their model. In addition, the concept of piecewise operators is being utilized by several authors to obtain numerical results for the food web model (see Ref. [28]). Numerous works have been documented by several researchers regarding piecewise differential and integral operators with various operators [29–33].

As for as the contribution of our article is concerned, we have converted the integer order problem to a global piecewise and fractional order model in the sense of Caputo and Atangana Baleanu operators (PCABC). As fractional operators are generalized because they have an extra degree of freedom and choices. Therefore, we checked the dynamics of different fractional orders lying between 0 and 1, and compared them with the integer order. On small fractional orders, stability is achieved quickly. The piecewise fractional model is investigated for the existence and uniqueness of the solution in the sense of fractional Caputo and Atangana Baleanu operator having a kernel of non-singularity in the form of the exponential function. The approximate or semi-analytical solution is obtained by the technique of piecewise fractional Caputo and ABC derivative. Taking different fractional orders we have simulated the obtained scheme for the first four terms. We have also compared the fractional dynamics with the integer order dynamics. All the quantities of the proposed problem are converging to their equilibrium points showing spectrum dynamics with the removal of singularity as well as the crossover or abrupt dynamics.

Motivated by the above-mentioned work, we study the system taken from [14] in the sense of piecewise Caputo and Atangana-Baleanu-Caputo operator as given below:

$$\begin{cases} {}_0^{PCABC}D_t^\nu S(t) = S[r(1 - \frac{S}{k}) - \frac{\beta I}{1+\alpha S} - p_1 Y], \\ {}_0^{PCABC}D_t^\nu I(t) = I(\frac{\beta S}{1+\alpha S} - \omega), \\ {}_0^{PCABC}D_t^\nu Y(t) = Y(-Y_1 + C_1 p_1 S - p_2 Z), \\ {}_0^{PCABC}D_t^\nu Z(t) = -Y_2 Z + C_2 p_2 YZ + \mu. \end{cases} \quad (2)$$

In order to elaborate further, equation (2) can be expressed as follows:

$$\begin{aligned} {}_0^{CABC}D_t^\nu(S(t)) &= \begin{cases} {}_0^C D_t^\nu(S(t)) = {}^C f_1(S, I, Y, Z, t), & 0 < t \leq t_1, \\ {}_0^{ABC} D_t^\nu(S(t)) = {}^{ABC} f_1(S, I, Y, Z, t), & t_1 < t \leq T, \end{cases} \\ {}_0^{CABC}D_t^\nu(I(t)) &= \begin{cases} {}_0^C D_t^\nu(I(t)) = {}^C f_2(S, I, Y, Z, t), & 0 < t \leq t_1, \\ {}_0^{ABC} D_t^\nu(I(t)) = {}^{ABC} f_2(S, I, Y, Z, t), & t_1 < t \leq T, \end{cases} \\ {}_0^{CABC}D_t^\nu(Y(t)) &= \begin{cases} {}_0^C D_t^\nu(Y(t)) = {}^C f_3(S, I, Y, Z, t), & 0 < t \leq t_1, \\ {}_0^{ABC} D_t^\nu(Y(t)) = {}^{ABC} f_3(S, I, Y, Z, t), & t_1 < t \leq T, \end{cases} \\ {}_0^{CABC}D_t^\nu(Z(t)) &= \begin{cases} {}_0^C D_t^\nu(Z(t)) = {}^C f_4(S, I, Y, Z, t), & 0 < t \leq t_1, \\ {}_0^{ABC} D_t^\nu(Z(t)) = {}^{ABC} f_4(S, I, Y, Z, t), & t_1 < t \leq T, \end{cases} \end{aligned} \quad (3)$$

In our study, we used piecewise fractional operators to describe the dynamics of the system, as they can capture crossover and abrupt dynamics effectively [34, 35]. Specifically, we applied different fractional operators to different intervals of the system and provided a qualitative analysis for each subinterval. To assess stability, we used the UH stability analysis. Furthermore, we investigated the utilization of piecewise terms and fractional orders in the final step of the system to obtain approximate solutions that can accommodate dynamics of both integer and rational orders.

The rest of the paper is organized as in the section 2 we include some preliminaries in form of definitions and lemmas. Section 3 comprised with the existence and uniqueness of solution of said model along with the stability of solution. In section 4 we established the numerical scheme

for the approximate solution of model in fractional piecewise format. To show the validness of the obtain scheme we provide the graphical representation in the section 5 of numerical simulation. At the end we give the concluding remarks.

## 2 Preliminaries

In this section, we recalled some definition from the literature.

**Definition 1** [16] The ABC operator of a function  $\mathbf{X}(t)$  with the condition  $\mathbf{X}(t) \in \mathcal{H}^1(0, T)$  is defined as follows:

$${}^{\text{ABC}}_0D_t^v(\mathbf{X}(t)) = \frac{\text{ABC}(v)}{1-v} \int_0^t \frac{d}{dy} \mathbf{X}(y) E_v \left[ \frac{-v(t-y)^v}{1-v} \right] dy. \quad (4)$$

**Definition 2** [16] If we consider  $\mathbf{X}(t) \in \mathcal{H}^1(0, T)$ , the ABC integral can be expressed as follows:

$${}^{\text{ABC}}_0I_t^v \mathbf{X}(t) = \frac{1-v}{\text{ABC}(v)} \mathbf{X}(t) + \frac{v}{\text{ABC}(v)\Gamma(v)} \int_0^t \mathbf{X}(y)(t-y)^{v-1} dy. \quad (5)$$

**Definition 3** [15] Let a function  $\mathbf{X}(t)$ , the Caputo derivative can be defined as:

$${}^{\text{C}}_0D_t^v \mathbf{X}(t) = \frac{1}{\Gamma(1-v)} \int_0^t \mathbf{X}'(y)(t-y)^{v-1} dy.$$

**Definition 4** [21] Assume that  $\mathbf{X}(t)$  is a function that is differentiable in a piecewise manner. In this case, one can compute the piecewise derivative of  $\mathbf{X}(t)$  using Caputo and ABC operator.

$${}^{\text{PCABC}}_0D_t^v \mathbf{X}(t) = \begin{cases} {}^{\text{C}}_0D_t^v \mathbf{X}(t), & 0 < t \leq t_1, \\ {}^{\text{ABC}}_0D_t^v \mathbf{X}(t) & t_1 < t \leq T. \end{cases}$$

The piecewise differential operator  ${}^{\text{PCABC}}_0D_t^v$  can be used to calculate the piecewise derivative of  $\mathbf{X}(t)$ . Specifically, the Caputo operator is employed in the interval  $0 < t \leq t_1$ , while the ABC operator is used in the interval  $t_1 < t \leq T$ .

**Definition 5** [21] Let  $\mathbf{X}(t)$  be a function that is piecewise integrable. We can then compute its piecewise derivative using the Caputo and ABC operators

$${}^{\text{PCABC}}_0I_t \mathbf{X}(t) = \begin{cases} \frac{1}{\Gamma v} \int_{t_1}^t \mathbf{X}(y)(t-y)^{v-1} d(y), & 0 < t \leq t_1, \\ \frac{1-v}{\text{ABC}v} \mathbf{X}(t) + \frac{v}{\text{ABC}v\Gamma v} \int_{t_1}^t \mathbf{X}(y)(t-y)^{v-1} d(y) & t_1 < t \leq T. \end{cases}$$

We can represent the piecewise integral operator as  ${}^{\text{PCABC}}_0I_t^v$ , where the Caputo operator is applied in the interval  $0 < t \leq t_1$ , and the ABC operator is applied in the interval  $t_1 < t \leq T$ .

## 3 Theoretical analysis

This section focuses on establishing the existence results and uniqueness of solution for the proposed system in the context of piecewise functions. We will investigate whether a solution exists for the hypothetical piecewise differentiable function and its particular solution attribute.

For the required solution, we will utilize the model (3) and provide additional clarification as follows:

$$\begin{aligned} {}_0^{\text{PCABC}}\mathbf{D}_t^v \mathcal{U}(t) &= \mathbf{G}(t, \mathcal{U}(t)), \quad 0 < v \leq 1, \\ \mathcal{U}(0) &= \mathcal{U}_0 \end{aligned}$$

is equal to

$$\mathcal{U}(t) = \begin{cases} \mathcal{U}_0 + \frac{1}{\Gamma(v)} \int_0^t \mathbf{G}(y, \mathcal{U}(y))(t-y)^{v-1} dy, & 0 < t \leq t_1, \\ \mathcal{U}(t_1) + \frac{1-v}{\text{ABC}(v)} \mathbf{G}(t, \mathcal{U}(t)) + \frac{v}{\text{ABC}(v)\Gamma(v)} \int_{t_1}^t (t-y)^{v-1} \mathbf{G}(y, \mathcal{U}(y)) d(y), & t_1 < t \leq T, \end{cases} \quad (6)$$

where

$$\mathcal{U}(t) = \begin{cases} \mathbf{S}(t) \\ \mathbf{I}(t) \\ \mathbf{Y}(t) \\ \mathbf{Z}(t) \end{cases}, \quad \mathcal{U}_0 = \begin{cases} \mathbf{S}_0 \\ \mathbf{I}_0 \\ \mathbf{Y}_0 \\ \mathbf{Z}_0 \end{cases}, \quad \mathcal{U}_{t_1} = \begin{cases} \mathbf{S}_{t_1} \\ \mathbf{I}_{t_1} \\ \mathbf{Y}_{t_1} \\ \mathbf{Z}_{t_1} \end{cases}, \quad \mathbf{G}(t, \mathcal{U}(t)) = \begin{cases} \mathbf{f}_i = \begin{cases} {}^{\text{C}}\mathbf{f}_i(\mathbf{S}, \mathbf{I}, \mathbf{Y}, \mathbf{Z}, t) \\ {}^{\text{ABC}}\mathbf{f}_i(\mathbf{S}, \mathbf{I}, \mathbf{Y}, \mathbf{Z}, t) \end{cases} \end{cases}, \quad (7)$$

we consider  $i = 1, 2, 3, 4$  and take  $0 < t \leq t < \infty$ . Let  $E_1$  represent the space for all piecewise differential function from  $C[0, t]$  to  $R$ , obviously it is a complete normed space and thus the Banach space  $E_1 = C[0, t]$ , equipped with a norm

$$\|\mathcal{U}\| = \max_{t \in [0, t]} |\mathcal{U}(t)|.$$

We assume the following growth condition:

(C1)  $\exists \mathcal{L}_{\mathbf{G}} > 0; \forall \mathbf{G}, \bar{\mathcal{U}} \in E$  we have

$$|\mathbf{G}(t, \mathcal{U}) - \mathbf{G}(t, \bar{\mathcal{U}})| \leq \mathcal{L}_{\mathbf{G}} |\mathcal{U} - \bar{\mathcal{U}}|,$$

(C2)  $\exists C_{\mathbf{G}} > 0$  &  $M_{\mathbf{G}} > 0;$ ;

$$|\mathbf{G}(t, \mathcal{U}(t))| \leq C_{\mathbf{G}} |\mathcal{U}| + M_{\mathbf{G}}.$$

If  $\mathbf{G}$  is piece-wise continuous on  $(0, t_1]$  and  $[t_1, T]$  on  $[0, \mathcal{T}]$ , also satisfying the assumption (C2), then (3) has  $\geq 1$  solution.

**Proof 1** We can apply the Schauder theorem to define a closed subset  $\mathbf{B}$  and  $E$  in both subintervals of the interval  $[0, \mathcal{T}]$ .

$$B = \{\mathcal{U} \in E : \|\mathcal{U}\| \leq R_{1,2}, R_{1,2} > 0\},$$

Consider a mapping  $\mathcal{S} : \mathbf{B} \rightarrow \mathbf{B}$  and using (6) as

$$\mathcal{S}(\mathcal{U}) = \begin{cases} \mathcal{U}_0 + \frac{1}{\Gamma(v)} \int_0^{t_1} \mathbf{G}(y, \mathcal{U}(y))(t-y)^{v-1} dy, & 0 < t \leq t_1, \\ \mathcal{U}(t_1) + \frac{1-v}{\text{ABC}(v)} \mathbf{G}(t, \mathcal{U}(t)) + \frac{v}{\text{ABC}(v)\Gamma(v)} \int_{t_1}^t (t-y)^{v-1} \mathbf{G}(y, \mathcal{U}(y)) d(y), & t_1 < t \leq T. \end{cases} \quad (8)$$

Any  $\mathcal{U} \in B$ , we have

$$\begin{aligned} |\mathcal{S}(\mathcal{U})(t)| &\leq \begin{cases} |\mathcal{U}_0| + \frac{1}{\Gamma(v)} \int_0^{t_1} (t-y)^{v-1} |\mathbf{G}(y, \mathcal{U}(y))| dy, \\ |\mathcal{U}(t_1)| + \frac{1-v}{\text{ABC}(v)} |\mathbf{G}(t, \mathcal{U}(t))| + \frac{v}{\text{ABC}(v)\Gamma(v)} \int_{t_1}^t (t-y)^{v-1} |\mathbf{G}(y, \mathcal{U}(y))| d(y), \end{cases} \\ &\leq \begin{cases} |\mathcal{U}_0| + \frac{1}{\Gamma(v)} \int_0^{t_1} (t-y)^{v-1} [C_G |\mathcal{U}| + M_G] dv, \\ |\mathcal{U}(t_1)| + \frac{1-v}{\text{ABC}(v)} [C_G |\mathcal{U}| + M_G] + \frac{v}{\text{ABC}(v)\Gamma(v)} \int_{t_1}^t (t-y)^{v-1} [C_G |\mathcal{U}| + M_G] dy, \end{cases} \\ &\leq \begin{cases} |\mathcal{U}_0| + \frac{\mathbf{T}^v}{\Gamma(v+1)} [C_H |\mathcal{U}| + M_G] = R_1, & 0 < t \leq t_1, \\ |\mathcal{U}(t_1)| + \frac{1-v}{\text{ABC}(v)} [C_G |\mathcal{U}| + M_G] + \frac{v(T-\mathbf{T})^v}{\text{ABC}(v)\Gamma(v)+1} [C_G |\mathcal{U}| + M_G] d(v) = R_2, & t_1 < t \leq T, \end{cases} \\ &\leq \begin{cases} R_1, & 0 < t \leq t_1, \\ R_2, & t_1 < t \leq T. \end{cases} \end{aligned}$$

Upon analyzing the previous equation, it can be concluded that  $\mathcal{U}$  belongs to the set  $\mathbf{B}$ . As a result, it follows that  $\mathcal{S}(\mathbf{B}) \subseteq \mathbf{B}$ , indicating the closure and completeness of  $\mathcal{S}$ . To further showcase its complete continuity, let us consider the initial interval in the Caputo sense as  $t_i < t_j \in [0, t_1]$ .

$$\begin{aligned} |\mathcal{S}(\mathcal{U})(t_j) - \mathcal{S}(\mathcal{U})(t_i)| &= \left| \frac{1}{\Gamma(v)} \int_0^{t_j} (t_j-y)^{v-1} \mathbf{G}(y, \mathcal{U}(y)) dy - \frac{1}{\Gamma(v)} \int_0^{t_i} (t_i-y)^{v-1} \mathbf{G}(y, \mathcal{U}(y)) dy \right|, \\ &\leq \frac{1}{\Gamma(v)} \int_0^{t_i} [(t_i-y)^{v-1} - (t_j-y)^{v-1}] |\mathbf{G}(y, \mathcal{U}(y))| dy \\ &\quad + \frac{1}{\Gamma(v)} \int_{t_i}^{t_j} (t_j-y)^{v-1} |\mathbf{G}(y, \mathcal{U}(y))| dy, \\ &\leq \frac{1}{\Gamma(v)} \left[ \int_0^{t_i} [(t_i-y)^{v-1} - (t_j-y)^{v-1}] dy + \int_{t_i}^{t_j} (t_j-y)^{v-1} dy \right] (C_H |\mathcal{U}| + M_G), \\ &\leq \frac{(C_G \mathcal{U} + M_G)}{\Gamma(v+1)} [t_j^y - t_i^v + 2(t_j - t_i)^v]. \end{aligned} \quad (9)$$

Next (9), we obtain  $t_i \rightarrow t_j$ , and then

$$|\mathcal{S}(\mathcal{U})(t_j) - \mathcal{S}(\mathcal{U})(t_i)| \rightarrow 0, \text{ as } t_i \rightarrow t_j.$$

So,  $\mathcal{S}$  is equi-continuous in  $[0, t_1]$ . Consider  $t_i, t_j \in [t_1, T]$  in the sense of ABC as

$$\begin{aligned}
|\mathcal{S}(\mathcal{U})(t_j) - \mathcal{S}(\mathcal{U})(t_i)| &= \left| \frac{1-v}{\text{ABC}(v)} \mathbf{G}(t, \mathcal{U}(t)) + \frac{v}{\text{ABC}(v)\Gamma(v)} \int_{t_1}^{t_j} (t_j - y)^{v-1} \mathbf{G}(y, \mathcal{U}(y)) dy, \right. \\
&\quad \left. - \frac{1-v}{\text{ABC}(v)} \mathbf{G}(t, \mathcal{U}(t)) + \frac{v}{\text{ABC}(v)\Gamma(v)} \int_{t_1}^{t_i} (t_i - y)^{v-1} \mathbf{G}(y, \mathcal{U}(y)) dy \right|, \\
&\leq \frac{v}{\text{ABC}(v)\Gamma(v)} \int_{t_1}^{t_i} [(t_i - y)^{v-1} - (t_j - y)^{v-1}] |\mathbf{G}(y, \mathcal{U}(y))| dy \\
&\quad + \frac{v}{\text{ABC}(v)\Gamma(v)} \int_{t_i}^{t_j} (t_j - y)^{v-1} |\mathbf{G}(y, \mathcal{U}(y))| dy, \\
&\leq \frac{v}{\text{ABC}(v)\Gamma(v)} \left[ \int_{t_1}^{t_i} [(t_i - y)^{v-1} - (t_j - y)^{v-1}] dy \right. \\
&\quad \left. + \int_{t_i}^{t_j} (t_j - y)^{v-1} dy \right] (C_{\mathbf{G}} |\mathcal{U}| + M_{\mathbf{G}}), \\
&\leq \frac{v(C_{\mathbf{G}} \mathcal{U} + M_{\mathbf{G}})}{\text{ABC}(v)\Gamma(v+1)} [t_j^v - t_i^v + 2(t_j - t_i)^v]. \tag{10}
\end{aligned}$$

If  $t_i \rightarrow t_j$ , then

$$|\mathcal{S}(\mathcal{U})(t_j) - \mathcal{S}(\mathcal{U})(t_i)| \rightarrow 0, \text{ as } t_i \rightarrow t_j.$$

Therefore, it can be concluded that the operator  $\mathcal{S}$  exhibits equi-continuity in the interval  $[t_1, T]$ , thus making it an equi-continuous map. By applying the Arzelà-Ascoli theorem, it can be inferred that  $\mathcal{S}$  is uniformly continuous, continuous, and bounded. Furthermore, based on the Schauder theorem, it can be established that problem (3) has at least one solution in the subintervals.

Moreover, if the operator  $\mathcal{S}$  satisfies the condition of being a contraction mapping with assumption (C1), then the proposed system possesses a unique solution. The mapping  $\mathcal{S} : \mathbf{B} \rightarrow \mathbf{B}$  is characterized by being piece-wise continuous, let us consider two elements  $\mathcal{U}$  and  $\bar{\mathcal{U}} \in B$  on the interval  $[0, t_1]$  in the sense of Caputo, as follows:

$$\begin{aligned}
\|\mathcal{S}(\mathcal{U}) - \mathcal{S}(\bar{\mathcal{U}})\| &= \max_{t \in [0, t_1]} \left| \frac{1}{\Gamma(v)} \int_0^t (t-y)^{v-1} \mathbf{G}(y, \mathcal{U}(y)) dy - \frac{1}{\Gamma(v)} \int_0^t (t-y)^{v-1} \mathbf{G}(y, \bar{\mathcal{U}}(y)) dy \right|, \\
&\leq \frac{\mathbf{T}^v}{\Gamma(v+1)} L_{\mathbf{G}} \|\mathcal{U} - \bar{\mathcal{U}}\|. \tag{11}
\end{aligned}$$

From (11), we have

$$\|\mathcal{S}(\mathcal{U}) - \mathcal{S}(\bar{\mathcal{U}})\| \leq \frac{\mathbf{T}^v}{\Gamma(v+1)} L_{\mathbf{G}} \|\mathcal{U} - \bar{\mathcal{U}}\|. \tag{12}$$

Consequently, it follows that  $\mathcal{S}$  satisfies the contraction mapping condition. Thus, according to the Banach fixed-point theorem, the problem at hand possesses a unique solution in the given subinterval. Additionally, it is worth noting that  $t \in [t_1, T]$  in the ABC sense:

$$\|\mathcal{S}(\mathcal{U}) - \mathcal{S}(\bar{\mathcal{U}})\| \leq \frac{1-v}{\text{ABC}(v)} L_{\mathbf{G}} \|\mathcal{U} - \bar{\mathcal{U}}\| + \frac{v(\mathbf{T} - T^v)}{\text{ABC}(v)\Gamma(v+1)} L_{\mathbf{f}} \|\mathcal{U} - \bar{\mathcal{U}}\|, \tag{13}$$

or

$$\|\$(\mathcal{U}) - \$(\bar{\mathcal{U}})\| \leq L_G \left[ \frac{1 - v}{ABC(v)} + \frac{v(T - \mathbf{T})^v}{ABC(v)\Gamma(v + 1)} \right] \|\mathcal{U} - \bar{\mathcal{U}}\|. \quad (14)$$

This implies that  $\$$  satisfies the contraction mapping property. Consequently, the problem being considered has a unique solution in the given sub-interval by virtue of the Banach fixed-point theorem. Therefore, taking into account equations (12) and (14), it can be concluded that the proposed problem has a unique solution on each sub-interval.

### Analysis of stability

To prove the Ulam-Hyers stability for the considered model, we need to show that small perturbations in the initial conditions or the parameters of the model result in small perturbations in the solution of the model. This can be done by showing that the operator  $\$$  is Lipschitz continuous with respect to the initial conditions or the parameters of the model.

**Definition 6** The considered system (1) is said to be U-H stable if, for every  $\aleph > 0$ , the inequality holds true.

$$\left| {}^{PCABC}D_t^v \mathbf{U}(t) - \mathbf{f}(t, \mathbf{U}(t)) \right| < \aleph, \text{ for all, } t \in \mathcal{T}, \quad (15)$$

There exists a unique solution  $\bar{\mathbf{U}} \in Z$  that is constant  $\mathcal{A} > 0$ ,

$$\|\mathbf{U} - \bar{\mathbf{U}}\|_Z \leq \mathcal{A}\aleph, \text{ for all, } t \in \mathcal{T}, \quad (16)$$

Furthermore, if we consider an increasing function  $\Psi : [0, \infty) \rightarrow R^+$ , the inequality described above can be expressed as follows:

$$\|\mathbf{U} - \bar{\mathbf{U}}\|_Z \leq \mathcal{A}\Psi(\aleph), \text{ for each, } t \in \mathcal{T},$$

If  $\Psi(0) = 0$ , then the resulting solution is considered to be generalized U-H (G-H-U) stable.

**Remark 1.** Assuming that a function  $\Psi \in C(\mathcal{T})$  does not depend on  $\mathbf{U} \in \mathscr{W}$  and satisfies  $\Psi(0) = 0$ , we can conclude that:

$$\begin{aligned} |\Psi(t)| &\leq \aleph, t \in \mathcal{T} \\ {}^{PCABC}D_t^v \mathbf{U}(t) &= \mathbf{f}(t, \mathbf{U}(t)) + \Psi(t), t \in \mathcal{T}. \end{aligned}$$

**Lemma 1** Consider the function

$${}_0^{PCABC}D_t^v \mathbf{U}(t) = \mathbf{f}(t, \mathbf{U}(t)), \quad 0 < v \leq 1. \quad (17)$$

The solution of (17) is

$$\mathbf{U}(t) = \begin{cases} \mathbf{U}_0 + \frac{1}{\Gamma(v)} \int_0^t \mathbf{f}(y, \mathbf{U}(y))(t-y)^{v-1} dy, & 0 < t \leq t_1 \\ \mathbf{U}(t_1) + \frac{1-v}{ABC(v)} \mathbf{f}(t, \mathbf{U}(t)) + \frac{v}{ABC(v)\Gamma(v)} \int_{t_1}^t (t-y)^{v-1} \mathbf{f}(y, \mathbf{U}(y)) d(y), & t_1 < t \leq T, \end{cases} \quad (18)$$

$$\|F(\mathbf{U}) - F(\bar{\mathbf{U}})\| \leq \begin{cases} \frac{\mathcal{T}_1^v}{\Gamma(v+1)} \aleph, & t \in \mathcal{T}_1 \\ \left[ \frac{(1-v)\Gamma(v) + (\mathcal{T}_2^v)}{ABC(v)\Gamma(v)} \right] \aleph = \Lambda \aleph, & t \in \mathcal{T}_2. \end{cases} \quad (19)$$

**Theorem 1** The implication of Lemma (1) is that if  $\frac{L_f \mathcal{T}^v}{\Gamma(v)} < 1$ , the solution to model (2) is H-U stable as well as G-H-U stable.

**Proof 2** If  $\mathbf{U} \in \mathcal{W}$  is a solution of (2) and  $\bar{\mathbf{U}} \in \mathcal{W}$  is also a unique solution of (2), then we can conclude that

**Case:1** for  $t \in \mathcal{T}$ , we have

$$\begin{aligned} \|\mathbf{U} - \bar{\mathbf{U}}\| &= \sup_{t \in \mathcal{T}} \left| \mathbf{U} - \left( \mathbf{U}_0 + \frac{1}{\Gamma(v)} \int_0^{t_1} (t_1 - y)^{v-1} \mathbf{f}(y, \bar{\mathbf{U}}(y)) dy \right) \right|, \\ &\leq \sup_{t \in \mathcal{T}} \left| \mathbf{U} - \left( \mathbf{U}_0 + \frac{1}{\Gamma(v)} \int_0^{t_1} (t_1 - y)^{v-1} \mathbf{f}(y, \bar{\mathbf{U}}(y)) dy \right) \right| \\ &+ \sup_{t \in \mathcal{T}} \left| + \frac{1}{\Gamma(v)} \int_0^{t_1} (t_1 - y)^{v-1} \mathbf{f}(y, \mathbf{U}(y)) dy - \frac{1}{\Gamma(v)} \int_0^{t_1} (t_1 - y)^{v-1} \mathbf{f}(y, \bar{\mathbf{U}}(y)) dy \right|, \\ &\leq \frac{\mathcal{T}_\infty^v}{\Gamma(v+1)} \aleph + \frac{L_f \mathcal{T}_\infty}{\Gamma(v+1)} \|\mathbf{U} - \bar{\mathbf{U}}\|. \end{aligned} \quad (20)$$

On more calculation

$$\|\mathbf{U} - \bar{\mathbf{U}}\| \leq \left( \frac{\mathcal{T}_\infty}{\Gamma(v+1)} \right) \aleph. \quad (21)$$

**Case:2**

$$\begin{aligned} \|\mathbf{U} - \bar{\mathbf{U}}\| &\leq \sup_{t \in \mathcal{T}} \left| \mathbf{U} - \left[ \mathbf{U}(t_1) + \frac{1-v}{ABC(v)} [\mathbf{f}(t, \mathbf{U}(t))] \right. \right. \\ &+ \left. \left. \frac{v}{ABC(v)\Gamma(v)} \left[ \int_{t_1}^t (t-y)^{v-1} \mathbf{f}(y, \bar{\mathbf{U}}(y)) d(y) \right] \right] \right| \\ &+ \sup_{t \in \mathcal{T}} \frac{1-v}{ABC(v)} |\mathbf{f}(t, \mathbf{U}(t)) - \mathbf{f}(t, \bar{\mathbf{U}}(t))| \\ &+ \sup_{t \in \mathcal{T}} \frac{v}{ABC(v)\Gamma(v)} \int_{t_1}^t (t-y)^{v-1} |\mathbf{f}(y, \mathbf{U}(y)) - \mathbf{f}(y, \bar{\mathbf{U}}(y))| ds. \end{aligned}$$

Using  $\Lambda = \left[ \frac{(1-v)\Gamma(v)+T_2^v}{ABC(v)\Gamma(v)} \right]$  and further calculation we have

$$\|U - \bar{U}\|_{\mathcal{W}} \leq \Lambda \aleph + \Lambda L_f \|U - \bar{U}\|_{\mathcal{W}},$$

or

$$\|U - \bar{U}\|_{\mathcal{W}} \leq \left( \frac{\Lambda}{1 - \frac{\Lambda}{L_f}} \right) \aleph. \tag{22}$$

We use

$$\mathcal{A} = \max \left\{ \left( \frac{\frac{\mathcal{T}_1}{\Gamma(v+1)}}{1 - \frac{L_f \mathcal{T}_1}{\Gamma(v+1)}} \right), \frac{\Lambda}{1 - \frac{\Lambda L_f}{1 - M_f}} \right\}.$$

Now, from Eq. (21) and (22), we have

$$\|U - \bar{U}\|_{\mathcal{W}} \leq \mathcal{A} \aleph, \text{ at every } t \in \mathcal{T}.$$

Thus, we can conclude that the solution to model (2) is H-U stable. Additionally, if we substitute  $\aleph$  with  $\Psi(\aleph)$  in (23), we get:

$$\|U - \bar{U}\|_{\mathcal{W}} \leq \mathcal{A} \Psi(\aleph), \text{ at each } t \in \mathcal{T}.$$

Therefore, we can infer that the solution to our proposed model (2) is G-H-U stable based on the fact that  $\Psi(0) = 0$ .

### 4 Numerical scheme

Here, we will find the numerical scheme for the considered system (2).

$$\begin{cases} {}_0^{PCABC} \mathbf{D}_t^v \mathbf{S}(t) = \mathbf{S} \left[ r \left( 1 - \frac{\mathbf{S}}{k} \right) - \frac{\beta \mathbf{I}}{1 + \alpha \mathbf{S}} - p_1 \mathbf{Y} \right], \\ {}_0^{PCABC} \mathbf{D}_t^v \mathbf{I}(t) = \mathbf{I} \left( \frac{\beta \mathbf{S}}{1 + \alpha \mathbf{S}} - \omega \right), \\ {}_0^{PCABC} \mathbf{D}_t^v \mathbf{Y}(t) = \mathbf{Y} \left( -\mathbf{Y}_1 + C_1 p_1 \mathbf{S} - p_2 \mathbf{Z} \right), \\ {}_0^{PCABC} \mathbf{D}_t^v \mathbf{Z}(t) = -\mathbf{Y}_2 \mathbf{Z} + C_2 p_2 \mathbf{Y} \mathbf{Z} + \mu. \end{cases} \tag{23}$$

Using the piecewise-integral of Caputo and ABC derivative, we have

$$\begin{aligned}
 S(t) &= \begin{cases} S_0 + \frac{1}{\Gamma(v)} \int_0^{t_1} (t-y)^{v-1} C \mathbf{f}_1(t, S) dy & 0 < t \leq t_1, \\ S(t_1) + \frac{1-v}{AB(v)} \mathbf{f}_1(t, S) dy + \frac{v}{AB(v)\Gamma(v)} \int_{t_1}^t (t-y)^{v-1} \mathbf{f}_1(t, S) dy & t_1 < t \leq T, \end{cases} \\
 I(t) &= \begin{cases} I_0 + \frac{1}{\Gamma(v)} \int_0^{t_1} (t-y)^{v-1} C \mathbf{f}_2(t, I) dy & 0 < t \leq t_1, \\ I(t_1) + \frac{1-v}{AB(v)} \mathbf{f}_2(t, I) dy + \frac{v}{AB(v)\Gamma(v)} \int_{t_1}^t (t-y)^{v-1} \mathbf{f}_2(t, I) dy & t_1 < t \leq T, \end{cases} \\
 Y(t) &= \begin{cases} Y_0 + \frac{1}{\Gamma(v)} \int_0^{t_1} (t-y)^{v-1} C \mathbf{f}_3(t, Y) dy & 0 < t \leq t_1, \\ Y(t_1) + \frac{1-v}{AB(v)} \mathbf{f}_3(t, Y) dy + \frac{v}{AB(v)\Gamma(v)} \int_{t_1}^t (t-y)^{v-1} \mathbf{f}_3(t, Y) dy & t_1 < t \leq T, \end{cases} \\
 Z(t) &= \begin{cases} Z_0 + \frac{1}{\Gamma(v)} \int_0^{t_1} (t-y)^{v-1} C \mathbf{f}_4(t, Z) dy & 0 < t \leq t_1, \\ Z(t_1) + \frac{1-v}{AB(v)} \mathbf{f}_4(t, Z) dy + \frac{v}{AB(v)\Gamma(v)} \int_{t_1}^t (t-y)^{v-1} \mathbf{f}_4(t, Z) dy & t_1 < t \leq T. \end{cases}
 \end{aligned} \tag{24}$$

At  $t = t_{n+1}$

$$\begin{aligned}
 S(t) &= \begin{cases} S_0 + \frac{1}{\Gamma(v)} \int_0^{t_1} (t-y)^{v-1} C \mathbf{f}_1(t, S) dy & 0 < t \leq t_1, \\ S(t_1) + \frac{1-v}{AB(v)} \mathbf{f}_1(t, S) dy + \frac{v}{AB(v)\Gamma(v)} \int_{t_1}^{t_{n+1}} (t-y)^{v-1} \mathbf{f}_1(t, S) dy & t_1 < t \leq T, \end{cases} \\
 I(t) &= \begin{cases} I_0 + \frac{1}{\Gamma(v)} \int_0^{t_1} (t-y)^{v-1} C \mathbf{f}_2(t, I) dy & 0 < t \leq t_1, \\ I(t_1) + \frac{1-v}{AB(v)} \mathbf{f}_2(t, I) dy + \frac{v}{AB(v)\Gamma(v)} \int_{t_1}^{t_{n+1}} (t-y)^{v-1} \mathbf{f}_2(t, I) dy & t_1 < t \leq T, \end{cases} \\
 Y(t) &= \begin{cases} Y_0 + \frac{1}{\Gamma(v)} \int_0^{t_1} (t-y)^{v-1} C \mathbf{f}_3(t, Y) dy & 0 < t \leq t_1, \\ Y(t_1) + \frac{1-v}{AB(v)} \mathbf{f}_3(t, Y) dy + \frac{v}{AB(v)\Gamma(v)} \int_{t_1}^{t_{n+1}} (t-y)^{v-1} \mathbf{f}_3(t, Y) dy & t_1 < t \leq T, \end{cases} \\
 Z(t) &= \begin{cases} Z_0 + \frac{1}{\Gamma(v)} \int_0^{t_1} (t-y)^{v-1} C \mathbf{f}_4(t, Z) dy & 0 < t \leq t_1, \\ Z(t_1) + \frac{1-v}{AB(v)} \mathbf{f}_4(t, Z) dy + \frac{v}{AB(v)\Gamma(v)} \int_{t_1}^{t_{n+1}} (t-y)^{v-1} \mathbf{f}_4(t, Z) dy & t_1 < t \leq T. \end{cases}
 \end{aligned}$$

Using the Newton polynomials and some calculation, we have

$$S(t_{n+1}) = \begin{cases} S_0 + \left\{ \begin{aligned} & \frac{(\Delta t)^{v-1}}{\Gamma(v+1)} \sum_{x=2}^i \left[ {}^C \mathbf{f}_1(S^{x-2}, t_{x-2}) \right] \Pi + \frac{(\Delta t)^{v-1}}{\Gamma(v+2)} \sum_{x=2}^i \left[ {}^C \mathbf{f}_1(S^{x-1}, t_{x-1}) - {}^C \mathbf{f}_1(S^{x-2}, t_{x-2}) \right] \wedge \\ & + \frac{v(\Delta t)^{v-1}}{2\Gamma(v+3)} \sum_{x=2}^i \left[ {}^C \mathbf{f}_1(S^x, t_x) - 2 {}^C \mathbf{f}_1(S^{x-1}, t_{x-1}) + {}^C \mathbf{f}_1(S^{x-2}, t_{x-2}) \right] \Delta \end{aligned} \right. \\ S(t_1) + \left\{ \begin{aligned} & \frac{1-v}{ABC(v)} {}^{ABC} \mathbf{f}_1(S^n, t_n) + \frac{v}{ABC(v)\Gamma(v+1)} \sum_{x=i+3}^n \left[ {}^{ABC} \mathbf{f}_1(S^{x-2}, t_{x-2}) \right] \Pi \\ & + \frac{v}{ABC(v)\Gamma(v+2)} \sum_{x=i+3}^n \left[ {}^{ABC} \mathbf{f}_1(S^{x-1}, t_{x-1}) + {}^{ABC} \mathbf{f}_1(S^{x-2}, t_{x-2}) \right] \wedge \\ & + \frac{v}{ABC(v)\Gamma(v+3)} \sum_{x=i+3}^n \left[ {}^{ABC} \mathbf{f}_1(S^x, t_x) - 2 {}^{ABC} \mathbf{f}_1(S^{x-1}, t_{x-1}) + {}^{ABC} \mathbf{f}_1(S^{x-2}, t_{x-2}) \right] \Delta, \end{aligned} \right. \end{cases} \tag{25}$$

$$I(t_{n+1}) = \begin{cases} I_0 + \left\{ \begin{aligned} & \left[ \frac{(\Delta t)^{v-1}}{\Gamma(v+1)} \sum_{x=2}^i \left[ \mathbf{f}_2(I^{x-2}, t_{x-2}) \right] \Pi + \frac{(\Delta t)^{v-1}}{\Gamma(v+2)} \sum_{x=2}^i \left[ \mathbf{f}_2(I^{x-1}, t_{x-1}) - {}^C \mathbf{f}_2(I^{x-2}, t_{x-2}) \right] \right] \wedge \\ & + \frac{v(\Delta t)^{v-1}}{2\Gamma(v+3)} \sum_{x=2}^i \left[ \mathbf{f}_2(I^x, t_x) - 2 {}^C \mathbf{f}_2(I^{x-1}, t_{x-1}) + {}^C \mathbf{f}_2(I^{x-2}, t_{x-2}) \right] \Delta \end{aligned} \right. \\ I(t_1) + \left\{ \begin{aligned} & \left[ \frac{1-v}{ABC(v)} {}^{ABC} \mathbf{f}_2(I^n, t_n) + \frac{v}{ABC(v)} \frac{(\delta t)^{v-1}}{\Gamma(v+1)} \sum_{x=i+3}^n \left[ {}^{ABC} \mathbf{f}_2(I^{x-2}, t_{x-2}) \right] \right] \Pi \\ & + \frac{v}{ABC(v)} \frac{(vt)^{v-1}}{\Gamma(v+2)} \sum_{x=i+3}^n \left[ {}^{ABC} \mathbf{f}_2(I^{x-1}, t_{x-1}) + ABC \mathbf{f}_2(I^{x-2}, t_{x-2}) \right] \right] \wedge \\ & + \frac{v}{ABC(v)} \frac{v(vt)^{v-1}}{\Gamma(v+3)} \sum_{x=i+3}^n \left[ {}^{ABC} \mathbf{f}_2(I^x, t_x) - 2 {}^{ABC} \mathbf{f}_2(I^{x-1}, t_{x-1}) + {}^{ABC} \mathbf{f}_2(I^{x-2}, t_{x-2}) \right] \Delta, \end{aligned} \right. \end{cases} \quad (26)$$

$$Y(t_{n+1}) = \begin{cases} Y_0 + \left\{ \begin{aligned} & \left[ \frac{(\Delta t)^{v-1}}{\Gamma(v+1)} \sum_{x=2}^i \left[ \mathbf{f}_3(Y^{x-2}, t_{x-2}) \right] \Pi + \frac{(\Delta t)^{v-1}}{\Gamma(v+2)} \sum_{x=2}^i \left[ \mathbf{f}_3(Y^{x-1}, t_{x-1}) - {}^C \mathbf{f}_3(Y^{x-2}, t_{x-2}) \right] \right] \wedge \\ & + \frac{v(\Delta t)^{v-1}}{2\Gamma(v+3)} \sum_{x=2}^i \left[ \mathbf{f}_3(Y^x, t_x) - 2 {}^C \mathbf{f}_3(Y^{x-1}, t_{x-1}) + {}^C \mathbf{f}_3(Y^{x-2}, t_{x-2}) \right] \Delta \end{aligned} \right. \\ Y(t_1) + \left\{ \begin{aligned} & \left[ \frac{1-v}{ABC(v)} {}^{ABC} \mathbf{f}_3(Y^n, t_n) + \frac{v}{ABC(v)} \frac{(\delta t)^{v-1}}{\Gamma(v+1)} \sum_{x=i+3}^n \left[ {}^{ABC} \mathbf{f}_3(Y^{x-2}, t_{x-2}) \right] \right] \Pi \\ & + \frac{v}{ABC(v)} \frac{(vt)^{v-1}}{\Gamma(v+2)} \sum_{x=i+3}^n \left[ {}^{ABC} \mathbf{f}_3(Y^{x-1}, t_{x-1}) + ABC \mathbf{f}_3(Y^{x-2}, t_{x-2}) \right] \right] \wedge \\ & + \frac{v}{ABC(v)} \frac{v(vt)^{v-1}}{\Gamma(v+3)} \sum_{x=i+3}^n \left[ {}^{ABC} \mathbf{f}_3(Y^x, t_x) - 2 {}^{ABC} \mathbf{f}_3(Y^{x-1}, t_{x-1}) + {}^{ABC} \mathbf{f}_3(Y^{x-2}, t_{x-2}) \right] \Delta, \end{aligned} \right. \end{cases} \quad (27)$$

$$Z(t_{n+1}) = \begin{cases} Z_0 + \left\{ \begin{aligned} & \left[ \frac{(\Delta t)^{v-1}}{\Gamma(v+1)} \sum_{x=2}^i \left[ \mathbf{f}_4(Z^{x-2}, t_{x-2}) \right] \Pi + \frac{(\Delta t)^{v-1}}{\Gamma(v+2)} \sum_{x=2}^i \left[ \mathbf{f}_4(Z^{x-1}, t_{x-1}) - {}^C \mathbf{f}_4(Z^{x-2}, t_{x-2}) \right] \right] \wedge \\ & + \frac{v(\Delta t)^{v-1}}{2\Gamma(v+3)} \sum_{x=2}^i \left[ \mathbf{f}_4(Z^x, t_x) - 2 {}^C \mathbf{f}_4(Z^{x-1}, t_{x-1}) + {}^C \mathbf{f}_4(Z^{x-2}, t_{x-2}) \right] \Delta \end{aligned} \right. \\ Z(t_1) + \left\{ \begin{aligned} & \left[ \frac{1-v}{ABC(v)} {}^{ABC} \mathbf{f}_4(Z^n, t_n) + \frac{v}{ABC(v)} \frac{(\delta t)^{v-1}}{\Gamma(v+1)} \sum_{x=i+3}^n \left[ {}^{ABC} \mathbf{f}_4(Z^{x-2}, t_{x-2}) \right] \right] \Pi \\ & + \frac{v}{ABC(v)} \frac{(vt)^{v-1}}{\Gamma(v+2)} \sum_{x=i+3}^n \left[ {}^{ABC} \mathbf{f}_4(Z^{x-1}, t_{x-1}) + ABC \mathbf{f}_4(Z^{x-2}, t_{x-2}) \right] \right] \wedge \\ & + \frac{v}{ABC(v)} \frac{v(vt)^{v-1}}{\Gamma(v+3)} \sum_{x=i+3}^n \left[ {}^{ABC} \mathbf{f}_4(Z^x, t_x) - 2 {}^{ABC} \mathbf{f}_4(Z^{x-1}, t_{x-1}) + {}^{ABC} \mathbf{f}_4(Z^{x-2}, t_{x-2}) \right] \Delta. \end{aligned} \right. \end{cases} \quad (28)$$

Here

$$\Pi = \begin{bmatrix} (1 - \mathbf{X} + m)^v \left( 2(-\mathbf{X} + m)^2 + (3v + 10)(-\mathbf{X} + m) + 2v^2 + 9v + 12 \right) \\ -(-\mathbf{X} + m) \left( 2(-\mathbf{X} + m)^2 + (5v + 10)(m - \mathbf{X}) + 6v^2 + 18v + 12 \right) \end{bmatrix},$$

$$\Lambda = \begin{bmatrix} (1 - \mathbf{X} + m)^v (3 + n + 2v - \mathbf{X}) \\ -(-\mathbf{X} + m) (m + 3v - \mathbf{X} + 3) \end{bmatrix},$$

$$\Delta = [(1 - \mathbf{X} + m)^v - (-\mathbf{X} + m)^v],$$

and

$$\begin{aligned} {}^C f_1(S, t) &= {}^{ABC} f_1(S, t) = S[r(1 - \frac{S}{k}) - \frac{\beta I}{1+\alpha S} - p_1 Y], \\ {}^C f_3(I, t) &= {}^{ABC} f_3(I, t) = I(\frac{\beta S}{1+\alpha S} - \omega), \\ {}^C f_2(Y, t) &= {}^{ABC} f_2(Y, t) = Y(-Y_1 + C_1 p_1 S - p_2 Z), \\ {}^C f_4(Z, t) &= {}^{ABC} f_4(Z, t) = -Y_2 Z + C_2 p_2 YZ + \mu. \end{aligned}$$

The above Eqs. (25)–(28) are the required solution for the aforementioned system.

### 5 Results and discussion

In this section we provide the numerical simulation of all four quantities of the considered piecewise problem on different fractional orders using the data of Table 2 taken from [14]. We also check the dynamics on two different intervals in the sense of Caputo and ABC fractional operators. The biological interpretation and their explanation are given in the article [14]. Further, the graphical results are simulated on different values lying between 0 and 1 which shows the total density of each quantity in the form of a continuous spectrum. Furthermore, chaotic dynamics are present in both divergent and convergent cases. All four quantities in the ecosystem oscillate which shows the dependence of one quantity over another one. The piecewise simulation is also provided on two subintervals the total time showing the sudden change dynamics or the crossover behavior

**Table 2.** Parameters and their description in model (1)

Notations	Numerical values - I	Numerical Values - II
r	4.5	3.8
k	5	15
$\beta$	2	2
$\alpha$	0.25	0.5
$\omega$	1.6	1.6
$d_1$	1	1
$c_1, c_2$	1, 1	1, 1
$\mu$	1	1.24143
$p_1, p_2$	2, 1	2, 1

The graphical representation of the four compartments is given in Figures 1a-1d with chaotic behaviors or phase portraits are given in Figures 1e-1f on different fractional orders using data of Table 2 numerical values-I. The extra information is provided by the fractional operators by taking extra orders lying between 0 and 1. For such data, the susceptible as well as infected plants are fluctuated or oscillated along with the other two quantities of Herbivores having the same dynamic. For this data, the said analysis is not converging faster as shown in the phase portrait figures.

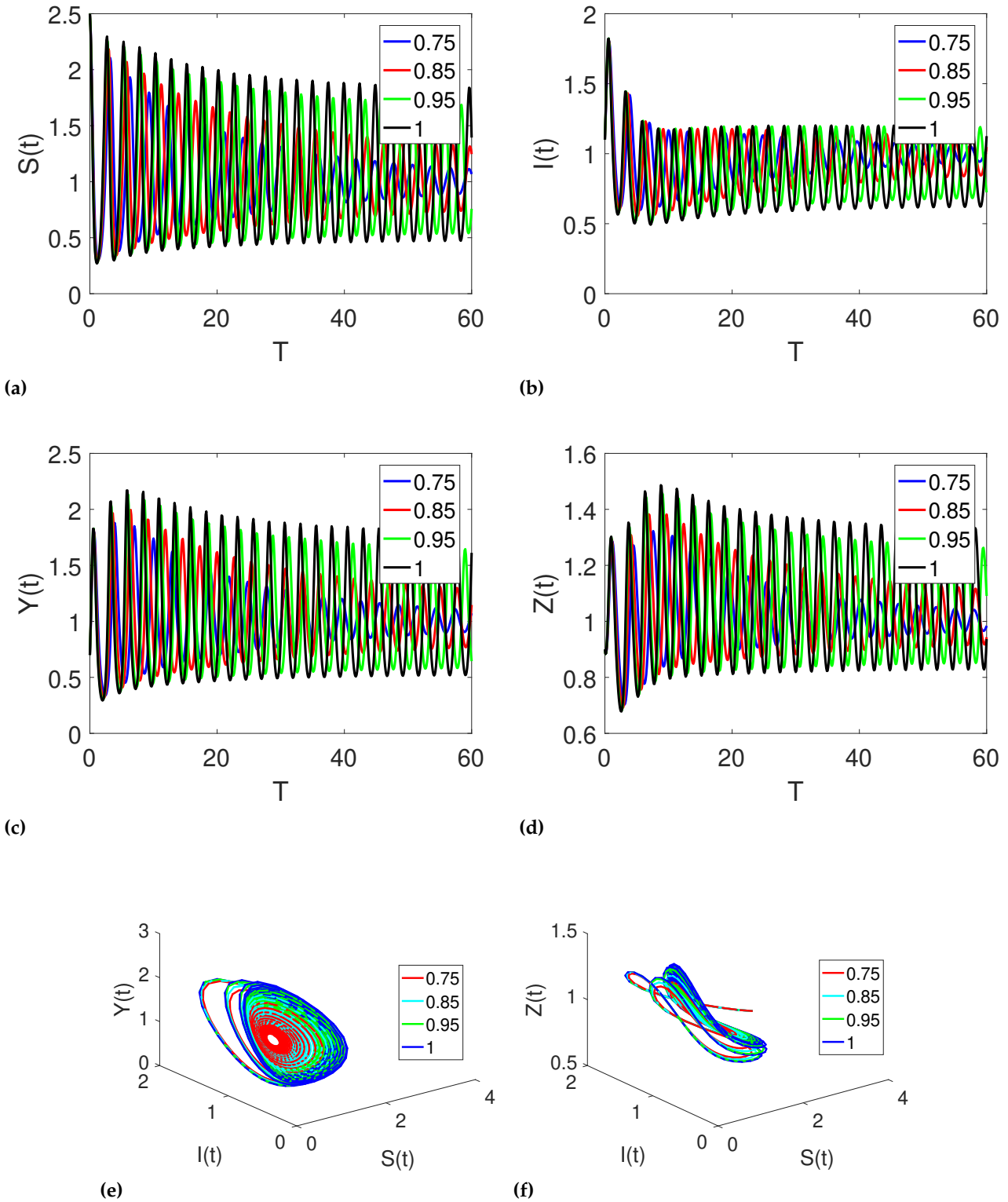


**Figure 1.** Dynamics of all the four compartments, on different arbitrary fractional orders  $\nu = 0.75, 0.85, 0.95, 1$  and time durations on any of the interval for the numerical value-I.

In figures 2a-2f, the graphical representation of the four compartments are given with chaotic behaviors or phase portrait are given on different fractional orders using data of table 2 numerical values-II. The extra information are provided by the fractional derivatives by taking extra orders lies between 0 and 1. For such data the susceptible as well as infected plants are fluctuated or

oscillating along with other two quantities of Herbivores having the same dynamics. But this time the said analysis is converging faster as shown in the phase portrait figures.

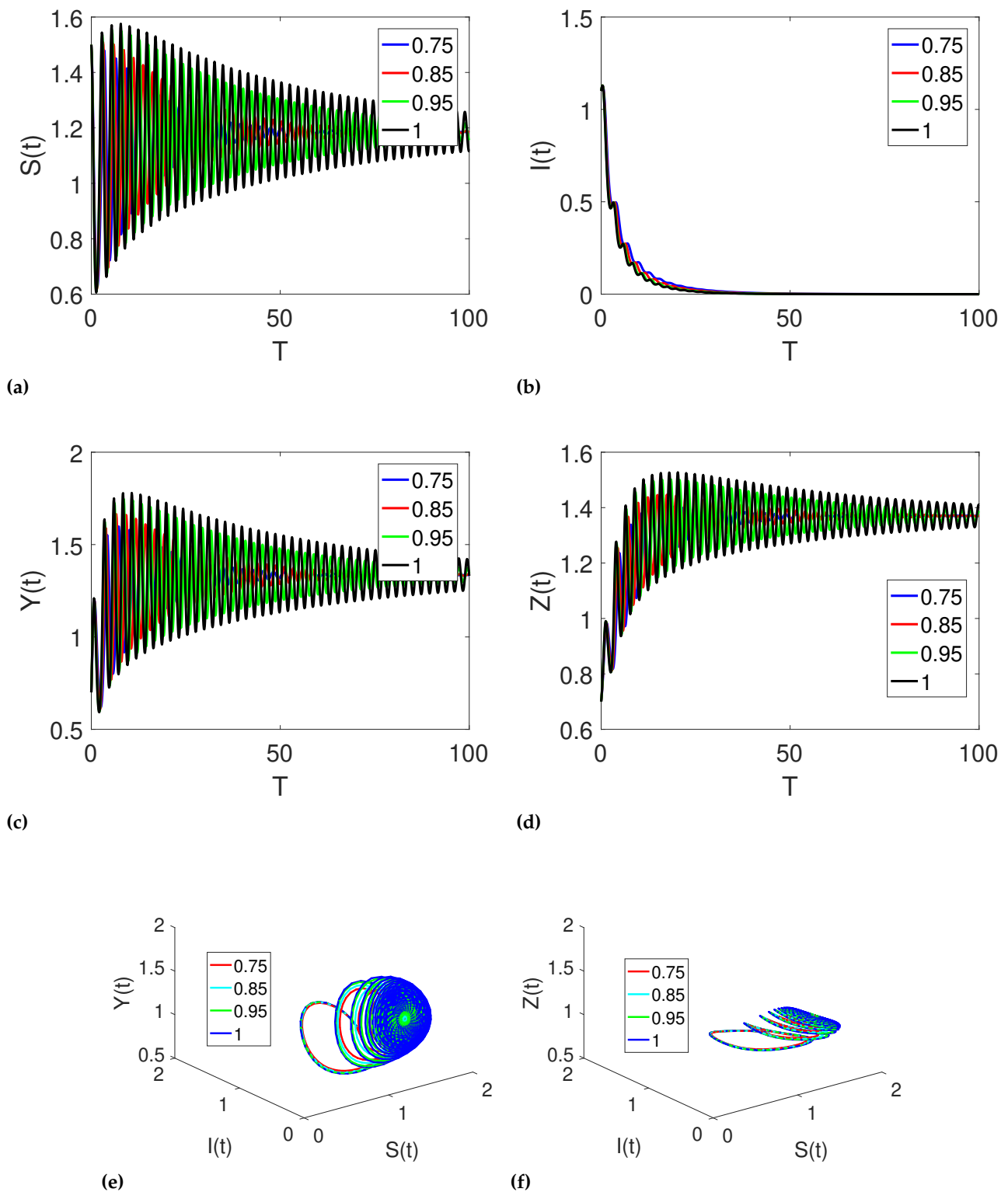


**Figure 2.** Dynamics of all the four compartments, on different arbitrary fractional orders  $\nu = 0.75, 0.85, 0.95, 1$  and time durations on any of the interval for the numerical value-II.

In Figures 3a-3f, the graphical representation of the four compartments are given with chaotic

behaviors or phase portrait are given on different fractional orders using data of table 2 numerical values-I on two sub intervals showing the crossover behaviors. The extra information are provided by the fractional derivatives by taking extra orders lies between 0 and 1. For such data the susceptible as well as infected plants are fluctuated or oscillating along with other two quantities of Herbivores having the oscillating dynamics. But this time the said analysis is not converging faster as shown in the phase portrait figures.

In figures 4a-4d, the graphical representation of the four compartments are given with chaotic behaviors or phase portrait are given on different fractional orders using data of table 2 numerical values-I on two sub intervals showing the crossover behaviors. The more information are provided by the fractional derivatives by taking extra orders lies between 0 and 1. For such data the susceptible as well as infected plants are shifting in one another oscillating along with other two quantities of Herbivores having the overlapping dynamics.

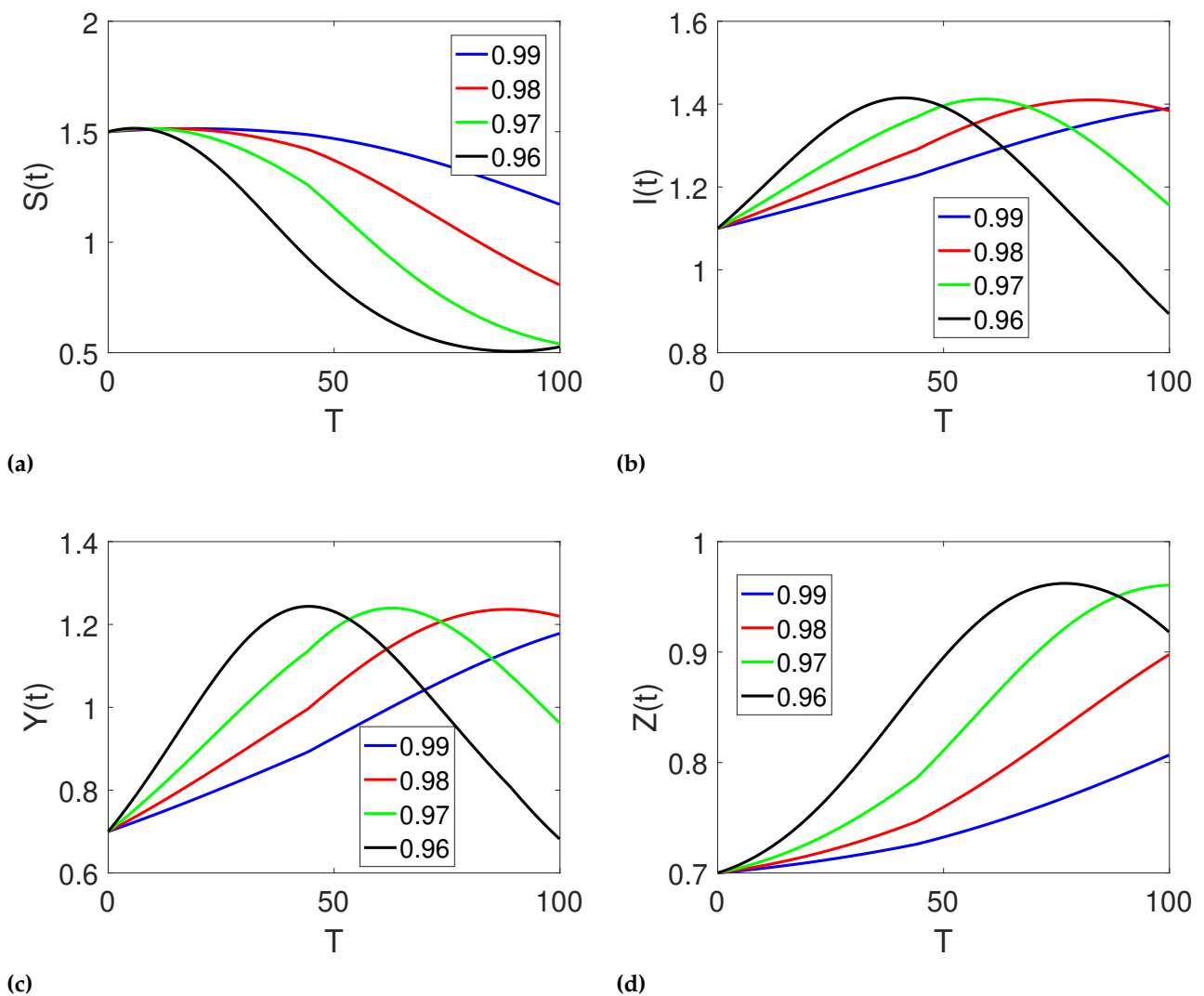


**Figure 4.** Dynamics of all the four compartments, on different arbitrary fractional orders  $\nu = 0.99, 0.98, 0.97, 0.96$  and time durations on any of two sub intervals  $[0, t_1], [t_1, t]$  for the numerical value-I showing the crossover dynamics.

In figures 5a-5f, the graphical representation of the four compartments are given with one another depending behaviors or phase portrait are given on different fractional orders using data of table 2

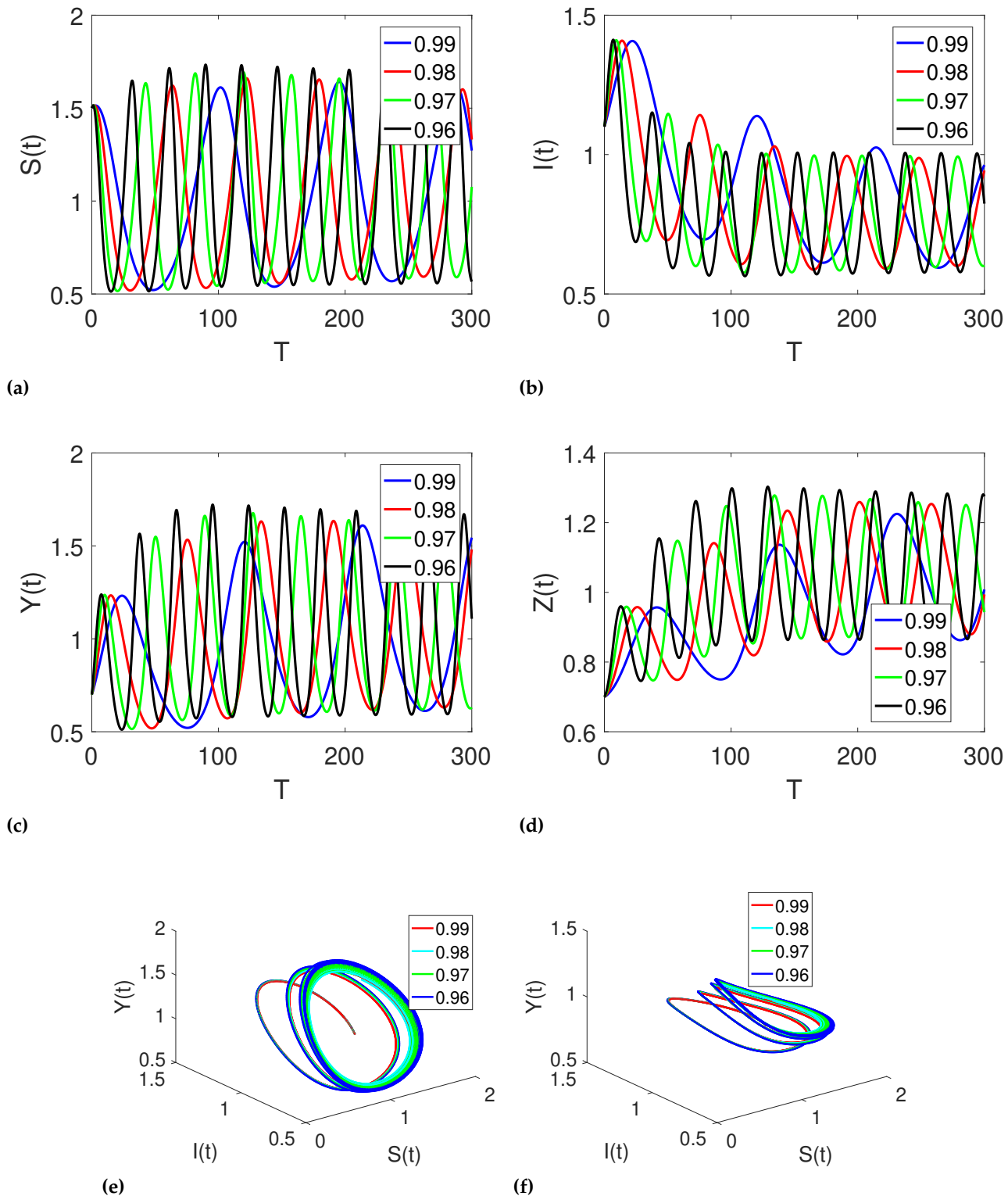


**Figure 3.** Dynamics of all the four compartments, on different arbitrary fractional orders  $\nu = 0.99, 0.98, 0.97, 0.96$  and time durations on any of two sub intervals  $[0, t_1], [t_1, t]$  for the numerical value-I.

numerical values-II on two sub intervals showing the crossover behaviors. The extra information are provided by the fractional derivatives by taking extra orders lies between 0 and 1. For such data the susceptible as well as infected plants are fluctuated or oscillating along with other two quantities of Herbivores having the oscillating dynamics which converges faster as shown in the

phase portrait figures.

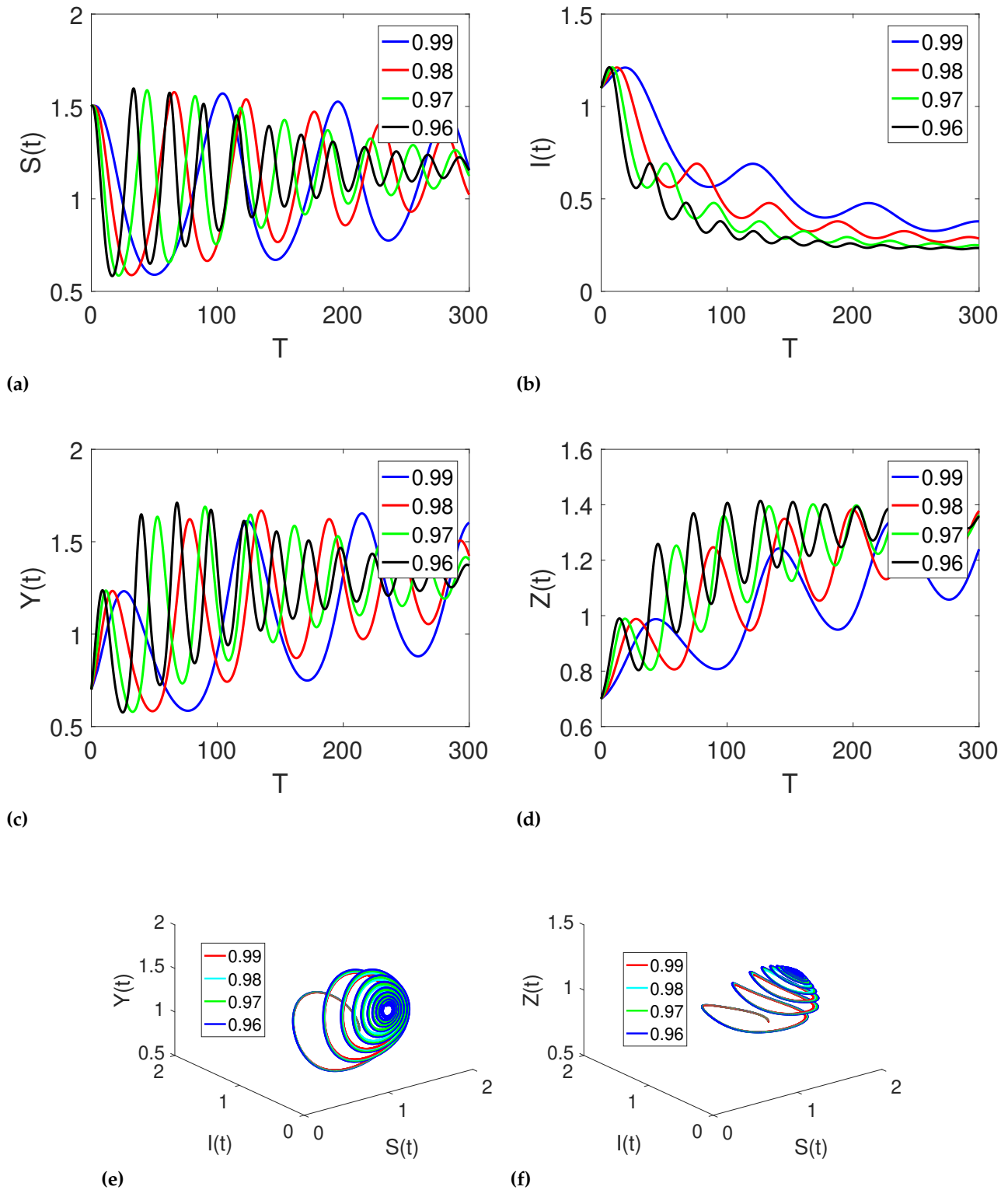


**Figure 5.** Dynamics of all the four compartments, on different arbitrary fractional orders  $\nu = 0.99, 0.98, 0.97, 0.96$  and time durations on any of two sub intervals  $[0, t_1], [t_1, t]$  for the numerical value-II.

## 6 Conclusion

Fractional-order differential equations with short memory play a crucial role in describing various real-world problems. Based on this premise, the current work explores a four-compartmental fractional-order plant model using the concept of piecewise derivative in both the Caputo and ABC sense. The study has further successfully investigated for the existence results, uniqueness of solution, and stability analysis of the considered problem, utilizing the fixed point concept and nonlinear functional analysis tools. Substantial results were obtained and presented in this work. The numerical solutions of the piecewise fractional model were computed using the Newton Polynomial technique in this study. MATLAB-18 was utilized to depict the numerical results for various fractional orders and time durations in this study. The results indicated that the piecewise data provided additional information that described crossover dynamics for different fractional orders. The graphical results obtained from both the piecewise and fractional order analysis were found to be highly intriguing as such analysis are more informative and generalized in the contrast of other relative work. The convergence and stability results are obtained by using fractional, piece wise fractional aspects. Fractional operators are generalized because they have an extra degree of freedom and choices. Therefore, we checked successfully the dynamics of different fractional orders lying between 0 and 1, and compare them with the integer order. On small fractional orders, stability is achieved quickly. Further, the piecewise fractional model is also tested validly for the existence and uniqueness of the solution in the sense of fractional Caputo and Atangana Baleanu operators having a kernel of non-singularity in the form of an exponential function. The approximate or semi-analytical solution is obtained by the technique of piecewise fractional Caputo and ABC derivative having the fractional parameter which shows the extra degree of freedom. Taking different fractional orders, we have simulated the obtained scheme for the first four terms. We also compare the fractional dynamics with the integer order dynamics. All the quantities of the proposed problem are converging to their equilibrium points showing spectrum dynamics with the removal of singularity as well as the crossover or abrupt dynamics.

### Declarations

#### Ethical approval

Not applicable

#### Consent for publication

Not applicable

#### Conflicts of interest

The authors declare that they have no conflict of interest.

#### Funding

Not applicable

#### Author's contributions

M.U.R.: Writing original draft preparation, Methodology, Validation. M.A.: Investigation, Software, Methodology. D.B.: Writing-Reviewing and Editing, Visualization, Supervision. All authors discussed the results and contributed to the final manuscript.

## Acknowledgements

Not applicable

## References

- [1] Schoonhoven, L.M., Van Loon, J.J. and Dicke, M. Insect-plant biology. *Oxford University Press on Demand*, (2005).
- [2] Strange, R.N. and Scott, P.R. Plant disease: a threat to global food security. *Annual Review of Phytopathology*, 43, 83-116, (2005). [[CrossRef](#)]
- [3] Mithofer, A. and Boland, W. Recognition of herbivory-associated molecular patterns. *Plant Physiology*, 146(3), 825-831, (2008). [[CrossRef](#)]
- [4] Dicke, M. and Sabelis, M.W. How plants obtain predatory mites as bodyguards. *Netherlands Journal of Zoology*, 38(2-4), 148-165, (1987).
- [5] Price, P.W., Bouton, C.E., Gross, P., McPherson, B.A., Thompson, J.N. and Weis, A.E. Interactions among three trophic levels: influence of plants on interactions between insect herbivores and natural enemies. *Annual review of Ecology and Systematics*, 11(1), 41-65, (1980). [[CrossRef](#)]
- [6] Takabayashi, J. and Dicke, M. Plant—carnivore mutualism through herbivore-induced carnivore attractants. *Trends in Plant Science*, 1(4), 109-113, (1996). [[CrossRef](#)]
- [7] Dudareva, N., Negre, F., Nagegowda, D.A. and Orlova, I. Plant volatiles: recent advances and future perspectives. *Critical Reviews in Plant Sciences*, 25(5), 417-440, (2006). [[CrossRef](#)]
- [8] Arimura, G.I., Kost, C. and Boland, W. Herbivore-induced, indirect plant defences. *Biochimica et Biophysica Acta (BBA)-Molecular and Cell Biology of Lipids*, 1734(2), 91-111, (2005). [[CrossRef](#)]
- [9] Dicke, M. Evolution of induced indirect defense of plants (Vol. 1999). Princeton, NJ: Princeton University Press, (1999).
- [10] Tumlinson, J.H., Paré, P.W. and Lewis, W.J. Plant production of volatile semiochemicals in response to insect-derived elicitors. In *Novartis Foundation Symposium*, pp. 95-104, Wiley, Chichester, (1999, January).
- [11] Price, P.W., Denno, R.F., Eubanks, M.D., Finke, D.L. and Kaplan, I. *Insect Ecology: Behavior, Populations and Communities*. Cambridge University Press, (2011).
- [12] Liu, Y.H., Li Liu, D., An, M., Fu, Y.L., Zeng, R.S., Luo, S.M., Wu, H. and Pratley, J. Modelling tritrophic interactions mediated by induced defence volatiles. *Ecological Modelling*, 220(23), 3241-3247, (2009). [[CrossRef](#)]
- [13] Fergola, P. and Wang, W. On the influences of defensive volatiles of plants in tritrophic interactions. *Journal of Biological Systems*, 19(02), 345-363, (2011). [[CrossRef](#)]
- [14] Mukherjee, D. Effect of constant immigration in plant–pathogen–herbivore interactions. *Mathematics and Computers in Simulation*, 160, 192-200, (2019). [[CrossRef](#)]
- [15] Podlubny, I. *Fractional Differential Equations, Mathematics in Science and Engineering*. Academic Press, New York, (1999).
- [16] Atangana, A. and Baleanu, D. New fractional derivatives with nonlocal and non-singular kernel: theory and application to heat transfer model. *Thermal Science*, 20(2), 763-785, (2016). [[CrossRef](#)]
- [17] Miller, K.S. Derivatives of noninteger order. *Mathematics magazine*, 68(3), 183-192, (1995). [[CrossRef](#)]
- [18] Zhang, L., ur Rahman, M., Arfan, M. and Ali, A. Investigation of mathematical model of

- transmission co-infection TB in HIV community with a non-singular kernel. *Results in Physics*, 28, 104559, (2021). [[CrossRef](#)]
- [19] Du, M., Wang, Z. and Hu, H. Measuring memory with the order of fractional derivative. *Scientific Reports*, 3(1), 3431, (2013). [[CrossRef](#)]
- [20] Wu, G.C., Gu, C.Y., Huang, L.L. and Baleanu, D. Fractional differential equations of variable order: existence results, numerical method and asymptotic stability conditions. *Miskolc Mathematical Notes*, 23(1), 485-493, (2022). [[CrossRef](#)]
- [21] Atangana, A. and Araz, S.I. New concept in calculus: Piecewise differential and integral operators. *Chaos, Solitons & Fractals*, 145, 110638, (2021). [[CrossRef](#)]
- [22] Ansari, K.J., Asma, Ilyas, F., Shah, K., Khan, A. and Abdeljawad, T. On new updated concept for delay differential equations with piecewise Caputo fractional-order derivative. *Waves in Random and Complex Media*, 1-20, (2023). [[CrossRef](#)]
- [23] Heydari, M.H., Razzaghi, M. and Baleanu, D. Orthonormal piecewise Vieta-Lucas functions for the numerical solution of the one-and two-dimensional piecewise fractional Galilei invariant advection-diffusion equations. *Journal of Advanced Research*, (2022). [[CrossRef](#)]
- [24] Patanarapeelert, N., Asma, A., Ali, A., Shah, K., Abdeljawad, T. and Sitthiwirattam, T. Study of a coupled system with anti-periodic boundary conditions under piecewise Caputo-Fabrizio derivative. *Thermal Science*, 27(1), 287-300, (2023). [[CrossRef](#)]
- [25] Sohail, A., Yu, Z., Arif, R., Nutini, A. and Nofal, T.A. Piecewise differentiation of the fractional order CAR-T cells-SARS-2 virus model. *Results in Physics*, 33, 105046, (2022). [[CrossRef](#)]
- [26] Zeb, A., Atangana, A., Khan, Z.A. and Djillali, S. A robust study of a piecewise fractional order COVID-19 mathematical model. *Alexandria Engineering Journal*, 61(7), 5649-5665, (2022). [[CrossRef](#)]
- [27] Atangana, A. and Araz, S.İ. Modeling third waves of Covid-19 spread with piecewise differential and integral operators: Turkey, Spain and Czechia. *Results in Physics*, 29, 104694, (2021). [[CrossRef](#)]
- [28] Cao, Y., Alamri, S., Rajhi, A.A., Anqi, A.E., Riaz, M. B., Elagan, S.K. and Jawa, T.M. A novel piece-wise approach to modeling interactions in a food web model. *Results in Physics*, 31, 104951, (2021). [[CrossRef](#)]
- [29] El-Shorbagy, M.A., ur Rahman, M. and Alyami, M.A. On the analysis of the fractional model of COVID-19 under the piecewise global operators. *Mathematical Biosciences and Engineering*, 20(4), 6134-6173, (2023). [[CrossRef](#)]
- [30] Khan, J., Ur Rahman, M., Riaz, M.B. and Awrejcewicz, J. A Numerical study on the dynamics of dengue disease model with fractional piecewise derivative. *Fractals*, 30(08), 2240260, (2022). [[CrossRef](#)]
- [31] Qu, H., Saifullah, S., Khan, J., Khan, A., Ur Rahman, M. and Zheng, G. Dynamics of leptospirosis disease in context of piecewise classical-global and classical-fractional operators. *Fractals*, 30(08), 2240216, (2022). [[CrossRef](#)]
- [32] Ansari, K.J., Asma, Ilyas, F., Shah, K., Khan, A. and Abdeljawad, T. On new updated concept for delay differential equations with piecewise Caputo fractional-order derivative. *Waves in Random and Complex Media*, 1-20, (2023). [[CrossRef](#)]
- [33] Shah, K., Abdeljawad, T. and Alrabaiah, H. On coupled system of drug therapy via piecewise equations. *Fractals*, 30(08), 2240206, (2022). [[CrossRef](#)]

- [34] Sohail, A., Yu, Z., Arif, R., Nutini, A. and Nofal, T.A. Piecewise differentiation of the fractional order CAR-T cells-SARS-2 virus model. *Results in Physics*, 33, 105046, (2022). [[CrossRef](#)]
- [35] Atangana, A. and Toufik, M. A piecewise heat equation with constant and variable order coefficients: A new approach to capture crossover behaviors in heat diffusion. *AIMS Mathematics*, 7(5), 8374-8389, (2022). [[CrossRef](#)]

Bulletin of Biomathematics (BBM)  
(<https://bulletinbiomath.org>)



**Copyright:** © 2023 by the authors. This work is licensed under a Creative Commons Attribution 4.0 (CC BY) International License. The authors retain ownership of the copyright for their article, but they allow anyone to download, reuse, reprint, modify, distribute, and/or copy articles in *BBM*, so long as the original authors and source are credited. To see the complete license contents, please visit (<http://creativecommons.org/licenses/by/4.0/>).

**How to cite this article:** Rahman, M., Arfan, M. & Baleanu, D. (2023). Piecewise fractional analysis of the migration effect in plant-pathogen-herbivore interactions. *Bulletin of Biomathematics*, 1(1), 1-23. <https://doi.org/10.59292/bulletinbiomath.2023001>

RESEARCH PAPER

## Analysis of the disturbance effect in intracellular calcium dynamic on fibroblast cells with an exponential kernel law

Hardik Joshi <sup>1,\*</sup>, Mehmet Yavuz <sup>2,†</sup> and Ivanka Stamova <sup>3,‡</sup>

<sup>1</sup>Department of Mathematics, LJ Institute of Engineering and Technology, LJ University, Ahmedabad-382210, India, <sup>2</sup>Department of Mathematics and Computer Sciences, Necmettin Erbakan University, 42090 Konya, Türkiye, <sup>3</sup>Department of Mathematics, The University of Texas at San Antonio, San Antonio, TX 78249, USA

\*Corresponding Author

† hardik.joshi8185@gmail.com (Hardik Joshi); mehmetyavuz@erbakan.edu.tr (Mehmet Yavuz); Ivanka.Stamova@utsa.edu (Ivanka Stamova)

### Abstract

The maintenance of free calcium in the cytoplasm is requisite for cell integrity and the regime of the multi-cellular process. Overproduction and degradation to manage this cellular entity produce offensive changes in tissue performance and as a result, commence fibrotic diseases. Thus, there is a necessity to know the cellular process for the inclusion and extrusion of free calcium. Here, a mathematical model is framed to investigate the role of buffer and calcium concentration on fibroblast cells. In this context, the Caputo-Fabrizio advection reaction-diffusion model along with apposite biophysical initial and boundary conditions is considered. The analytical solution is obtained and used to analyze the diverse mechanisms of calcium on fibroblast cells. The obtained results reveal that when the fractional order goes to one, the Caputo–Fabrizio fractional derivative provides a concise calcium profile and well-managed cellular entity due to the exponential kernel law.

**Keywords:** Calcium concentration; buffer; fibroblast cells; fractional advection reaction-diffusion equation; Caputo-Fabrizio fractional derivative

**AMS 2020 Classification:** 26A33, 35Q92, 35R11, 92B05, 97M10

### 1 Introduction

Fibroblast is non-excitabile and heterogeneous structural cells whose primary function is the production of extracellular matrix for tissue maintenance and repair. It plays a pivotal role in maintaining tissue integrity, and in healing processes. They participate in fibrotic disorders in the lung, skin, and other tissues. All these events are closely related to another mechanism in cells, particularly with the signals from the local environment or extracellular medium and the

calcium diffusion mechanisms [1]. Calcium ion acts as a messenger to perform all these functions in fibroblasts cell. Fibroblast cell regulates calcium concentration at different levels in response to the requirements for activation and performance of various physiological processes like wound healing, tissue remodeling, and tissue growth. This calcium regulation mechanism and the calcium concentration levels are required for cellular activities and their maintenance [2]. Therefore, it is necessary to understand calcium regulation processes in fibroblast cells. This calcium regulation mechanism involves processes like diffusion, advection, flux, and buffering phenomena.

Buffer binds the excess calcium present in the cell to form bound buffers and lower the calcium concentration in the cell [3]. The calcium in excess of a limit for a longer span will be toxic and can cause cell death [4]. On the requirement for a higher concentration of calcium for any physiological process in fibroblast cells, these bound buffers release it to fulfill the requirement. Thus, the buffers act as stores of calcium concentration and also perform functions like source and sinks to regulate the concentration levels.

Experimental studies have shown that fibroblast shows excitability in particular growth stages. The excitability of a cell is an important mechanism in calcium signaling since a strong interplay exists between the membrane potential and the internal calcium concentration. The increase in intracellular calcium associated with action potentials provides a mechanism for long-range and fast-coordinated calcium signaling in excitable cells. Although in-excitable cells it has been reported that fibroblast functions are unclear. Thus to fully understand the calcium regulation mechanisms in fibroblast cells, it will be important to understand the local changes in calcium levels.

Several theoretical investigations are reported in the literature to study calcium dynamics in fibroblast cells [5, 6]. Also, some mathematical model has been developed in the literature to study calcium dynamics in astrocyte [7–9], neuron [10–18], myocytes [19], oocyte [20, 21], T lymphocyte [22, 23], cholangiocyte [24] and another cell. But, no attempt is reported in the literature to study the effect of disturbances in intracellular calcium dynamic on fibroblast cells with an exponential kernel law. In the view of above, here an attempt has been made to develop a mathematical model to investigate the role of buffer and calcium concentration on fibroblast cells with the Caputo-Fabrizio fractional operator. To the best of the author's knowledge, no attempts are registered to investigate the effect of calcium dynamics on fibroblast cells by using fractional calculus approaches. Fractional derivative is a natural extension of classical derivative to study differential equations with a memory-dependent derivative [25–30]. Fractional derivative provides great freedom for the choice of order of derivative and thus illustrates the reality of complex phenomena in a more understanding and expressive way [31–37]. In this attempt, we use the Caputo-Fabrizio derivative due to its non-singular exponential kernel.

The structure of the paper is as follows: In Section 2, we introduce some mathematical preliminaries. In Section 3, we developed the Caputo-Fabrizio advection reaction-diffusion model for calcium dynamics in fibroblast cells. In Section 4, we present numerical simulations for various physiological conditions of the calcium model. Finally, the conclusion is provided in section 5.

## 2 Mathematical preliminaries

In this section, some preliminaries are provided about the Caputo-Fabrizio fractional derivative with a nonsingular kernel. According to [26], the formal definition of Caputo-Fabrizio fractional derivatives is defined as follows:

**Definition 1** Let  $f \in H^1(x, y)$ , with  $y > x$ , then the Caputo-Fabrizio derivative of function  $f(t)$  of order

$\alpha \in [0, 1]$  is defined as

$${}^{CF}D_t^\alpha f(t) = \frac{M(\alpha)}{1-\alpha} \int_x^t f'(w) \exp \left[ -\alpha \frac{t-w}{1-\alpha} \right] dw, \quad (1)$$

where  $M(\alpha)$  is a normalization function and satisfies  $M(0) = M(1) = 1$ .

If  $f \notin H^1(x, y)$ , then the derivative of function  $f(t)$  is defined as

$${}^{CF}D_t^\alpha f(t) = \frac{\alpha M(\alpha)}{1-\alpha} \int_x^t (f(t) - f(w)) \exp \left[ -\alpha \frac{t-w}{1-\alpha} \right] dw. \quad (2)$$

**Remark 1** If  $\beta = \frac{1-\alpha}{\alpha} \in [0, \infty)$ ,  $\alpha = \frac{1}{1+\beta}$ , then the equation (2) can be modified as

$${}^{CF}D_t^\alpha f(t) = \frac{N(\alpha)}{\alpha} \int_x^t f'(t) \exp \left[ -\frac{t-w}{\beta} \right] dw, \quad (3)$$

where  $N(0) = N(\infty) = 1$ . Moreover,

$$\lim_{\beta \rightarrow 0} \left( \frac{1}{\alpha} \exp \left( -\frac{t-w}{\beta} \right) \right) = \delta(w-t). \quad (4)$$

According to [38], the Caputo-Fabrizio integral is defined as follows:

**Definition 2** The Caputo-Fabrizio integral of function  $f(t)$  of order  $\alpha \in [0, 1]$  and  $t \geq 0$  is defined as

$${}^{CF}I_t^\alpha f(t) = \frac{2(1-\alpha)}{(2-\alpha)M(\alpha)} f(t) + \frac{2\alpha}{(2-\alpha)M(\alpha)} \int_0^t f(s) ds. \quad (5)$$

Further simplification gives us as

$$\frac{2(1-\alpha)}{(2-\alpha)M(\alpha)} + \frac{2\alpha}{(2-\alpha)M(\alpha)} = 1. \quad (6)$$

### 3 Mathematical model and solution

The mathematical model includes diffusion of calcium and buffer in calcium signaling phenomena. The process occurs inside the plasma membrane of the cells. The calcium kinetics in fibroblast cells is governed by a set of advection reaction-diffusion equations in the form of a bimolecular reaction between  $Ca^{2+}$  and buffer [3, 39, 40].



The remaining reaction-diffusion equations can be derived using Fickian diffusion as [39, 40]

$$\frac{\partial [Ca^{2+}]}{\partial t} = D_C \cdot \nabla^2 [Ca^{2+}] + \sum_k R_k, \quad (8)$$

$$\frac{\partial [B]}{\partial t} = D_B \cdot \nabla^2 [B] + R_k, \quad (9)$$

$$\frac{\partial [CaB]}{\partial t} = D_{CB} \cdot \nabla^2 [CaB] - R_k, \quad (10)$$

where  $R_k = -k^+ [B] [Ca^{2+}] + k^- [CaB]$ , known as the reaction term and  $D_K$  is the diffusion coefficient for the respective entity. Although, the buffer do not capable to diffuse with other entity is considered a stationary buffer and mathematically described by setting  $D_B = D_{CB} = 0$ . Now, including equations (7-10) the mathematical model is become as

$$\frac{\partial u}{\partial t} = D_c \frac{\partial^2 u}{\partial x^2} - v \frac{\partial u}{\partial x} - k^+ \cdot [B]_{\infty} (u - u_{\infty}), \quad (11)$$

where  $u = [Ca^{2+}]$ .

The apposite biophysical initial condition is defined as

$$u(x, 0) = u_{\infty}, x > 0, \quad (12)$$

and the boundary conditions are

$$u(0, t) = u_0, t > 0, \quad \frac{\partial u}{\partial x} = 0, x \rightarrow \infty, t > 0. \quad (13)$$

For simplicity, we replaced  $u - u_{\infty} = u$  and  $k^+ \cdot [B]_{\infty} = f$  then the mathematical model is rearranged as

$$\frac{\partial u}{\partial t} = D_c \frac{\partial^2 u}{\partial x^2} - v \frac{\partial u}{\partial x} - fu. \quad (14)$$

The apposite biophysical initial and boundary conditions are modified as

$$\begin{aligned} u(x, 0) &= 0, x > 0, \\ u(0, t) &= u_{\infty} - u_0, t > 0, \quad \frac{\partial u}{\partial x} = 0, x \rightarrow \infty, t > 0. \end{aligned} \quad (15)$$

The non-dimensional calcium model is formulated by introducing the dimensionless variables

$$x^* = x \sqrt{\frac{f}{D_C}}, \quad t^* = ft, \quad u^* = \frac{u}{u_0}, \quad k = \frac{v}{\sqrt{fD_C}}.$$

Hence, equation (14) turns out to be the following equation as

$$\frac{\partial u}{\partial t} = \frac{\partial^2 u}{\partial x^2} - k \frac{\partial u}{\partial x} - u, \quad (16)$$

and the corresponding conditions are

$$\begin{aligned} u(x, 0) &= 0, \quad x > 0, \\ u(0, t) &= u_\infty - u_0, \quad t > 0, \quad \frac{\partial u}{\partial x} = 0, \quad x \rightarrow \infty, \quad t > 0. \end{aligned} \quad (17)$$

Next, we defined a new solute concentration  $u(x, t) = \exp\left(\frac{kx}{2}\right) \gamma(x, t)$  and it is easy to verify that  $\gamma(x, t)$  satisfies the following non-dimensional calcium problem.

$$\frac{\partial \gamma}{\partial t} = \frac{\partial^2 \gamma}{\partial x^2} - \left(\frac{k^2}{2} + 1\right) \gamma. \quad (18)$$

For simplicity, we replaced  $\left(\frac{k^2}{2} + 1\right) = \xi^2$ . Finally, the calcium model is formulated as follows

$$\frac{\partial \gamma}{\partial t} = \frac{\partial^2 \gamma}{\partial x^2} - \xi^2 \gamma, \quad (19)$$

and the corresponding conditions are

$$\begin{aligned} \gamma(x, 0) &= 0, \quad x > 0, \\ \gamma(0, t) &= u_0 - u_\infty, \quad t > 0, \quad \gamma(x, t) = 0, \quad x \rightarrow \infty, \quad t > 0. \end{aligned} \quad (20)$$

Now we convert the calcium model into the Caputo-Fabrizio sense to improve the accuracy and introduce a memory and hereditary behavior of cells. Thus the Caputo-Fabrizio calcium model for fibroblast cells is represented as follows:

$${}^{CF}D_t^\alpha \gamma(x, t) = \frac{\partial^2 \gamma}{\partial x^2} - \xi^2 \gamma. \quad (21)$$

Applying the Laplace transform on equation (21), we obtain the following transformed problem as

$$\frac{s\bar{\gamma}(x, s) - \gamma(x, 0)}{(1-\alpha)s + \alpha} = \frac{\partial^2 \bar{\gamma}(x, s)}{\partial x^2} - \xi^2 \bar{\gamma}(x, s), \quad (22)$$

where  $\bar{\gamma}(x, s)$  is the Laplace transformation of  $\gamma(x, t)$ .

Next, applying the Fourier sine transform on equation (22), the transformed problem is recast as

$$\frac{\hat{s}\bar{\gamma}(w, s)}{(1-\alpha)s + \alpha} = -w^2 \bar{\gamma}(w, s) + w\bar{\gamma}(0, s) - \xi^2 \bar{\gamma}(w, s), \quad (23)$$

where  $\hat{s}\bar{\gamma}(w, s)$  is the Fourier sine transform of  $\bar{\gamma}(x, s)$ . By using equation (20) we obtain as

$$\frac{\hat{s}\bar{\gamma}(w, s)}{(1-\alpha)s + \alpha} = -w^2 \bar{\gamma}(w, s) + w(u_0 - u_\infty) - \xi^2 \bar{\gamma}(w, s). \quad (24)$$

By simple rearrangement give us the following expression

$$\hat{\gamma}(w, s) = \frac{w(u_0 - u_\infty)}{w^2 + m + \zeta^2} + \frac{\alpha m^2 w(u_0 - u_\infty)}{(w^2 + m + \zeta^2)^2} \frac{1}{s + \frac{\alpha m(w^2 + \zeta^2)}{w^2 + m + \zeta^2}}, \quad (25)$$

where  $m = 1/(1 - \alpha)$ . Next, by inverting the Laplace and Fourier transform of equation (25), we have

$$\begin{aligned} \gamma(x, t) &= \frac{2(u_0 - u_\infty)\delta(t)}{\pi} \int_0^\infty \frac{w \sin(wx)}{w^2 + m + \zeta^2} dw \\ &+ \frac{2(u_0 - u_\infty)}{\pi} \int_0^\infty \frac{\alpha m^2 w \sin(wx)}{(w^2 + m + \zeta^2)^2} \exp\left(\frac{\alpha m(w^2 + \zeta^2)t}{w^2 + m + \zeta^2}\right) dw. \end{aligned} \quad (26)$$

By using the relation

$$\int_0^\infty \frac{w \sin(wx)}{w^2 + b^2} dw = \frac{\pi}{2} e^{-bx}. \quad (27)$$

Equation (26) turns out to be

$$\begin{aligned} \gamma(x, t) &= (u_0 - u_\infty)\delta(t) \exp\left(-x\sqrt{m + \zeta^2}\right) \\ &+ \frac{2(u_0 - u_\infty)}{\pi} \int_0^\infty \frac{\alpha m^2 w \sin(wx)}{(w^2 + m + \zeta^2)^2} \exp\left(\frac{\alpha m(w^2 + \zeta^2)t}{w^2 + m + \zeta^2}\right) dw. \end{aligned} \quad (28)$$

Then by transforming equation (28) to the original coordinate system, we get the calcium concentration in fibroblast cells at any instant as

$$\begin{aligned} u(x, t) &= (u_0 - u_\infty)\delta(t) \exp\left(-x\sqrt{m + \zeta^2} + \frac{kx}{2}\right) \\ &+ \frac{2(u_0 - u_\infty)}{\pi} \exp\left(\frac{kx}{2}\right) \int_0^\infty \frac{\alpha m^2 w \sin(wx)}{(w^2 + m + \zeta^2)^2} \exp\left(-\frac{\alpha m(w^2 + \zeta^2)t}{w^2 + m + \zeta^2}\right) dw. \end{aligned} \quad (29)$$

### Limiting case of the model (Caputo-Fabrizio order $\alpha \rightarrow 1$ )

The classical solution of the calcium model is obtained here as a special case or limiting case of the Caputo-Fabrizio calcium model by approaching  $\alpha \rightarrow 1$ .

When  $\alpha \rightarrow 1$  we have,

$$\begin{aligned} \gamma(x, t) &= \lim_{\alpha \rightarrow 1} \frac{2(u_0 - u_\infty)}{\pi} \int_0^\infty \frac{\alpha m^2 w \sin(wx)}{(w^2 + m + \zeta^2)^2} \exp\left(-\frac{\alpha m(w^2 + \zeta^2)t}{w^2 + m + \zeta^2}\right) dw \\ &= \frac{2(u_0 - u_\infty)}{\pi} \int_0^\infty w \sin(wx) \exp\left(-(w^2 + \zeta^2)t\right) dw. \end{aligned} \quad (30)$$

Then by using equation (30), equation (29) rearrange as follows

$$\gamma(x, t) = \frac{(u_0 - u_\infty)}{2\sqrt{\pi}} \frac{x}{t\sqrt{t}} \exp\left(-\zeta^2 t - \frac{x^2}{4t}\right), \quad (31)$$

and again by transforming equation (31) to the original coordinate system, we get the calcium concentration in fibroblast cells for the classical case as

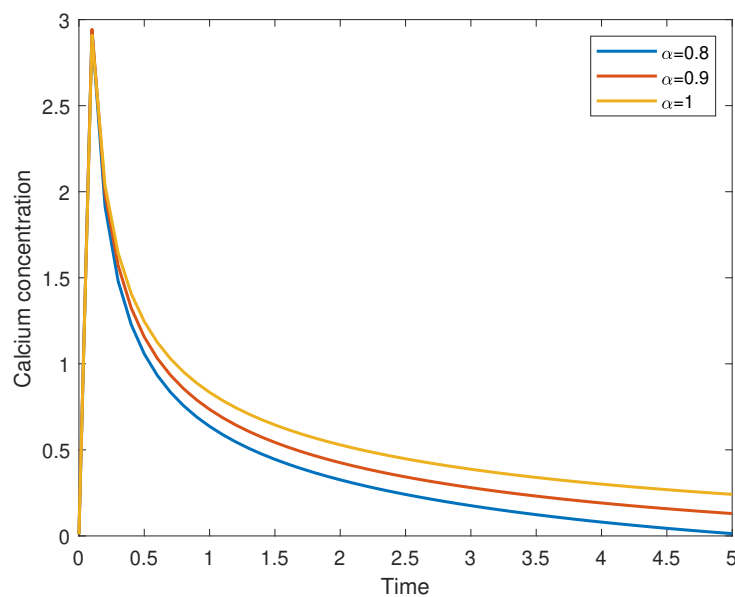
$$u(x, t) = \frac{(u_0 - u_\infty)}{2\sqrt{\pi}} \frac{x}{t\sqrt{t}} \exp\left(-\zeta^2 t - \frac{x^2}{4t} + \frac{kx}{2}\right). \quad (32)$$

#### 4 Numerical results and discussion

In this section, we portrayed the spatial and temporal calcium concentration in fibroblast cells for various amounts of buffer, diffusion coefficient, advection flux, and Caputo-Fabrizio derivative. The numerical values of a bio-physiological parameter used to simulate the result are provided in Table 1.

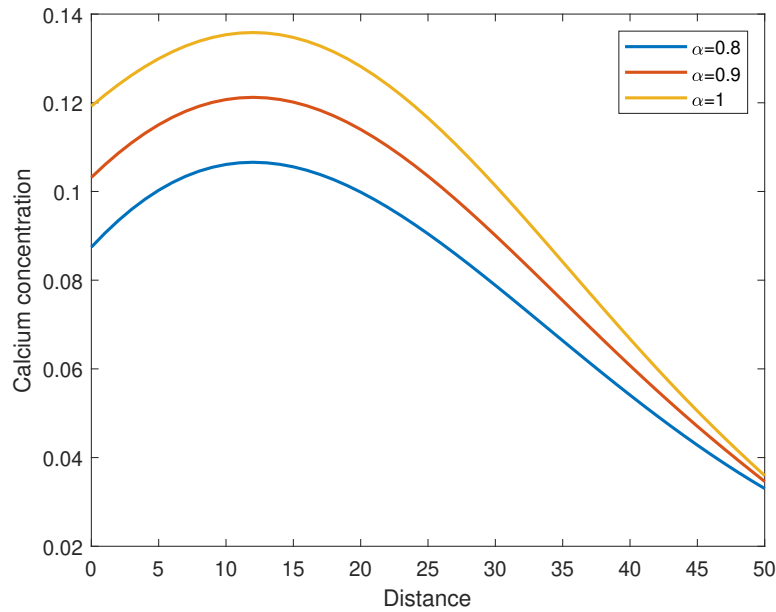
**Table 1.** Values of bio-physiological parameters [3, 5, 40]

Symbol	Parameter	Value
$D_C$	Diffusion coefficient	260-400 $\mu\text{m}^2/\text{s}$
$[B_m]$	Buffer concentration	60-200 $\mu\text{M}$
$k^+$ (EGTA)	Buffer association rate	1.6-30 $\mu\text{M}^{-1}\text{s}^{-1}$
$k^+$ (BAPTA)	Buffer association rate	600-900 $\mu\text{M}^{-1}\text{s}^{-1}$
$[Ca^{2+}]_\infty$	Background $Ca^{2+}$ concentration	0.1 $\mu\text{M}$
$v$	Advection flux	0-30 $\mu\text{m}/\text{s}$



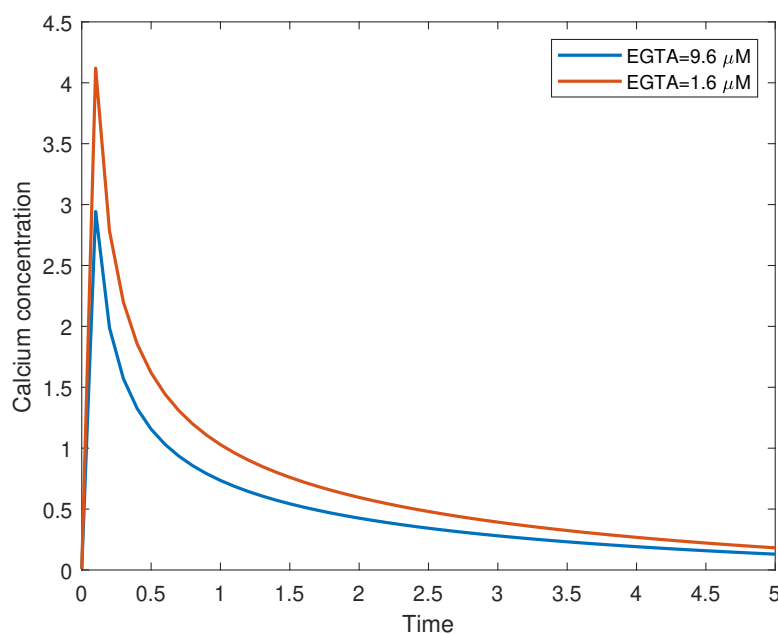
**Figure 1.** Calcium concentration against time for various orders of Caputo-Fabrizio derivative

Figure 1 shows the calcium concentration in a fibroblast cell against time for diffusion coefficient  $290 \mu\text{m}^2/\text{s}$ , advection flux  $10 \mu\text{m}/\text{s}$ , and EGTA buffer  $1.6 \mu\text{M}$ . The highest concentration is observed near the source then it decreases to reach its equilibrium conditions. This happened near the source as free calcium reacted with the buffer and made a calcium-bound buffer. As a result, the sharp fall is observed after 0.5 seconds and it shows the notable role of a buffer up to 0.5 seconds. Also, the kernel of the Caputo-Fabrizio derivative plays a significant role due to the exponential kernel law and forces the calcium profile to early achieved stable conditions.



**Figure 2.** Calcium concentration against distance for various orders of Caputo-Fabrizio derivative

Figure 2 shows the calcium concentration in a fibroblast cell against distance for diffusion coefficient  $290 \mu m^2/s$ , advection flux  $10 \mu m/s$ , and EGTA buffer  $1.6 \mu M$ . The highest concentration is observed near the source then subtle rises due to the entry of buffer affinity and then decreases gradually to reach its equilibrium conditions. The sharp fall is observed after  $20 \mu m$ , and it shows the notable role of buffer in the initial stage of cellular activities. As Caputo-Fabrizio derivative moves to integer order, the calcium concentration is increasing then finally achieved stable conditions. Figures 1 and 2 show the significant role of the Caputo-Fabrizio derivative due to the exponential kernel law and hence Figures 3-10 are produced only for Caputo-Fabrizio fractional order  $\alpha = 0.9$ .



**Figure 3.** Calcium concentration against time for various amounts of EGTA buffer

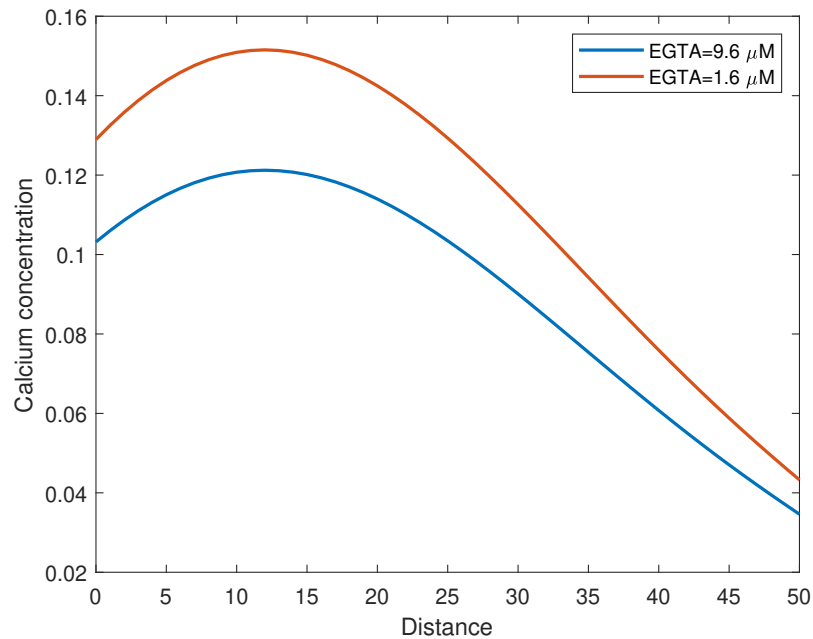


**Figure 4.** Calcium concentration against distance for various amounts of EGTA buffer

Figures 3 and 4 show the calcium concentration in a fibroblast cell against time and space respectively. The bio-physiological parameters used to simulate the result are the same as listed above. Here, we examine the effect of EGTA buffer over time and space. From the figures, we confirmed that as the value of buffer increases calcium concentration initiates to decrease due to the free buffer binds with free calcium.

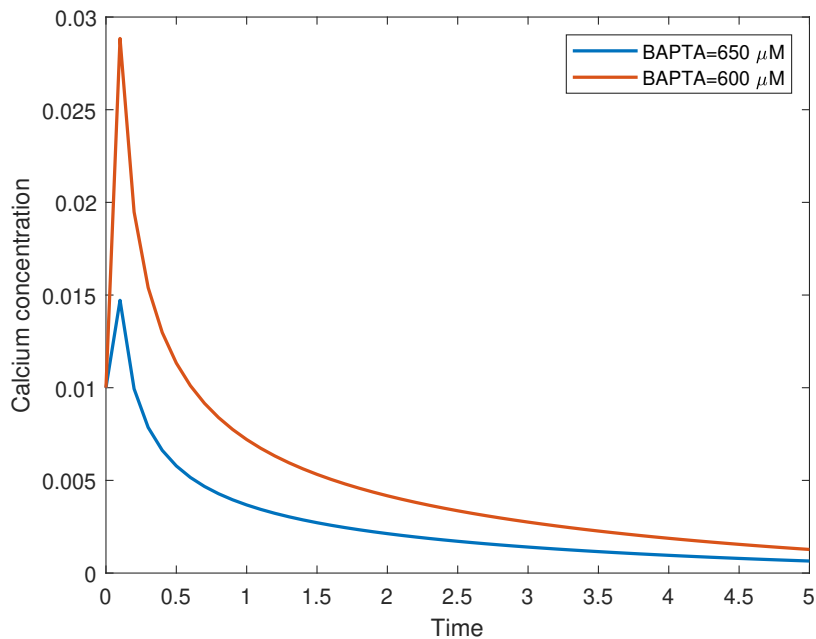


**Figure 5.** Calcium concentration against time for various amounts of BAPTA buffer

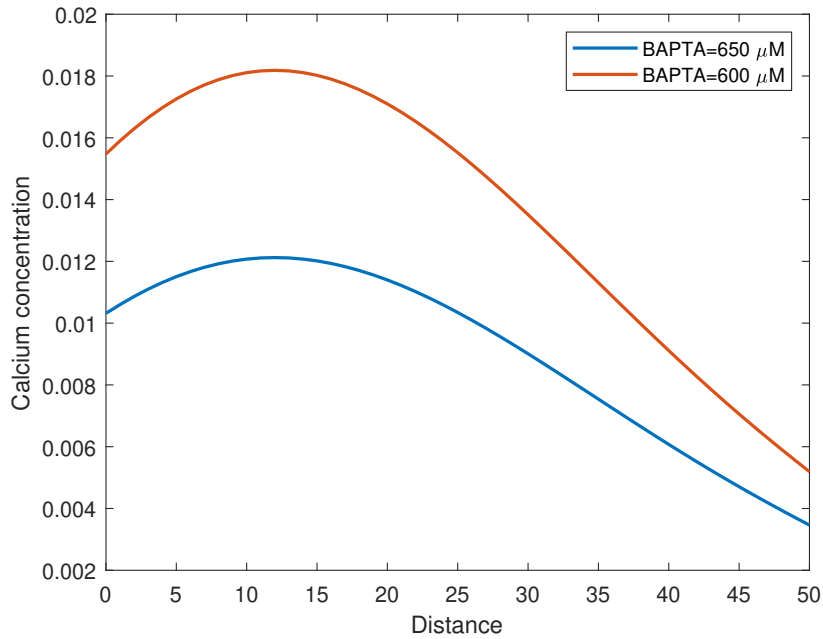


**Figure 6.** Calcium concentration against distance for various amounts of BAPTA buffer

Figures 5 and 6 show the calcium concentration in a fibroblast cell against time and space respectively. Here, we examine the effect of BAPTA buffer over time and space. From the figures, we confirmed that as the value of the buffer increases calcium concentration decrease. Also, it is observed that calcium concentration is dramatically reduced as compared to EGTA buffer due to the association rate of BAPTA buffer.

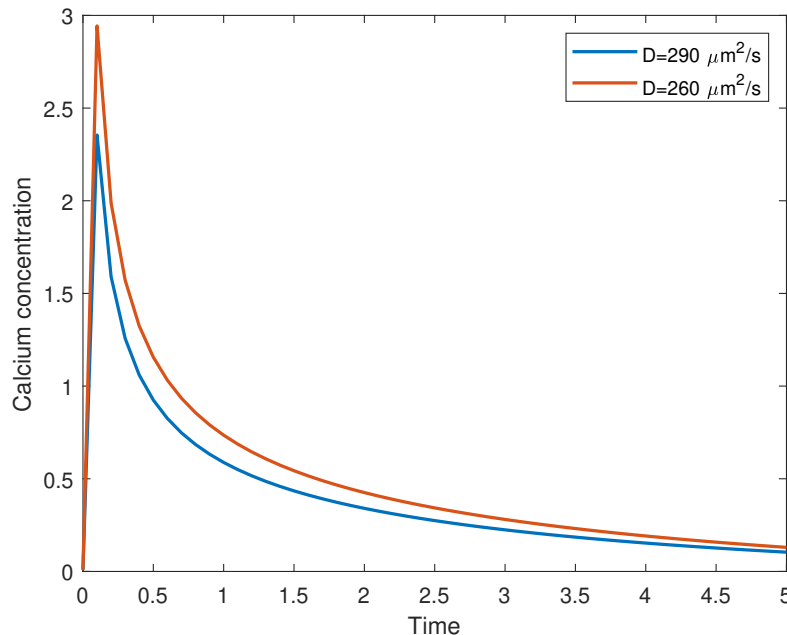


**Figure 7.** Calcium concentration against time for various diffusion coefficient

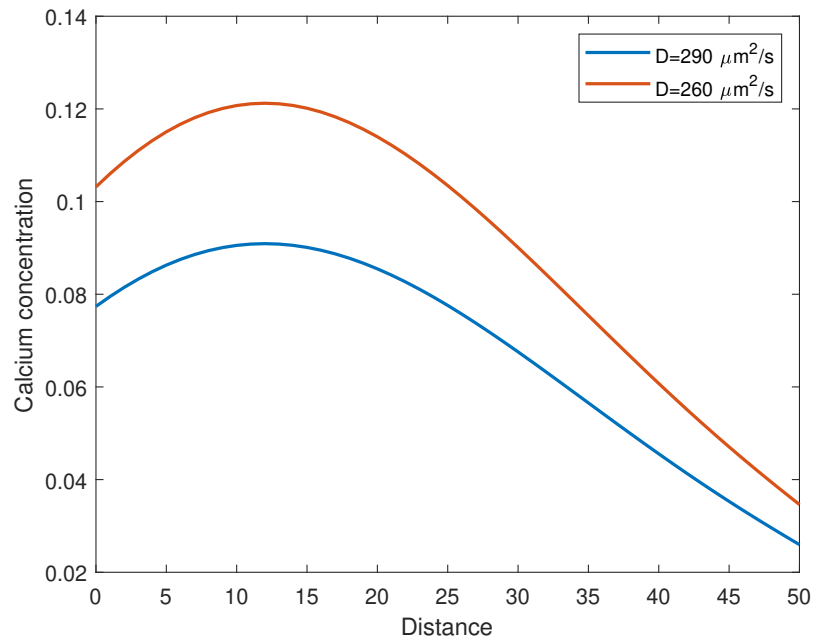


**Figure 8.** Calcium concentration against distance for various diffusion coefficient

Figures 7 and 8 show the calcium concentration in a fibroblast cell against time and space for various diffusion coefficients. From the figures, we confirmed that as the value of diffusion coefficients increases calcium concentration decreases and hence it plays a dual role in the absence of buffer and contributes to managing cellular activities.

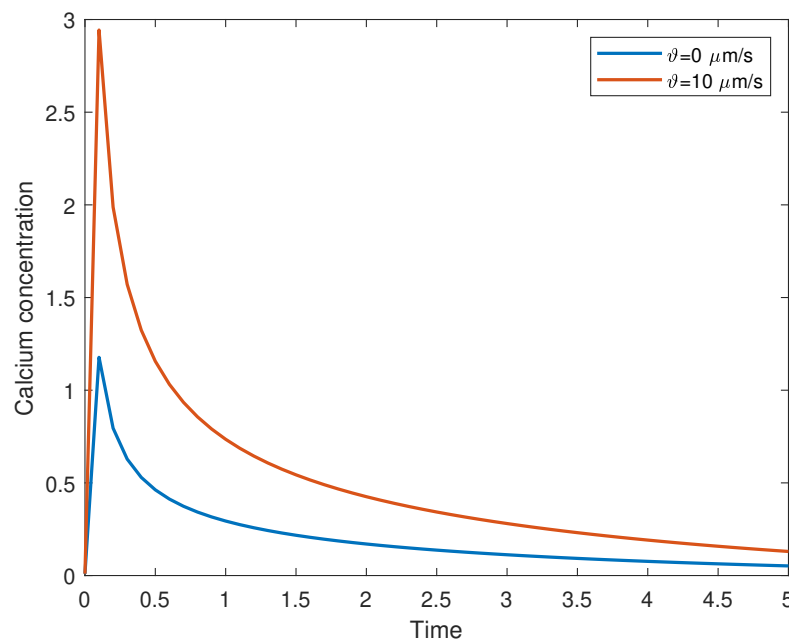


**Figure 9.** Calcium concentration against time for presence and absence of advection flux

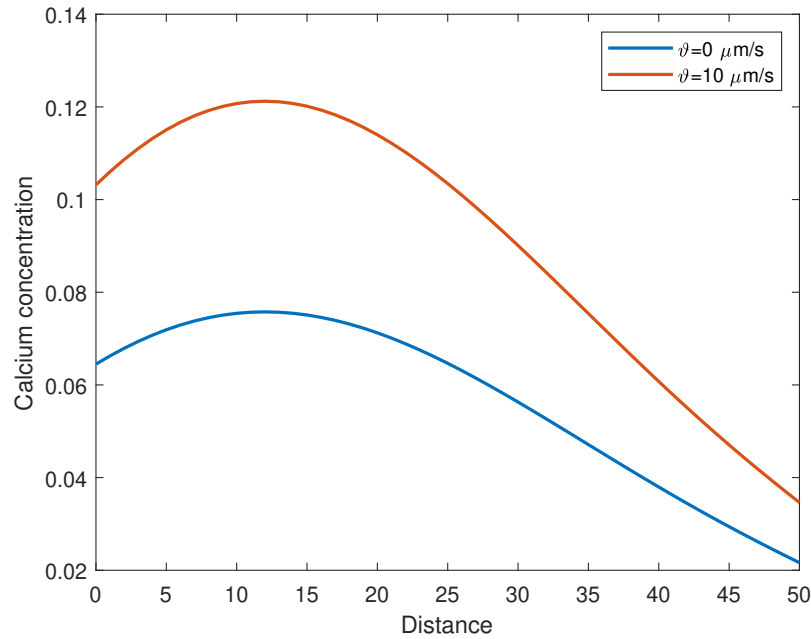


**Figure 10.** Calcium concentration against distance for presence and absence of advection flux

Figures 9 and 10 show the calcium concentration in a fibroblast cell against time and space for the presence and absence of advection flux. From the figures, we confirmed that the presence of flux significantly rise the calcium concentration and is thus involved in cellular activities such as secretion, cell integrity, and so on.

## 5 Conclusion

We analyzed the effect of disturbances in intracellular calcium dynamic on fibroblast cells with the Caputo-Fabrizio advection reaction-diffusion equation. The analytical solution is derived by use of Laplace and Fourier transform techniques. Also, the limiting case of the model is obtained by setting the Caputo-Fabrizio fractional operator to unity. Numerical simulation is presented for various physiological conditions to study calcium diffusion in a fibroblast cell. This approach provides us with a comparably good approximation of the complex geometry of the cell including various biophysical parameters like buffer, diffusion coefficient, and advection flux. The results imply that buffer concentration, the binding affinity of EGTA and BAPTA, the presence and absence of advection flux, and the Caputo-Fabrizio fractional operator has a significant effect on calcium concentration in fibroblast cells. Moreover, the results shown here are in agreement with the physiological facts and hence they play an important role in generating specific calcium concentration patterns necessary for activation, continuation, and termination of fibroblast during wound healing, fibrotic diseases, and cardiovascular disease. Recently, there are many new fractional derivatives introduced such as the generalized fractional derivative known as the Abu-Shady-Kaabar fractional derivative. This fractional derivative can work and obtain the same results as other well-known fractional derivatives in a very simple way. Therefore, it is a good direction for future research works to study the present problem in the sense of the Abu-Shady Kaabar fractional derivative.

## Declarations

### Consent for publication

Not applicable

### Conflicts of interest

The authors declare that they have no conflict of interest.

### Funding

None. No funding to declare.

### Author's contributions

H.J.: Methodology, Writing-Original draft preparation, Software. M.Y.: Investigation, Writing-Reviewing and Editing. I.S.: Visualization, Supervision, Validation. All authors discussed the results and contributed to the final manuscript.

### Acknowledgements

The authors are thankful to the associate editor and referees for their valuable time and suggestions that improved the quality of this manuscript.

### References

- [1] Camelliti, P., Borg, T.K. and Kohl P. Structural and functional characterisation of cardiac fibroblasts. *Cardiovascular Research*, 65(1), 40-51, (2005). [[CrossRef](#)]
- [2] Michailova, A., DelPrincipe, F., Egger, M. and Niggli, E. Spatiotemporal features of  $Ca^{2+}$  buffering and diffusion in atrial cardiac myocytes with inhibited sarcoplasmic reticulum. *Biophysical Journal*, 83(6), 3134–3151, (2002). [[CrossRef](#)]
- [3] Schwaller, B. Cytosolic  $Ca^{2+}$  buffers. *Cold Spring Harbor Perspectives in Biology*, 2(11), a004051, (2010). [[CrossRef](#)]
- [4] Clapham, D.E. Calcium signaling. *Cell*, 131(6), 1047-1058, (2007). [[CrossRef](#)]
- [5] Kotwani, M., Adlakha, N. and Mehta, M.N. Numerical model to study calcium diffusion in fibroblasts cell for one dimensional unsteady state case. *Applied Mathematical Sciences*, 6(102), 5063-5072, (2012).
- [6] Kothiya, A.B. and Adlakha, N. Cellular nitric oxide synthesis is affected by disorders in the interdependent  $Ca^{2+}$  and  $IP_3$  dynamics during cystic fibrosis disease. *Journal of Biological Physics*, (2023). [[CrossRef](#)]
- [7] Joshi, H. and Jha, B.K. Advection diffusion model to study the astrocyte calcium regulation in neurodegenerative disease. *Mathematics in Engineering, Science & Aerospace (MESA)*, 13(2), (2022).
- [8] Jha, B.K., Adlakha, N. and Mehta, M.N. Two-dimensional finite element model to study calcium distribution in astrocytes in presence of excess buffer. *International Journal of Biomathematics*, 7(03), 1450031, (2014). [[CrossRef](#)]
- [9] Jha, B.K., Adlakha, N. and Mehta, M.N. Two-dimensional finite element model to study calcium distribution in astrocytes in presence of VGCC and excess buffer. *International Journal of Modeling, Simulation, and Scientific Computing*, 4(02), 1250030, (2013). [[CrossRef](#)]
- [10] Joshi, H. and Jha, B.K. Modeling the spatiotemporal intracellular calcium dynamics in nerve

- cell with strong memory effects. *International Journal of Nonlinear Sciences and Numerical Simulation*, (2021). [[CrossRef](#)]
- [11] Dave, D.D. and Jha, B.K. Mathematical modeling of calcium oscillatory patterns in a neuron. *Interdisciplinary Sciences: Computational Life Sciences*, 13, 12-24, (2021). [[CrossRef](#)]
- [12] Jha, A. and Adlakha, N. Two-dimensional finite element model to study unsteady state  $Ca^{2+}$  diffusion in neuron involving ER LEAK and SERCA. *International Journal of Biomathematics*, 8(01), 1550002, (2015). [[CrossRef](#)]
- [13] Joshi, H. and Jha, B.K. Generalized diffusion characteristics of calcium model with concentration and memory of cells: A spatiotemporal approach. *Iranian Journal of Science and Technology, Transactions A: Science*, 46, 309-322, (2022). [[CrossRef](#)]
- [14] Jha, A., Adlakha, N. and Jha, B.K. Finite element model to study effect of  $Na^+ - Ca^{2+}$  exchangers and source geometry on calcium dynamics in a neuron cell. *Journal of Mechanics in Medicine and Biology*, 16(02), 1650018, (2016). [[CrossRef](#)]
- [15] Joshi, H. and Jha, B.K. 2D dynamic analysis of the disturbances in the calcium neuronal model and its implications in neurodegenerative disease. *Cognitive Neurodynamics*, (2022). [[CrossRef](#)]
- [16] Joshi, H. and Jha, B.K. 2D memory-based mathematical analysis for the combined impact of calcium influx and efflux on nerve cells. *Computers & Mathematics with Applications*, 134, 33-44, (2023). [[CrossRef](#)]
- [17] Joshi, H. and Jha, B.K. Chaos of calcium diffusion in Parkinson's infectious disease model and treatment mechanism via Hilfer fractional derivative. *Mathematical Modelling and Numerical Simulation with Applications*, 1(2), 84-94, (2021). [[CrossRef](#)]
- [18] Pawar, A. and Pardasani, K.R. Effects of disorders in interdependent calcium and  $IP_3$  dynamics on nitric oxide production in a neuron cell. *The European Physical Journal Plus*, 137(5), 543, (2022). [[CrossRef](#)]
- [19] Pathak, K. and Adlakha, N. Finite element model to study two dimensional unsteady state calcium distribution in cardiac myocytes. *Alexandria Journal of Medicine*, 52(3), 261-268, (2016). [[CrossRef](#)]
- [20] Naik, P.A. and Pardasani, K.R. Finite element model to study calcium signalling in oocyte cell. *International Journal of Modern Mathematical Sciences*, 15(01), 58-71, (2017).
- [21] Naik, P.A. and Pardasani, K.R. Finite element model to study effect of  $Na^+ / K^+$  pump and  $Na^+ / Ca^{2+}$  exchanger on calcium distribution in oocytes in presence of buffers. *Asian Journal of Mathematics and Statistics*, 7(01), 21-28, (2014).
- [22] Naik, P.A. and Zu, J. Modeling and simulation of spatial-temporal calcium distribution in T lymphocyte cell by using a reaction-diffusion equation. *Journal of Bioinformatics and Computational Biology*, 18(02), 2050013, (2020). [[CrossRef](#)]
- [23] Naik, P.A. Modeling the mechanics of calcium regulation in T lymphocyte: a finite element method approach. *International Journal of Biomathematics*, 13(05), 2050038, (2020). [[CrossRef](#)]
- [24] Nakul, N., Mishra, V. and Adlakha, N. Finite volume simulation of calcium distribution in a cholangiocyte cell. *Mathematical Modelling and Numerical Simulation with Applications*, 3(1), 17-32, (2023). [[CrossRef](#)]
- [25] Kilbas, A.A., Marichev, O.I. and Samko, S.G. *Fractional Integrals and Derivatives (Theory and Applications)*, (1993).
- [26] Caputo, M., and Fabrizio, M. A new definition of fractional derivative without singular kernel.

*Progress in Fractional Differentiation and Applications*, 1(2), 73-85, (2015).

- [27] Podlubny I. *Fractional Differential Equations: An Introduction to Fractional Derivatives, Fractional Differential Equations, to Methods of Their Solution and Some of Their Applications* (Vol. 1). Academic Press, Elsevier, (1998).
- [28] Kilbas, A.A., Srivastava, H.M. and Trujillo, J.J. *Theory and Applications of Fractional Differential Equations* (Vol. 204). Elsevier, (2006).
- [29] Atangana, A. and Baleanu, D. New fractional derivatives with nonlocal and non-singular kernel: Theory and application to heat transfer model. *Thermal Science*, 20(2), 763-769, (2016). [[CrossRef](#)]
- [30] Abu-Shady, M. and Kaabar, M.K. A generalized definition of the fractional derivative with applications. *Mathematical Problems in Engineering*, 2021, 9444803, (2021). [[CrossRef](#)]
- [31] Din, A. and Abidin, M.Z. Analysis of fractional-order vaccinated Hepatitis-B epidemic model with Mittag-Leffler kernels. *Mathematical Modelling and Numerical Simulation with Applications*, 2(2), 59-72, (2022). [[CrossRef](#)]
- [32] Ahmad, S., Qiu, D. and ur Rahman, M. Dynamics of a fractional-order COVID-19 model under the nonsingular kernel of Caputo-Fabrizio operator. *Mathematical Modelling and Numerical Simulation with Applications*, 2(4), 228-243, (2022). [[CrossRef](#)]
- [33] Yavuz, M. and Ozdemir, N. Analysis of an epidemic spreading model with exponential decay law. *Mathematical Sciences and Applications E-Notes*, 8(1), 142-154, (2020). [[CrossRef](#)]
- [34] Avci, D., Yavuz, M. and Ozdemir, N. Fundamental solutions to the Cauchy and Dirichlet problems for a heat conduction equation equipped with the Caputo-Fabrizio differentiation. In *Heat Conduction: Methods, Applications and Research* (pp. 95-107). Hauppauge, New York, USA: Nova Science Publishers, (2019).
- [35] Premakumari, R.N., Baishya, C. and Kaabar, M.K. Dynamics of a fractional plankton–fish model under the influence of toxicity, refuge, and combine-harvesting efforts. *Journal of Inequalities and Applications*, 2022, 137, (2022). [[CrossRef](#)]
- [36] Achar, S.J., Baishya, C. and Kaabar, M.K. Dynamics of the worm transmission in wireless sensor network in the framework of fractional derivatives. *Mathematical Methods in the Applied Sciences*, 45(8), 4278-4294, (2022). [[CrossRef](#)]
- [37] Martínez, F. and Kaabar, M.K. A Novel theoretical investigation of the Abu-Shady–Kaabar fractional derivative as a modeling tool for science and engineering. *Computational and Mathematical Methods in Medicine*, 2022, 4119082, (2022). [[CrossRef](#)]
- [38] Losada, J. and Nieto, J.J. Properties of a new fractional derivative without singular kernel. *Progress in Fractional Differentiation and Applications*, 1(2), 87-92, (2015).
- [39] Crank, J. *The Mathematics of Diffusion*. Oxford university press, (1979).
- [40] Smith, G.D. Analytical steady-state solution to the rapid buffering approximation near an open  $Ca^{2+}$  channel. *Biophysical Journal*, 71(6), 3064-3072, (1996).



**Copyright:** © 2023 by the authors. This work is licensed under a Creative Commons Attribution 4.0 (CC BY) International License. The authors retain ownership of the copyright for their article, but they allow anyone to download, reuse, reprint, modify, distribute, and/or copy articles in *BBM*, so long as the original authors and source are credited. To see the complete license contents, please visit (<http://creativecommons.org/licenses/by/4.0/>).

**How to cite this article:** Joshi, H., Yavuz, M. & Stamova, I. (2023). Analysis of the disturbance effect in intracellular calcium dynamic on fibroblast cells with an exponential kernel law. *Bulletin of Biomathematics*, 1(1), 24-39. <https://doi.org/10.59292/bulletinbiomath.2023002>



RESEARCH PAPER

## Numerical investigations and simulation of calcium distribution in the alpha-cell

Tejaswi Singh <sup>1,‡</sup>, Vaishali <sup>1,\*,‡</sup> and Neeru Adlakha <sup>1,‡</sup>

<sup>1</sup>Sardar Vallabhbhai National Institute of Technology, Surat, Gujarat 395007, India

\*Corresponding Author

<sup>‡</sup>ittejaswi@gmail.com (Tejaswi Singh); d20ma002@amhd.svnit.ac.in (Vaishali); nad@amhd.svnit.ac.in (Neeru Adlakha)

### Abstract

The  $\alpha$ -cells are a part of islets of Langerhans located in the pancreas and are responsible for glucagon secretion. Calcium signaling is crucial for the regulation of the functions and structure of these  $\alpha$ -cells and the same is still not well understood. Here a mathematical model is framed to obtain more insights into calcium signaling in  $\alpha$ -cells. The non-linear reaction-diffusion equation for calcium signaling along with boundary conditions is employed to propose the model for a one-dimensional steady-state case. The numerical solutions were obtained using the Newton-Raphson method and the cubic spline method. The combination of Newton-Raphson and cubic spline has proved to be quite effective in numerical simulations and in generating deeper insights into calcium regulation in an  $\alpha$ -cell under various conditions. The results provide information about changes in source influx, buffers, ER leak, and SERCA pump leading to disturbances in calcium homeostasis, which can be responsible for the development of diabetes and other metabolic disorders.

**Keywords:** Cubic spline method; Newton-Raphson method; calcium distribution; ER leak; SERCA

**AMS 2020 Classification:** 92B05; 92C37; 65D07; 34A45

### 1 Introduction

In order to maintain normal physiology and metabolism, calcium homeostasis mechanisms regulate ionized plasma calcium ( $Ca^{2+}$ ) concentration in the human body within a specific range. The cytosolic calcium is kept at a very low-level [1]. The cytosolic calcium level can rise by releasing calcium from intracellular reserves and bringing calcium in from external sources. The calcium level within the  $\alpha$ -cell regulates biophysical processes like the formation and secretion of glucagon hormone [2]. The free calcium level inside the  $\alpha$ -cell is maintained at  $0.1 \mu M$  under resting conditions. The  $\alpha$ -cells have pyramidal shape and size about  $8 \mu m$  in diameter and they appear in groups [3]. Due to the electrically excitable nature, the  $\alpha$ -cells continuously generate overshooting action potentials when the release of glucagon is induced at a low concentration of glucose.

Voltage-gated  $Na^+$  and  $Ca^{2+}$  channels are crucial for the upstroke of action potentials. Voltage-gated  $Ca^{2+}$  channels (VGCCs) are opened by the discharge of high-voltage action potentials allowing extracellular calcium to enter the cytosol. As a result, the number of intracellular calcium rises, which triggers the glucagon granule exocytosis process thereby leading to the fusion of hormone-containing granules with cell membranes and the secretion of the hormones contained inside. Glucagon secretion is inhibited as blood glucose levels rise. This is most likely accomplished via a decrease in the activity of P/Q-type calcium channel of  $\alpha$ -cells and by SERCA pump, which stimulates  $Ca^{2+}$ -sequestration into the ER [4]. In stable conditions, the glucose level lies between 70 to 180  $mg/dl$ , i.e., normoglycemia. If it falls below 70  $mg/dl$ , the body experiences hypoglycemia. The pancreatic  $\alpha$ -cells then secrete glucagon, which causes the liver to release glucose back into the bloodstream, stabilizing its concentration. Contrarily, hyperglycemia occurs when blood sugar levels rise above 180  $mg/dl$ . The pancreatic  $\beta$ -cells then secrete insulin, which causes fatty tissue to absorb glucose to bring the blood sugar level back to normal [5]. A lot of similar secretory machinery has been found in  $\beta$  and  $\alpha$ -cells [6]. Disruptions in these mechanisms are the key factor in the growth of diabetes, which is commonly divided into two categories: Type-1 diabetes and Type-2 diabetes [5].

Many researchers and scientists have developed a variety of mathematical models for studying calcium signaling in different cells like myocytes [7–11], neurons [12–26], astrocytes [27–31], hepatocytes [32–34], fibroblasts [35–38], lymphocytes [39, 40], oocytes [41–48], acinar cells [49–51], dendritic spines [52], etc. In order to understand the kinetics of calcium signaling in endothelial cells, Wiesner et al. [53] constructed a model which gives a mathematical explanation of how calcium affects the ability of the endothelial cell to transmit signals. A mathematical model was created by Handy [27] to investigate the effects of calcium pumps, channels, ER leak, SERCA, and other elements on calcium dynamics in astrocytes. They proposed that modifications to this parameter's ratio had a direct impact on the cytosolic calcium levels in astrocyte cells. The calcium dynamics in a neuron have been examined by Futagi and Kitano [54]. They computationally analyzed the effect of the ryanodine receptor and how it can cause the fluctuation in the calcium profile. Proposing a finite element model, Tewari and Pardasani [19–23] demonstrated calcium distribution in neurons. They considered a number of buffers, including EGTA, BAPTA, Troponin, and Calmodulin for their study. A mathematical model has been created by Jha et al. [28–31] to investigate the calcium advection and diffusion phenomenon in astrocytes. This model includes an advection-diffusion equation, suitable boundary conditions, and physiological factors like diffusion coefficient, buffers and VGCC. To acquire the numerical results, they used the finite element method. Naik and Pardasani [41–46] used the same technique to investigate the calcium distribution in oocyte cells while buffer, VGCC, and receptor were present. Due to these variables, they saw a considerable variation in calcium profiles. Pathak and Adlakha [7–9] investigated the finite element model in order to confirm the physiological mechanism of calcium homeostasis in myocytes by considering factors such as a leak, pump and excess buffer. They discovered that while leaks help to increase calcium concentration, buffers are important to lower it. In recent years, some advancements have also been made by researchers in the field of computational modeling. Joshi and Jha [55, 56] considered the fractional reaction-diffusion equation to study the physiological phenomenon in depth in neurons. Additionally, they expanded their model to a two-dimensional study and correlated the findings with the physiology of neurodegenerative disorders [57, 58].

Nowadays, it is commonly acknowledged that insufficient pancreatic hormone secretion is the major cause of the emergence of diabetes [59]. Impaired insulin profile has been the main topic of study these days. Several computational and theoretical studies have been devoted to the

exocytosis and electrical behavior of  $\beta$ -cell [60, 61], but there is relatively little information available regarding the modeling of the calcium signaling in pancreatic  $\alpha$ -cell. Diderichsen and Gopel [62] established a mathematical model of electrical activity based on the ion channel properties of  $\alpha$ -cells found on the surface of healthy mouse islets in 2006. Additionally, their model was revised by Watts and Sherman [6] in 2014 to include calcium dynamics and secretion. Similar findings of secretion, calcium dynamics and electrical activity were described theoretically by Fridlyand and Philipson [63] in 2012. Exocytosis and secretion were mostly analyzed [6, 62, 63] as an impact of electrical activity, although the primary goal was on the modulation of  $\alpha$ -cell electrical activity. A mathematical model was constructed by Montefusco and Pedersen [64] to test the  $\alpha$ -cells electrical activity modulations that result in glucose administration. They describe the intracellular calcium profile with a focus on simulating calcium concentrations in the microdomains implicated in the release of glucagon. Briant et al. [4] investigated the mechanisms behind metabolic regulation of glucagon secretion of  $\alpha$ -cells with the help of a mathematical model. They also examined the paracrine and intrinsic mechanisms of  $\alpha$ -cells. Brereton et al. [65] in their work concluded that inter-islet communication is restored by both islet architecture and cellular functions. It is also responsible for glucose homeostasis in diabetes. González-Vélez et al. [2] investigated the importance of calcium and glucose maintaining the secretion of glucagon hormone through  $\alpha$ -cells. They also established that the secretion of glucagon is potentiated by calcium variation in comparison to a constant level of intracellular calcium. The model emphasized the exocytosis of  $\alpha$ -cell and gave the tools helping in the study of modulators involved in glucagon secretion. Moede et al. [66], in their research work, gave the relationship of  $\alpha$  and  $\beta$ -cells. Their main focus was the hormones secreted by  $\alpha$ -cells, such as acetylcholine and glucagon. The inter-relationship of  $\alpha$  and  $\beta$ -cells is affected by different architectures of the islet in various species.

From the literature survey, it can be observed that glucagon secretion is responsible for maintaining the glucose level and it depends on the calcium signaling of the cells. Most of the studies found in the literature are based on either the electrical activity of the  $\alpha$ -cells [6, 62, 63] or they describe the metabolic regulation of glucagon secretion theoretically [2, 4]. On the other hand, several attempts have been made to solve the linear form of the reaction-diffusion model for the other cells using different mathematical techniques like FEM and FVM [23, 31, 32, 46]. It has been noted that no attempts have been made to analyze the non-linear calcium distribution involving SERCA pump and ER leak in an  $\alpha$ -cell. Furthermore, little is known about how numerous factors including diffusion, influx, the SERCA pump and ER leak affect calcium signaling in  $\alpha$ -cells. The previous studies on calcium signaling in various cells with the help of the finite element method used linear interpolation functions which required a large number of elements to achieve the desired accuracy. In the present paper, the above-mentioned issues are addressed by developing a mathematical model of calcium signaling in an  $\alpha$ -cell. The non-linear reaction-diffusion equation along with boundary conditions is employed to construct a model in the form of a boundary value problem. The numerical results are calculated by using the combination of the cubic spline method and the Newton-Raphson method. The cubic spline method is employed to obtain an approximation of the field variable in the cell domain. The Newton-Raphson approach has been implemented to effectively obtain the numerical solution of the non-linear equations. The way the study is performed is as follows: the steady state distribution of calcium in an  $\alpha$ -cell is modeled by a non-linear reaction-diffusion equation in Section 2. In Section 3, the calcium profile for various physiological parameters is discussed. Section 4 completes our discussion with conclusions. Finally, in Section 5, the algorithms of the cubic spline method and Newton-Raphson method are given.

## 2 Construction of the mathematical model

The proposed model incorporates two mechanisms of calcium influx due to an ER leak and outflow caused by the SERCA pump. We begin by assuming a single well-mixed pool (like the cytoplasm of the  $\alpha$ -cell) where a bimolecular association interaction of calcium and buffer takes place. The calcium-buffer binding and unbinding equation is given by [67, 68]:



where  $Ca^{2+}$ ,  $B$  and  $CaB$  denote the free calcium, free buffer and calcium-bound buffer respectively. The terms  $k^+$  and  $k^-$  are the rate constants for association and dissociation, respectively.

The required equation for analyzing the calcium regulation in an  $\alpha$ -cell is given as follows [61, 64, 67, 68]:

$$\frac{\partial[Ca^{2+}]}{\partial t} = D_{Ca} \nabla^2 [Ca^{2+}] - k_i^+ [B]_{\infty} ([Ca^{2+}] - [Ca^{2+}]_{\infty}) + J_{leak} - J_{SERCA}, \quad (2)$$

where  $D_{Ca}$  is the diffusion coefficients of free  $Ca^{2+}$  and  $J_{leak}$  and  $J_{SERCA}$  represent the ER leak and SERCA pump flux, respectively and given as follow:

$$J_{leak} = P_{ER} ([Ca^{2+}]_{ER} - [Ca^{2+}]), \quad (3)$$

where  $P_{ER}$  leak permeability out of the ER and  $[Ca^{2+}]_{ER}$  is the free calcium concentration in ER.

$$J_{SERCA} = P_{SERCA}^{max} \frac{[Ca^{2+}]^2}{k_{pump}^2 + [Ca^{2+}]^2}, \quad (4)$$

where  $P_{SERCA}^{max}$  and  $k_{pump}$  are the maximum pumping rate and half maximum pump activity of SERCA pump, respectively [64, 69].

For one-dimensional steady-state case in cartesian coordinates, the equation (2) is given by:

$$\frac{\partial^2 [Ca^{2+}]}{\partial x^2} - \frac{k^+ [B]_{\infty}}{D_{Ca}} ([Ca^{2+}] - [Ca^{2+}]_{\infty}) + \frac{P_{ER}}{D_{Ca}} ([Ca^{2+}]_{ER} - [Ca^{2+}]) - \frac{P_{SERCA}^{max}}{D_{Ca}} \frac{[Ca^{2+}]^2}{k_{pump}^2 + [Ca^{2+}]^2} = 0. \quad (5)$$

The source term of the calcium is assumed at the point  $x=0 \mu m$ , thus the flux boundary is given as follows [68]:

$$\lim_{x \rightarrow 0} \left( -D_{Ca} \frac{\partial [Ca^{2+}]}{\partial x} \right) = \sigma_{Ca}. \quad (6)$$

The other end boundary is assumed at the resting state i.e., the background calcium concentration is assumed at that point and expressed as follows:

$$\lim_{x \rightarrow \infty} [Ca^{2+}] = 0.1 \mu M. \quad (7)$$

Re-writing equation (5), we get:

$$\frac{\partial^2 y}{\partial x^2} - Ay - B \frac{y^2}{k_{pump}^2 + y^2} + C = 0, \quad (8)$$

where

$$A = \frac{k^+[B]_{\infty} + P_{ER}}{D_{Ca}},$$

$$B = \frac{P_{SERCA}^{max}}{D_{Ca}},$$

$$C = \frac{k^+[B]_{\infty}[Ca^{2+}]_{\infty} + P_{ER}[Ca^{2+}]_{ER}}{D_{Ca}},$$

and  $y$  denotes the  $[Ca^{2+}]$ . In past studies, various research workers have used the finite element method with linear interpolation functions. The linear interpolation functions give linear approximation within each subdomain/interval giving a polygonal curve for the field variable as an approximation to a real/smooth curve within the whole domain/cell. Therefore to achieve good approximation the smaller step size is taken to discretize the domain in a larger number of elements/intervals to make a polygonal curve very close to the smooth curve of the field variable in the domain/cell to achieve good accuracy. Here the cell size is very small i.e. few microns. Further, the cubic splines are superior to linear interpolation as it satisfies higher-order continuity conditions to give smooth curves and its order of approximation is higher than the order of approximation of linear interpolation functions. Thus, we have two options to achieve good approximation: (i) Use linear interpolation functions and take a smaller step size to divide the domain into a larger number of intervals/elements or (ii) Use higher order interpolation functions like cubic splines and divide the domain in a smaller number of intervals/elements. The first option requires a larger number of elements which in the case of the nonlinear system becomes very complicated and requires large computational efforts. The second option of using cubic splines requires a smaller number of elements leading to a smaller number of nonlinear equations thereby reducing complications and requiring less computational effort but more mathematical manipulations. Here we use the second option and discretize the cell into eight equal elements to obtain better results by solving a more realistic model. The cubic spline method [70, 71] has been applied to solve the model given by equation (8) and the boundary conditions equation (6) and (7). Thus, equations for the internal nodes are given as follows:

$$\frac{h}{6}N_{j-1} + \frac{2h}{3}N_j + \frac{h}{6}N_{j+1} = \frac{y_{j+1} - 2y_j + y_{j-1}}{h}, \quad (9)$$

where

$$N_j = Ay_j + B \frac{y_j^2}{k_{pump}^2 + y_j^2} - C, \quad (10)$$

where  $j = 1, 2, 3, \dots, 7$  and  $h = x_j - x_{j-1}$ .

Substituting the value of equation (10) in equation (9) and after rearranging, we get:

$$\begin{aligned} & \left( \frac{Ah}{6} - \frac{1}{h} \right) y_{j-1} + 2 \left( \frac{Ah}{3} + \frac{1}{h} \right) y_j + \left( \frac{Ah}{6} - \frac{1}{h} \right) y_{j+1} \\ & + \frac{Bh}{6} \left( \frac{y_{j-1}^2}{k_{pump}^2 + y_{j-1}^2} + 4 \frac{y_j^2}{k_{pump}^2 + y_j^2} + \frac{y_{j+1}^2}{k_{pump}^2 + y_{j+1}^2} \right) - Ch = 0, \end{aligned} \quad (11)$$

where  $j = 1, 2, 3, \dots, 7$ .

Condition for the right boundary is obtained by using equation (7):

$$y_8 - 0.1 = 0. \quad (12)$$

Applying the cubic spline method on equation (6), the condition for the left boundary is given as follows:

$$-\frac{h}{3}N_j - \frac{h}{6}N_{j+1} + \frac{y_{j+1} - y_j}{h} = -\frac{\sigma_{Ca}}{D_{Ca}}, \quad (13)$$

$$N_0 = \frac{3}{h^2}(y_1 - y_0) - \frac{1}{2}N_1 + \frac{3}{h} \frac{\sigma_{Ca}}{D_{Ca}}. \quad (14)$$

Combining equations (11), (12) and (14), a non-linear system of 9 equations has been obtained. A MATLAB program of the Newton-Raphson method for the nonlinear system has been developed to solve the obtained system. In Table 1, biophysical parameters and corresponding numerical data are presented.

**Table 1.** Biophysical parameters and numerical data [64, 68, 69]

Notation	Name of the parameter	Numerical value
$D_{Ca}$	Diffusion Coefficient	$250 \mu m^2/sec$
$K^+$	Association rate of EGTA	$1.5 \mu M/sec$
$B_\infty$	EGTA	$5 \mu M$
$P_{ER}$	Calcium leak permeability of ER	$0.0001 /sec$
$P_{SERCA}^{max}$	Maximum pumping rate of SERCA	$0.105 \mu M/sec$
$k_{pump}$	Half-maximum pumping rate of SERCA	$0.5 \mu M$
$[Ca^{2+}]_\infty$	Cytosolic calcium at rest	$0.1 \mu M$
$[Ca^{2+}]_{ER}$	Calcium concentration in ER	$22.8 \mu M$
$\sigma_{Ca}$	Source influx	$15 pA$

### 3 Results and discussion

The data of the parameters listed in Table 1 were used to compute numerical solutions. The profiles for calcium concentration with respect to space for different conditions have been plotted. Figure 1 depicts the cytosolic calcium of the  $\alpha$ -cell with respect to space. It can be observed from the figure that concentration is initially high near the source influx and then gradually drops as we move away from the source. However, at the other end, it attains its equilibrium value which is  $0.1 \mu M$ . Active pumps and buffers within the  $\alpha$ -cell were the cause of the change in calcium concentration with regard to space.

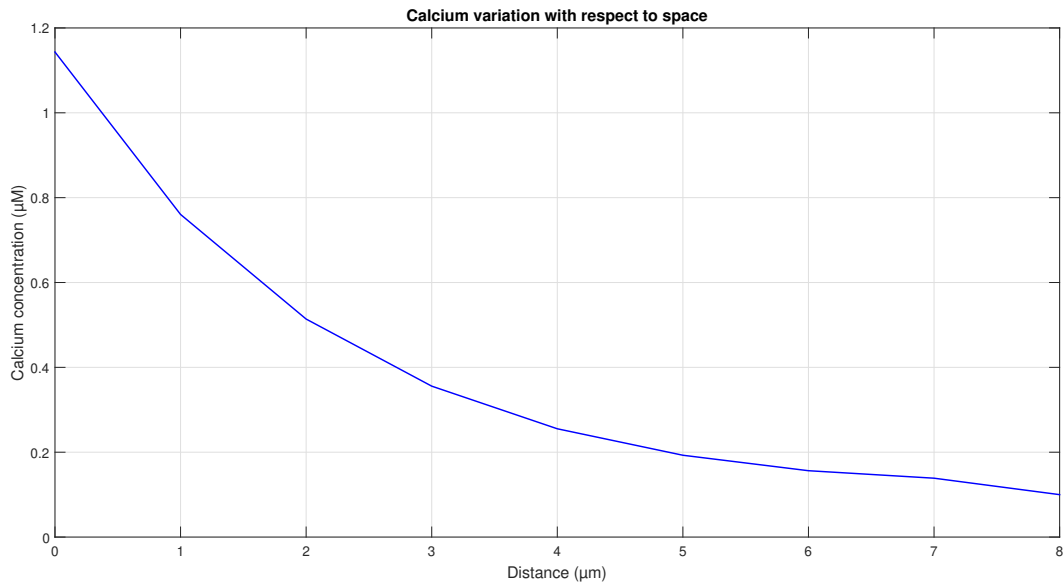


**Figure 1.** Calcium concentration for standard values of parameters given in Table 1

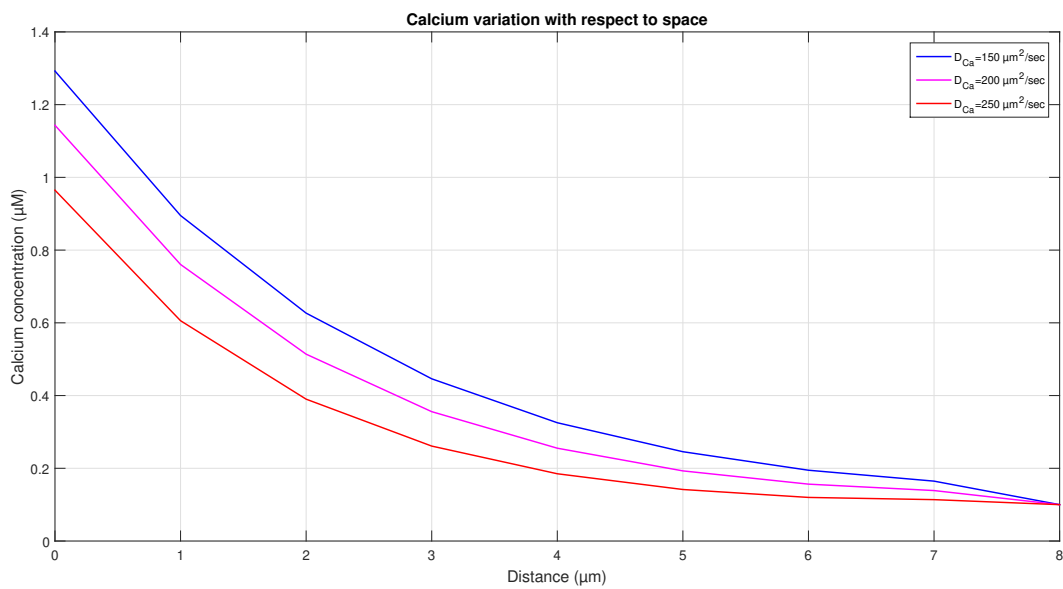


**Figure 2.** Calcium concentration for different values of diffusion coefficients

The spatial variation in calcium concentration as the diffusion coefficient values change from 150 to 200 and 200 to 250  $\mu\text{m}^2/\text{sec}$  is shown in Figure 2. The diffusion coefficient is defined as the amount of diffusing substance moved per unit area per unit of time from one portion of the cell to another. This indicates that calcium ions will flow quickly from the apical to the basal portion of the cell for a larger value of  $D_{Ca}$ . For  $D_{Ca} = 250 \mu\text{m}^2/\text{sec}$ , less free calcium accumulates in the space as more calcium is carried through the cell. Therefore, the concentration of calcium decreases as the magnitude of the diffusion coefficient increases. The amount of free calcium is clearly inversely proportional to the diffusion coefficient, as seen in the graph.

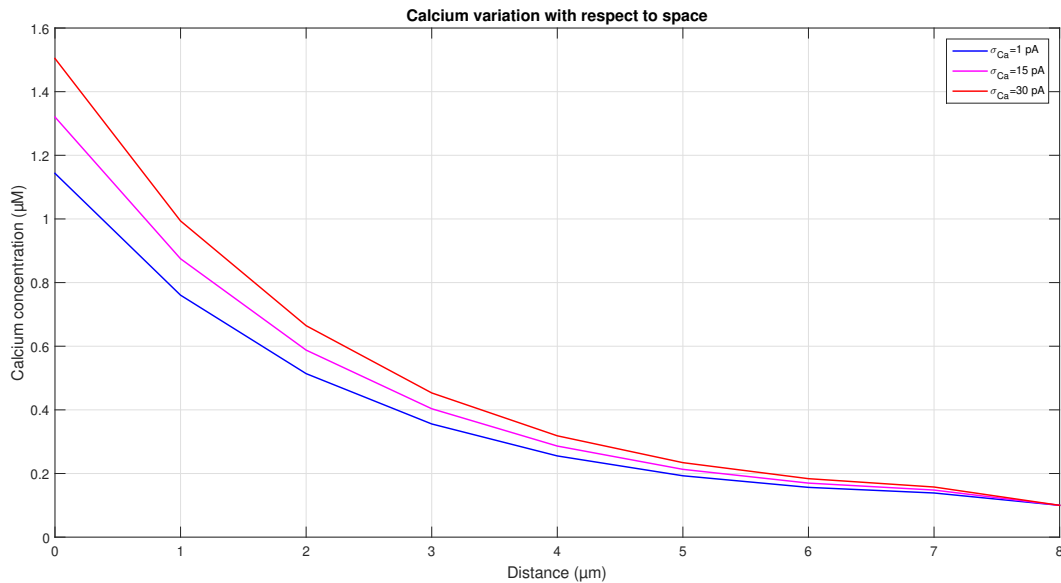
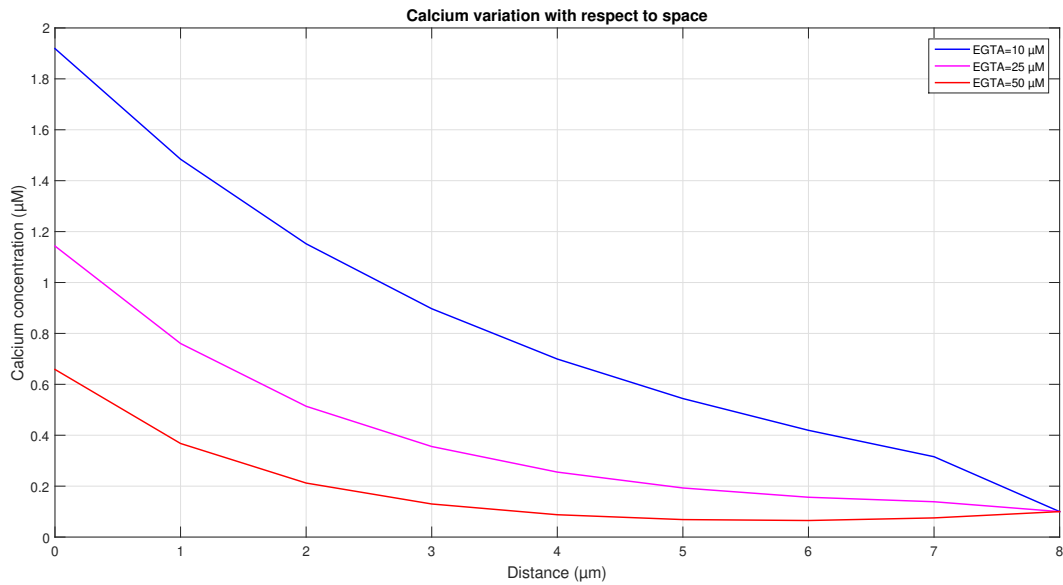


**Figure 3.** Calcium concentration for different values of source influx

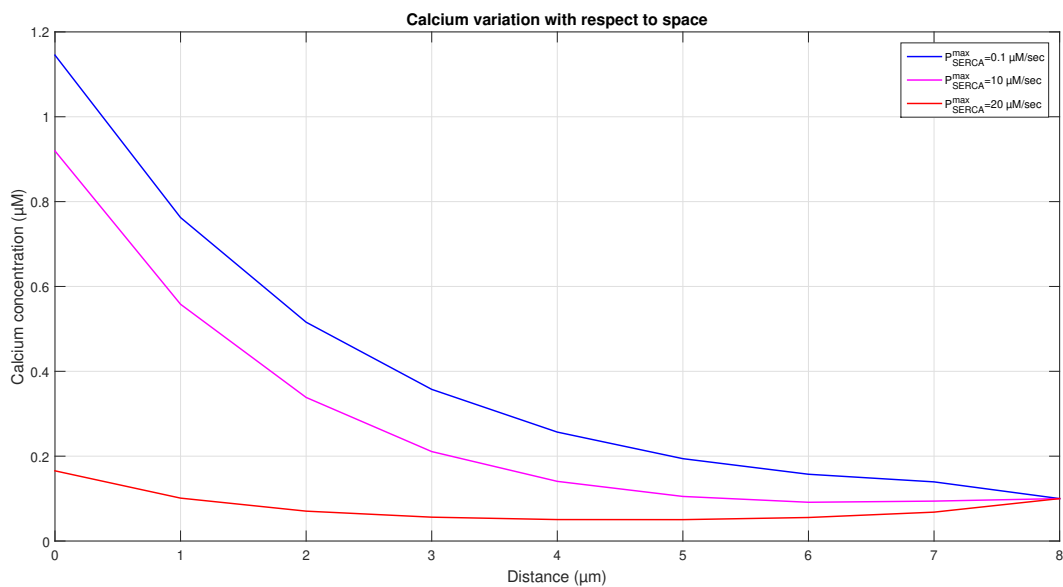
The spatial change in calcium concentration when the value of source amplitude  $\sigma_{Ca}$  is 1, 15 and 30  $pA$  respectively is shown in Figure 3. The unit of characteristic amplitude current passing through a channel is pico amperes ( $pA$ ). The open channel permits ions to pass and is measured as current. As the source amplitude's value increases, more calcium is released into the cytosol. Thus it leads to an increase in the concentration of free calcium. It can be seen from Figure 3 that the concentration of calcium is 1.1, 1.3 and 1.5  $\mu M$  respectively for 1, 15 and 30  $pA$  source amplitude at the mouth of a point source and thereafter it decreases uniformly up to 0.1  $\mu M$ . The appropriate experimental results are still not available for comparison, but however, the outcomes of the suggested model are consistent with biological facts.

Figure 4 represents the spatial change in calcium profile for various EGTA buffer quantities. It can be noticed that different quantities of buffers have different effects on the calcium profile. The maximum calcium concentration occurs for EGTA = 10  $\mu M$  and the minimum calcium concentration occurs for EGTA = 50  $\mu M$ . In all three EGTA buffers above with different quantities, the concentration of calcium decreases with an increase in the concentration of cytosolic buffer inside the  $\alpha$ -cell.

Figure 5 demonstrates the effect of different pumping rates on the calcium concentration inside the  $\alpha$ -cell. The graph shows three different pumping rates. When the pumping rate  $P_{SERCA}^{max}$  is 0.1  $\mu M/\text{sec}$ , the cytosolic calcium is higher and the concentration begins to decline as the pumping rate increases. Calcium concentration also decreases with an increase in the distance of the cell from the source.



**Figure 4.** Calcium concentration for different values of buffer concentration(EGTA buffer)



**Figure 5.** Calcium concentration for different pumping rates of SERCA

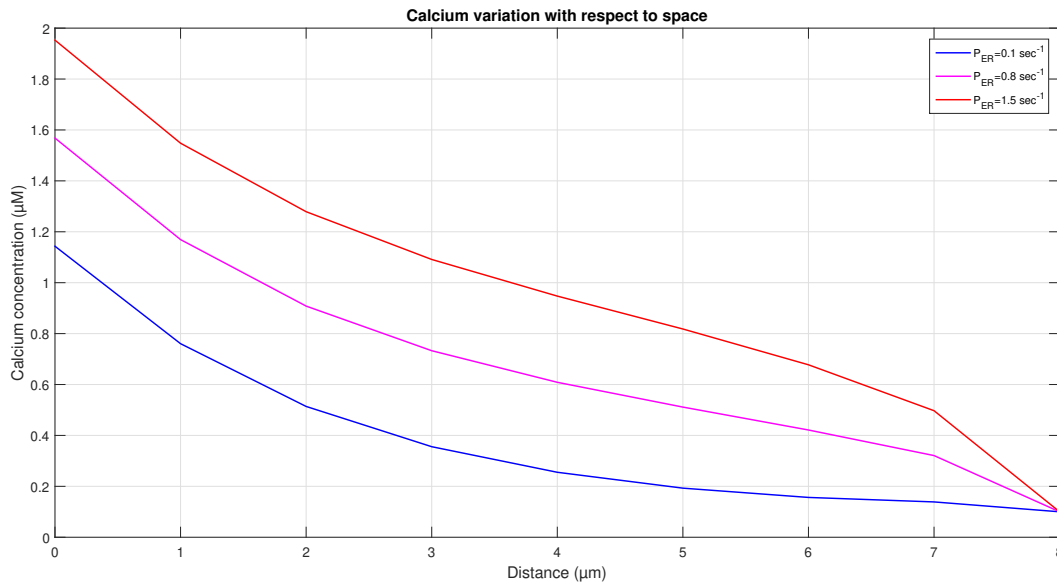


**Figure 6.** Calcium concentration for different values of ER leak

Figure 6 demonstrates the effect of different leak rates ( $P_{ER}$ ). Here with an increase in the distance from the source of the cell, the calcium concentration inside the cell decreases. The gaps observed among the curves in the figure indicate that leak helps in raising the cytosolic calcium with the increase in leak rate. The figure also shows how altering the leak rates causes variations in calcium concentration.

#### 4 Conclusion

A one-dimensional steady-state model for calcium distribution has been proposed and effectively used to examine the roles of different factors like EGTA buffers, source influx, leak, pump, etc. on the cytosolic calcium concentration of the  $\alpha$ -cell. The combination of the cubic spline and Newton-Raphson method has proved to be effective for solving non-linear reaction-diffusion and performing numerical simulations to obtain valuable results. The following conclusions have been drawn:

- i. The buffers and pumps are crucial in lowering calcium levels in an  $\alpha$ -cell.
- ii. The source influx and leak are crucial in raising the calcium concentration in an  $\alpha$ -cell.
- iii. The cell has a beautiful mechanism for balancing this calcium concentration by elevating and reducing mechanisms to regulate the calcium concentration at appropriate levels necessary for normal cell survival.
- iv. The proposed model is the first non-linear spatial model for studying relationships among the parameters like buffers, SERCA pump, ER leak and source influx involved in the calcium homeostasis of an  $\alpha$ -cell.
- v. Combination of cubic spline and Newton-Raphson method is superior as compared to the other methods like finite element method with linear shape functions, as the proposed approach required less number of elements and less amount of computational effort for solving non-linear reaction-diffusion model as compared to the finite element method with linear shape functions and Gauss elimination method used by most of the earlier research workers for solving linear reaction-diffusion model of calcium homeostasis in various other cells.

The proposed model gives better insight into the role of various parameters in regulating calcium

concentration in an  $\alpha$ -cell. This information is crucial in controlling the disorders and diseases caused by the dysfunction of  $\alpha$ -cell like diabetes, etc. The model can be applied in the study of diabetes, as it gives information about the factors involved in calcium regulation of  $\alpha$ -cell. Calcium directly regulates glucagon secretion through  $\alpha$ -cells. So, with the help of the model, it is possible to observe the factors responsible for the disruption of glucagon secretion, which is one of the main factors in regulating the blood glucose level and responsible for the development of diabetes and many other metabolic disorders. The information about the relationships among the various parameters involved in the regulation of calcium level in the  $\alpha$ -cell obtained from the proposed model can be useful for developing a framework for the diagnosis and treatment of various disorders like diabetes, etc. The proposed model and approach can also be extended for its applications in various other cells like neurons, astrocytes, myocytes, oocytes, and  $\beta$ -cells for calcium homeostasis and their respective disorders.

## 5 Appendix

### Cubic spline method

The essential idea for using the cubic spline method is to fit a piecewise function with the help of cubic polynomials:

$$Q(x) = \begin{cases} q_1(x), & x \in [x_1, x_2] \\ q_2(x), & x \in [x_2, x_3] \\ \vdots & \\ q_{n-1}(x), & x \in [x_{n-1}, x_n] \end{cases}, \quad (15)$$

$q_j$ 's denotes the cubic polynomial and is defined as follows:

$$q_j(x) = a_j(x_j - x)^3 + b_j(x_j - x)^2 + c_j(x_j - x) + d_j, \quad (16)$$

for  $j = 1, 2, 3, \dots, n-1$ .

As it is expected that the curve  $Q(x)$  must be continuous across its full interval, it follows that each sub-function must connect at the data points,

$$q_j(x_j) = q_{j-1}(x_j), \quad (17)$$

for  $j = 2, 3, \dots, n$ .

The derivatives at the data points must also be equal in order for the curve to be smooth over the interval; so,

$$q_j'(x_j) = q_{j-1}'(x_j), \quad (18)$$

for  $j = 2, 3, \dots, n$ .

Lastly, since  $q_j''(x)$  has to be continuous across the interval,

$$q_j''(j) = q_{j-1}''(x_j),$$

for  $j = 1, 2, 3, \dots, n-1$ .

After simplifying the above equations (15), (16), (17) and (18), the cubic spline  $Q(x)$  interpolating to the function  $y(x)$  at the knots  $x_j = x_0 + jh$  for  $j = 1, 2, 3, \dots, n-1$  is given in the interval

$x_{j-1} \leq x \leq x_j$  by the equation,

$$Q(x) = N_{j-1} \frac{(x_j - x)^3}{6h} + N_j \frac{(x - x_{j-1})^3}{6h} + \left( y_{j-1} - \frac{h^2}{6} N_{j-1} \right) \frac{(x_j - x)}{h} + \left( y_j - \frac{h^2}{6} N_j \right) \frac{(x - x_{j-1})}{h}, \quad (19)$$

where  $N_j = Q''(x_j)$  and  $y_j = y(x_j)$ .

$$Q'(x_j^+) = -\frac{h}{3} N_j - \frac{h}{6} N_{j+1} + \frac{y_{j+1} - y_j}{h}, \quad (20)$$

for  $j = 0, 1, 2, 3, \dots, n-1$ .

$$Q'(x_j^-) = \frac{h}{3} N_j + \frac{h}{6} N_{j-1} + \frac{y_j - y_{j-1}}{h}, \quad (21)$$

for  $j = 1, 2, 3, \dots, n$ . The continuity of the first derivative implies,

$$\frac{h}{6} N_{j-1} + \frac{2h}{3} N_j + \frac{h}{6} N_{j+1} = \frac{y_{j+1} - 2y_j + y_{j-1}}{h}, \quad (22)$$

where  $j = 1, 2, 3, \dots, n-1$  and  $h = x_j - x_{j-1}$ .

### Newton-Raphson method

Consider a non-linear system of equations,

$$\begin{aligned} f_1(x_1, x_2) &= 0, \\ f_2(x_1, x_2) &= 0. \end{aligned} \quad (23)$$

Let  $x^{(0)} = (x_1^{(0)}, x_2^{(0)})$  be the initial guess to estimate the solution and  $f$  be differentiable at  $x^{(0)}$ . The equation to the tangent plane to the function  $y_i = f_i(x_1, x_2)$  at  $x^{(0)}$  for  $i = 1, 2$  is,

$$y_i - f_i(x^{(0)}) = \frac{\partial}{\partial x_1} [f_i(x^{(0)})] (x_1 - x_1^{(0)}) + \frac{\partial}{\partial x_2} [f_i(x^{(0)})] (x_2 - x_2^{(0)}). \quad (24)$$

The above expression can be written in terms of the Jacobian matrix  $J(x_1^{(0)}, x_2^{(0)})$  as follows:

$$\begin{bmatrix} y_1 - f_1(x^{(0)}) \\ y_2 - f_2(x^{(0)}) \end{bmatrix} = \begin{bmatrix} \frac{\partial}{\partial x_1} [f_1(x^{(0)})] & \frac{\partial}{\partial x_2} [f_1(x^{(0)})] \\ \frac{\partial}{\partial x_1} [f_2(x^{(0)})] & \frac{\partial}{\partial x_2} [f_2(x^{(0)})] \end{bmatrix} \begin{bmatrix} (x_1 - x_1^{(0)}) \\ (x_2 - x_2^{(0)}) \end{bmatrix}. \quad (25)$$

If the given system is expressed as a vector  $V = F(x)$ , then from equation (25);

$$\Delta F \approx J(x_1^{(0)}, x_2^{(0)}) \Delta X. \quad (26)$$

Suppose that  $(p_1, p_2)$  be the solution of equation (23); that is,

$$\begin{aligned} f_1(p_1, p_2) &= 0, \\ f_2(p_1, p_2) &= 0. \end{aligned} \quad (27)$$

To solve the equation (23) using Newton's approach, we must take into account a little change in the function near the coordinates  $(p_1^{(0)}, p_2^{(0)})$ :

$$\begin{aligned}\Delta y_1 &= y_1 - f_1(x^{(0)}), & \Delta x_1 &= (x_1 - p_1^{(0)}), \\ \Delta y_2 &= y_2 - f_2(x^{(0)}), & \Delta x_2 &= (x_2 - p_2^{(0)}).\end{aligned}\tag{28}$$

Set  $(x_1^{(0)}, x_2^{(0)}) = (p_1, p_2)$  in equation (23) and use equation (27) to see that  $(y_1, y_2) = (0, 0)$ . Hence the changes in the dependent variables are:

$$\begin{aligned}y_1 - f_1(x^{(0)}) &= f_1(p_1, p_2) - f_1(p_1^{(0)}, p_2^{(0)}) = 0 - f_1(p_1^{(0)}, p_2^{(0)}), \\ y_2 - f_2(x^{(0)}) &= f_2(p_1, p_2) - f_2(p_1^{(0)}, p_2^{(0)}) = 0 - f_2(p_1^{(0)}, p_2^{(0)}).\end{aligned}\tag{29}$$

Use the result of equation (29) in equation (25) to get the linear transformation,

$$\begin{bmatrix} \frac{\partial}{\partial x_1}[f_1(P_0)] & \frac{\partial}{\partial x_2}[f_1(P_0)] \\ \frac{\partial}{\partial x_1}[f_2(P_0)] & \frac{\partial}{\partial x_2}[f_2(P_0)] \end{bmatrix} \begin{bmatrix} \Delta x_1 \\ \Delta x_2 \end{bmatrix} \approx \begin{bmatrix} f_1(P_0) \\ f_2(P_0) \end{bmatrix},\tag{30}$$

where  $P_0 = (p_1^{(0)}, p_2^{(0)})$ . If the Jacobian  $J(P_0)$  in (30) is nonsingular, we can solve for

$$\Delta P = [\Delta x_1, \Delta x_2]' = [p_1, p_2]' - [p_1^{(0)}, p_2^{(0)}]'$$

as follows:

$$\Delta P \approx J(P_0)^{-1}F(P_0).\tag{31}$$

Then the next approximation  $P_1$  to the solution  $P$  is,

$$P_1 = P_0 + \Delta P = P_0 - J(P_0)^{-1}F(P_0).\tag{32}$$

For a system of  $n$  number of equations, Newton's method can be written by generalizing the equation (30).

## Declarations

### Ethical approval

Not applicable.

### Consent for publication

Not applicable.

### Conflicts of interest

The authors declare that they have no conflict of interest.

### Funding

Not applicable.

## Author's contributions

T.S.: Literature Survey, Writing-Original draft preparation. V.: Conceptualization, Methodology, Investigation. N.A.: Visualization, Supervision, Reviewing and Editing. All authors discussed the results and contributed to the final manuscript.

## Acknowledgements

Not applicable.

## References

- [1] Idevall-Hagren, O. and Tengholm, A. Metabolic regulation of calcium signaling in beta cells. *In Seminars in Cell & Developmental Biology*, (Vol. 103, pp. 20-30), Academic Press, (2020). [[CrossRef](#)]
- [2] Gonzalez-Velez, V., Dupont, G., Gil, A., Gonzalez, A. and Quesada, I. Model for glucagon secretion by pancreatic  $\alpha$  -cells. *PLoS One*, 7(3), e32282, (2012). [[CrossRef](#)]
- [3] Zimny, M.L. and Blackard, W.G. The surface structure of isolated pancreatic islet cells. *Cell and Tissue Research*, 164(4), 467-471, (1975). [[CrossRef](#)]
- [4] Briant, L., Salehi, A., Vergari, E., Zhang, Q. and Rorsman, P. Glucagon secretion from pancreatic  $\alpha$ -cells. *Upsala Journal of Medical Sciences*, 121(2), 113-119, (2016). [[CrossRef](#)]
- [5] Munoz-Balbontin, M. Criticality control of insulin-release. *In Research Student Conference 2018 Faculty of Technology, Design and Environment Oxford Brookes University Ox*, p. 48, (2018).
- [6] Watts, M. and Sherman, A. Modeling the pancreatic  $\alpha$ -cell: dual mechanisms of glucose suppression of glucagon secretion. *Biophysical Journal*, 106(3), 741-751, (2014). [[CrossRef](#)]
- [7] Pathak, K.B. and Adlakha, N. Finite element model to study calcium signalling in cardiac myocytes involving pump, leak and excess buffer. *Journal of Medical Imaging and Health Informatics*, 5(4), 683-688, (2015). [[CrossRef](#)]
- [8] Pathak, K.B. and Adlakha, N. Finite element model to study one dimensional calcium dynamics in cardiac myocytes. *Journal of Multiscale Modelling*, 6(02), 1550003, (2015). [[CrossRef](#)]
- [9] Pathak, K. and Adlakha, N. Finite element model to study two dimensional unsteady state calcium distribution in cardiac myocytes. *Alexandria Journal of Medicine*, 52(3), 261-268, (2016). [[CrossRef](#)]
- [10] Singh, N. and Adlakha, N. A mathematical model for interdependent calcium and inositol 1, 4, 5-trisphosphate in cardiac myocyte. *Network Modeling Analysis in Health Informatics and Bioinformatics*, 8(1), 18, (2019). [[CrossRef](#)]
- [11] Singh, N. and Adlakha, N. Nonlinear dynamic modeling of 2-dimensional interdependent calcium and inositol 1, 4, 5-trisphosphate in cardiac myocyte. *Matematicheskaya Biologiya i Bioinformatika*, 14(1), 290-305, (2019). [[CrossRef](#)]
- [12] Jha, A. and Adlakha, N. Analytical solution of two dimensional unsteady state problem of calcium diffusion in a neuron cell. *Journal of Medical Imaging and Health Informatics*, 4(4), 547-553, (2014). [[CrossRef](#)]
- [13] Jha, A., Adlakha, N. and Jha, B.K. Finite element model to study effect of  $Na^+ - Ca^{2+}$  exchangers and source geometry on calcium dynamics in a neuron cell. *Journal of Mechanics in Medicine and Biology*, 16(02), 1650018, (2016). [[CrossRef](#)]
- [14] Pawar, A. and Pardasani, K.R. Effect of disturbances in neuronal calcium and  $IP_3$  dynamics on  $\beta$ -amyloid production and degradation. *Cognitive Neurodynamics*, 17(1), 239-256, (2023).

[CrossRef]

- [15] Pawar, A. and Raj Pardasani, K. Effects of disorders in interdependent calcium and  $IP_3$  dynamics on nitric oxide production in a neuron cell. *The European Physical Journal Plus*, 137(5), 1-19, (2022). [CrossRef]
- [16] Pawar, A. and Pardasani, K.R. Simulation of disturbances in interdependent calcium and  $\beta$ -amyloid dynamics in the nerve cell. *The European Physical Journal Plus*, 137(8), 1-23, (2022). [CrossRef]
- [17] Pawar, A. and Pardasani, K.R. Study of disorders in regulatory spatiotemporal neurodynamics of calcium and nitric oxide. *Cognitive Neurodynamics*, (2022). [CrossRef]
- [18] Pawar, A. and Pardasani, K.R. Computational model of calcium dynamics-dependent dopamine regulation and dysregulation in a dopaminergic neuron cell. *The European Physical Journal Plus*, 138(1), 30, (2023). [CrossRef]
- [19] Tewari, S. and Pardasani, K.R. Finite difference model to study the effects of  $Na^+$  influx on cytosolic  $Ca^{2+}$  diffusion. *Biological and Medical Sciences*, 1(04), 205-210, (2008).
- [20] Tewari, S. and Pardasani, K.R. Finite element model to study two dimensional unsteady state cytosolic calcium diffusion in presence of excess buffers. *IAENG International Journal of Applied Mathematics*, 40(3), 108-112, (2010).
- [21] Tewari, V., Tewari, S. and Pardasani, K.R. A model to study the effect of excess buffers and  $Na^+$  ions on  $Ca^{2+}$  diffusion in neuron cell. *International Journal of Bioengineering and Life Sciences*, 5(4), 251-256, (2011).
- [22] Tewari, S.G. and Pardasani, K.R. Finite element model to study two dimensional unsteady state cytosolic calcium diffusion. *Journal of Applied Mathematics & Informatics*, 29(1-2), 427-442, (2011).
- [23] Tewari, S.G. and Pardasani, K.R. Modeling effect of sodium pump on calcium oscillations in neuron cells. *Journal of Multiscale Modelling*, 4(03), 1250010, (2012). [CrossRef]
- [24] Tripathi, A. and Adlakha, N. Finite volume model to study calcium diffusion in neuron cell under excess buffer approximation. *International Journal of Mathematical Sciences and Engineering Applications (IJMSEA)*, 5, 437-447, (2011).
- [25] Tripathi, A. and Adlakha, N. Two dimensional coaxial circular elements in FEM to study calcium diffusion in neuron cells. *Applied Mathematical Sciences*, 6(10), 455-466, (2012).
- [26] Tripathi, A. and Adlakha, N. Finite element model to study calcium diffusion in a neuron cell involving J<sub>RyR</sub>, J<sub>Serca</sub> and J<sub>Leak</sub>. *Journal of Applied Mathematics & Informatics*, 31(5-6), 695-709, (2013). [CrossRef]
- [27] Handy, G., Taheri, M., White, J.A. and Borisyyuk, A. Mathematical investigation of  $IP_3$ -dependent calcium dynamics in astrocytes. *Journal of Computational Neuroscience*, 42(3), 257-273, (2017). [CrossRef]
- [28] Jha, B.K., Adlakha, N. and Mehta, M.N. Finite element model to study calcium diffusion in astrocytes. *International Journal of Pure and Applied Mathematics*, 78(7), 945-955, (2012).
- [29] Jha, B.K., Adlakha, N. and Mehta, M.N. Two-dimensional finite element model to study calcium distribution in astrocytes in presence of VGCC and excess buffer. *International Journal of Modeling, Simulation, and Scientific Computing*, 4(02), 1250030, (2013). [CrossRef]
- [30] Jha, B.K., Adlakha, N. and Mehta, M.N. Two-dimensional finite element model to study calcium distribution in astrocytes in presence of excess buffer. *International Journal of Biomathe-*

atics, 7(03), 1450031, (2014). [[CrossRef](#)]

- [31] Jha, B.K., Jha, A. and Adlakha, N. Three-dimensional finite element model to study calcium distribution in astrocytes in presence of VGCC and excess buffer. *Differential Equations and Dynamical Systems*, 28(3), 603-616, (2020). [[CrossRef](#)]
- [32] Jagtap, Y. and Adlakha, N. Finite volume simulation of two dimensional calcium dynamics in a hepatocyte cell involving buffers and fluxes. *Commun. Math. Biol. Neuroscience*, 2018, (2018). [[CrossRef](#)]
- [33] Jagtap, Y.D. and Adlakha, N. Simulation of buffered advection diffusion of calcium in a hepatocyte cell. *Matematicheskaya Biologiya i Bioinformatika*, 13(2), 609-619, (2018). [[CrossRef](#)]
- [34] Jagtap, Y. and Adlakha, N. Numerical study of one-dimensional buffered advection–diffusion of calcium and  $IP_3$  in a hepatocyte cell. *Network Modeling Analysis in Health Informatics and Bioinformatics*, 8(1), 25, (2019). [[CrossRef](#)]
- [35] Kothiya, A. and Adlakha, N. Model of calcium dynamics regulating  $IP_3$  and ATP production in a fibroblast cell. *Advances in Systems Science and Applications*, 22(3), 49-69, (2022). [[CrossRef](#)]
- [36] Kotwani, M., Adlakha, N. and Mehta, M.N. Numerical model to study calcium diffusion in fibroblasts cell for one dimensional unsteady state case. *Applied Mathematical Sciences*, 6(102), 5063-5072, (2012).
- [37] Kotwani, M., Adlakha, N. and Mehta, M.N. Finite element model to study the effect of buffers, source amplitude and source geometry on spatio-temporal calcium distribution in fibroblast cell. *Journal of Medical Imaging and Health Informatics*, 4(6), 840-847, (2014). [[CrossRef](#)]
- [38] Kotwani, M. and Adlakha, N. Modeling of endoplasmic reticulum and plasma membrane  $Ca^{2+}$  uptake and release fluxes with excess buffer approximation (EBA) in fibroblast cell. *International Journal of Computational Materials Science and Engineering*, 6(01), 1750004, (2017). [[CrossRef](#)]
- [39] Bhardwaj, H. and Adlakha, N. Radial basis function based differential quadrature approach to study reaction diffusion of  $Ca^{2+}$  in T lymphocyte. *International Journal of Computational Methods*, (2022). [[CrossRef](#)]
- [40] Naik, P.A. and Zu, J. Modeling and simulation of spatial-temporal calcium distribution in T lymphocyte cell by using a reaction-diffusion equation. *Journal of Bioinformatics and Computational Biology*, 18(02), 2050013, (2020). [[CrossRef](#)]
- [41] Naik, P.A. and Pardasani, K.R. Finite element model to study effect of  $Na^+ / K^+$  pump and  $Na^+ / Ca^{2+}$  exchanger on calcium distribution in oocytes in presence of buffers. *Asian Journal of Mathematics & Statistics*, 7(1), 21, (2014).
- [42] Naik, P.A. and Pardasani, K.R. One dimensional finite element model to study calcium distribution in oocytes in presence of VGCC, RyR and buffers. *Journal of Medical Imaging and Health Informatics*, 5(3), 471-476, (2015). [[CrossRef](#)]
- [43] Naik, P.A. and Pardasani, K.R. Two dimensional finite element model to study calcium distribution in oocytes. *Journal of Multiscale Modelling*, 6(01), 1450002, (2015). [[CrossRef](#)]
- [44] Naik, P.A. and Pardasani, K.R. Finite element model to study calcium distribution in oocytes involving voltage gated  $Ca^{2+}$  channel, ryanodine receptor and buffers. *Alexandria Journal of Medicine*, 52(1), 43-49, (2016). [[CrossRef](#)]
- [45] Naik, P.A. and Pardasani, K.R. 2D finite-element analysis of calcium distribution in oocytes. *Network Modeling Analysis in Health Informatics and Bioinformatics*, 7(1), 1-11, (2018). [[CrossRef](#)]

- [46] Naik, P.A. and Pardasani, K.R. Three-dimensional finite element model to study effect of RyR calcium channel, ER leak and SERCA pump on calcium distribution in oocyte cell. *International Journal of Computational Methods*, 16(01), 1850091, (2019). [[CrossRef](#)]
- [47] Panday, S. and Pardasani, K.R. Finite element model to study effect of advection diffusion and  $Na^+ / Ca^{2+}$  exchanger on  $Ca^{2+}$  distribution in oocytes. *Journal of Medical Imaging and Health Informatics*, 3(3), 374-379, (2013). [[CrossRef](#)]
- [48] Panday, S. and Pardasani, K.R. Finite element model to study the mechanics of calcium regulation in oocyte. *Journal of Mechanics in Medicine and Biology*, 14(02), 1450022, (2014). [[CrossRef](#)]
- [49] Manhas, N. and Pardasani, K.R. Mathematical model to study  $IP_3$  dynamics dependent calcium oscillations in pancreatic acinar cells. *Journal of Medical Imaging and Health Informatics*, 4(6), 874-880, (2014). [[CrossRef](#)]
- [50] Manhas, N. and Pardasani, K.R. Modelling mechanism of calcium oscillations in pancreatic acinar cells. *Journal of Bioenergetics and Biomembranes*, 46, 403-420, (2014). [[CrossRef](#)]
- [51] Manhas, N., Sneyd, J. and Pardasani, K.R. Modelling the transition from simple to complex  $Ca^{2+}$  oscillations in pancreatic acinar cells. *Journal of Biosciences*, 39(3), 463-484, (2014). [[CrossRef](#)]
- [52] Jha, A., & Adlakha, N. Finite element model to study the effect of exogenous buffer on calcium dynamics in dendritic spines. *International Journal of Modeling, Simulation, and Scientific Computing*, 5(02), 1350027, (2014). [[CrossRef](#)]
- [53] Wiesner, T.F., Berk, B.C. and Nerem, R.M. A mathematical model of cytosolic calcium dynamics in human umbilical vein endothelial cells. *American Journal of Physiology-Cell Physiology*, 270(5), C1556-C1569, (1996). [[CrossRef](#)]
- [54] Futagi, D. and Kitano, K. Ryanodine-receptor-driven intracellular calcium dynamics underlying spatial association of synaptic plasticity. *Journal of Computational Neuroscience*, 39(3), 329-347, (2015). [[CrossRef](#)]
- [55] Joshi, H. and Jha, B.K. Fractional reaction diffusion model for Parkinson's disease. In *Proceedings of the International Conference on ISMAC in Computational Vision and Bio-Engineering 2018 (ISMAC-CVB)*, pp. 1739-1748, Springer International Publishing, (2019). [[CrossRef](#)]
- [56] Joshi, H. and Jha, B.K. Chaos of calcium diffusion in Parkinson's infectious disease model and treatment mechanism via Hilfer fractional derivative. *Mathematical Modelling and Numerical Simulation with Applications*, 1(2), 84-94, (2021). [[CrossRef](#)]
- [57] Joshi, H. and Jha, B.K. 2D dynamic analysis of the disturbances in the calcium neuronal model and its implications in neurodegenerative disease. *Cognitive Neurodynamics*, (2022). [[CrossRef](#)]
- [58] Joshi, H. and Jha, B.K. 2D memory-based mathematical analysis for the combined impact of calcium influx and efflux on nerve cells. *Computers & Mathematics with Applications*, 134, 33-44, (2023). [[CrossRef](#)]
- [59] Kahn, S.E., Zraika, S., Utzschneider, K.M. and Hull, R.L. The beta cell lesion in type 2 diabetes: there has to be a primary functional abnormality. *Diabetologia*, 52(6), 1003-1012, (2009). [[CrossRef](#)]
- [60] Bertram, R., Sherman, A. and Satin, L.S. Metabolic and electrical oscillations: partners in controlling pulsatile insulin secretion. *American Journal of Physiology-Endocrinology And Metabolism*, 293(4), E890-E900, (2007). [[CrossRef](#)]
- [61] Pedersen, M.G., Cortese, G. and Eliasson, L. Mathematical modeling and statistical analysis

- of calcium-regulated insulin granule exocytosis in  $\beta$ -cells from mice and humans. *Progress in Biophysics and Molecular Biology*, 107(2), 257-264, (2011). [[CrossRef](#)]
- [62] Diderichsen, P.M. and Göpel, S.O. Modelling the electrical activity of pancreatic  $\alpha$ -cells based on experimental data from intact mouse islets. *Journal of Biological Physics*, 32, 209-229, (2006). [[CrossRef](#)]
- [63] Fridlyand, L.E. and Philipson, L.H. A computational systems analysis of factors regulating  $\alpha$ -cell glucagon secretion. *Islets*, 4(4), 262-283, (2012). [[CrossRef](#)]
- [64] Montefusco, F. and Pedersen, M.G. Mathematical modelling of local calcium and regulated exocytosis during inhibition and stimulation of glucagon secretion from pancreatic alpha cells. *The Journal of Physiology*, 593(20), 4519-4530, (2015). [[CrossRef](#)]
- [65] Brereton, M.F., Vergari, E., Zhang, Q. and Clark, A. Alpha-, delta-and PP-cells: are they the architectural cornerstones of islet structure and co-ordination?. *Journal of Histochemistry & Cytochemistry*, 63(8), 575-591, (2015). [[CrossRef](#)]
- [66] Moede, T., Leibiger, I.B. and Berggren, P.O. Alpha cell regulation of beta cell function. *Diabetologia*, 63(10), 2064-2075, (2020). [[CrossRef](#)]
- [67] Crank, J. *The Mathematics of Diffusion, Second Edition* (Vol. 4). Clarendon Press Oxford, (1975).
- [68] Smith, G.D. Modeling local and global calcium signals using reaction diffusion equations. *Computational neuroscience*, 49-85, (2001).
- [69] Dupont, G., Falcke, M., Kirk, V. and Sneyd, J. *Models of Calcium Signalling* (Vol. 43). Springer: New York, USA, (2016). [[CrossRef](#)]
- [70] Albasiny, E.L. and Hoskins, W.D. Cubic spline solutions to two-point boundary value problems. *The Computer Journal*, 12(2), 151-153, (1969). [[CrossRef](#)]
- [71] McKinley, S., Levine, M. Cubic spline interpolation. *College of the Redwoods*, 45(1), 1049-1060, (1998).

Bulletin of Biomathematics (BBM)  
(<https://bulletinbiomath.org>)



**Copyright:** © 2023 by the authors. This work is licensed under a Creative Commons Attribution 4.0 (CC BY) International License. The authors retain ownership of the copyright for their article, but they allow anyone to download, reuse, reprint, modify, distribute, and/or copy articles in *BBM*, so long as the original authors and source are credited. To see the complete license contents, please visit (<http://creativecommons.org/licenses/by/4.0/>).

**How to cite this article:** Singh, T., Vaishali & Adlakha, N. (2023). Numerical investigations and simulation of calcium distribution in the alpha-cell. *Bulletin of Biomathematics*, 1(1), 40-57. <https://doi.org/10.59292/bulletinbiomath.2023003>

RESEARCH PAPER

# Asymptotic extinction and persistence of a perturbed epidemic model with different intervention measures and standard Lévy jumps

Yassine Sabbar <sup>1,\*</sup> ‡

<sup>1</sup>MAIS Laboratory, MAMCS Group, FST Errachidia, Moulay Ismail University of Meknes, P.O. Box 509, Errachidia 52000, Morocco

\* Corresponding Author

‡ [y.sabbar@umi.ac.ma](mailto:y.sabbar@umi.ac.ma) (Yassine Sabbar)

## Abstract

Controlling an outbreak through response measures is critical to saving lives and protecting vulnerable populations. This article proposes an epidemic model with three intervention measures: media coverage, isolation, and medical therapy. Since randomness plays an important role in biology, from the molecular level to the organismal level, we extend our system to a more realistic framework, which then takes into account the effect of standard jumps due to some sudden environmental changes. After providing the associated framework, the sharp criteria for asymptotic extinction and persistence of illness are derived. To check the accuracy of our results, we perform two numerical examples.

**Keywords:** Epidemic model; isolation; therapy; coverage media; asymptotic analysis; Lévy jumps

**AMS 2020 Classification:** 37A50; 37C10; 92D30

## 1 Introduction

Mathematical modeling is a robust tool for understanding the attitude of infections and assessing the influence of various intervention strategies. In the context of biological modeling, "intervention measures" refer to the implementation of measures to reduce the spread of disease [1]. The most commonly used interventions include social distancing, wearing masks, contact tracing, isolation or quarantine, and hospitalization. To simulate the impact of these interventions, one can use a compartmental model, which divides the population into different compartments based on their infection status [2]. Also, it is possible to introduce parameters that represent the effectiveness of these interventions, such as the reduction in transmission due to social distancing or the effectiveness of a vaccine. By adjusting these parameters, one can simulate the impact of different intervention strategies on the evolution of the illness [3].

Media intervention can play a critical role in shaping public perception, awareness, and behavior during an epidemic. Effective media interventions can help to disseminate accurate information about the disease, promote healthy behaviors, and counter misinformation and rumors [4]. One way that media intervention can have an impact is by increasing knowledge and awareness about the disease. This can be done through the dissemination of accurate and up-to-date information about the disease, its transmission, symptoms, and prevention [5]. By providing clear and concise information, media intervention can help to increase public understanding of the disease and the need for preventive measures. Another way that media intervention can have an impact is by promoting healthy behaviors. During an epidemic, media intervention can be used to encourage individuals to adopt protective behaviors such as hand washing, wearing masks, and social distancing. By promoting these behaviors, media intervention can help to reduce the transmission of the disease and slow the spread of the epidemic. Media intrusion can also help to counter misinformation and rumors that may be circulating during an epidemic. Misinformation can lead to fear, panic, and irrational behavior, which can exacerbate the spread of the disease [6]. By providing accurate information and dispelling rumors, media intervention can help to reduce fear and promote rational decision-making.

Isolation is one of the key measures used to control the spread of an epidemic. It involves separating individuals who are infected with the disease from those who are not infected [7]. Generally, isolation can take different forms, depending on the severity of the epidemic and the resources available. In some cases, isolation may involve self-isolation at home for individuals who have mild symptoms or who have been exposed to the disease. In more severe cases, isolation may involve hospitalization of individuals who are severely ill or at high risk of complications. Isolation is effective for controlling the spread of an epidemic for several reasons [8]. First, it can prevent infected individuals from coming into contact with uninfected individuals, which can reduce the transmission of the disease. By separating infected individuals from others, isolation can help to break the chain of transmission and slow the spread of the disease [9]. Second, isolation can provide medical care and support for individuals who are infected. In some cases, infected individuals may require hospitalization and medical treatment to manage their symptoms and prevent complications. Isolation in a hospital setting can ensure that infected individuals receive the care and treatment they need. Third, isolation can provide time for public health officials to track and monitor the spread of the disease. By isolating infected individuals and tracing their contacts, public health officials can identify and isolate additional cases, which can further reduce the spread of the disease [10].

A hospitalization intervention is a strategy implemented during an epidemic to reduce the number of hospitalizations due to the illness [11]. This can involve various measures, such as increasing hospital capacity, improving triage processes to identify and prioritize the most severe cases, and implementing effective treatments. During an epidemic, hospitalizations can quickly overwhelm healthcare systems, leading to shortages of beds, equipment, and staff [12]. By implementing hospitalization interventions, health-care providers can work to ensure that those most in need receive the care they require, while also preventing the spread of the illness to others. Some examples of hospitalization interventions that may be used during an epidemic include setting up temporary field hospitals to increase capacity, using telemedicine to reduce in-person visits and decrease the risk of transmission, and developing effective treatments and therapies to help patients recover more quickly and avoid hospitalization altogether [13].

The incubation period of an epidemic is the time period between the initial infection with a pathogen and the onset of symptoms of the disease [14]. During this period, the infected individual may be asymptomatic, meaning that they are not yet showing any symptoms of the disease, but they may still be able to transmit the pathogen to others. The length of the incubation period

can vary depending on the pathogen and the individual's immune system [15]. For example, the incubation period for influenza is typically between 1 – 4 days, while the incubation period for COVID-19 can range from 2 – 14 days, with an average of 5 – 6 days. Understanding the incubation period of an epidemic is important for several reasons. First, it can help public health officials to identify and isolate infected individuals before they become symptomatic, which can help to prevent the spread of the disease [16]. Second, it can help to determine the length of time that exposed individuals need to be monitored for symptoms and potential infection. It is important to note that the incubation period is not the same as the infectious period, which is the length of time during which an infected individual can transmit the disease to others. The infectious period can be shorter or longer than the incubation period, depending on the pathogen and the individual's immune system [17].

In order to build a mathematical model that takes into consideration the above interventions and the different types of immunities, we assume that the total population is divided into seven groups of susceptible, exposed, infectious persons with actual viral symptoms, individuals asymptotically infected, isolated, individuals under treatment and persons with full cure, with concentrations expressed respectively by  $S(t)$ ,  $E(t)$ ,  $C(t)$ ,  $I(t)$ ,  $Q(t)$ ,  $Z(t)$  and  $P(t)$ . The epidemiological exchanges between these groups are depicted through the following dynamical system (denoted by SECIQZP):

$$\begin{aligned}
 dS(t) &= \left( \Pi - (m + a)S(t) - S(t)(I(t) + gC(t)) \left( b_1 - \frac{b_2 I(t)}{p + I(t)} \right) + \varepsilon Q(t) \right) dt, \\
 dE(t) &= \left( S(t)(I(t) + gC(t)) \left( b_1 - \frac{b_2 I(t)}{p + I(t)} \right) - (m + \beta)E(t) \right) dt, \\
 dC(t) &= \left( (1 - \vartheta) \beta E(t) - (m + \omega_C + s_C + h_C) C(t) \right) dt, \\
 dI(t) &= \left( \beta \vartheta E(t) - (m + \omega_I + s_I + h_I) I(t) \right) dt, \\
 dQ(t) &= \left( aS(t) - (m + \varepsilon) Q(t) \right) dt, \\
 dZ(t) &= \left( \omega_I I(t) + \omega_C C(t) - (m + s_Z + h_Z) Z(t) \right) dt, \\
 dP(t) &= \left( s_Z Z(t) + s_I I(t) + s_C C(t) - mP(t) \right) dt.
 \end{aligned} \tag{1}$$

The positive parameters of this model are defined as follows:

- $\Pi$  is the recruitment rate of the uninfected (but susceptible) persons that corresponds to normal births and immigration.
- $m$ ,  $h_C$ ,  $h_I$  and  $h_Z$  are denoting, in this order, the normal mortality rate of all individuals and the infection-induced mortality rates affecting only from groups  $C$ ,  $I$  and  $Z$ .
- $a$  and  $\varepsilon$  represent the exchange rates between  $S$  and  $Q$  classes.
- $b_1$  is the standard contamination rate before applying media intervention.  $b_2$  is the extra reduced contact rate under the application of media intrusion such that  $b_1 - b_2$  is positive.  $p$  is the saturation coefficient.
- $0 < g < 1$  is the parameter that ensures the high infectivity of infected individuals.
- $\beta$  is the transfer rate from  $E$  group to  $I$  population with the probability  $0 < \vartheta < 1$  of becoming infectious and  $(1 - \vartheta)$  for entering  $C$  class.
- $\omega_I$  and  $\omega_C$  are respectively the treatment rates  $I$  and  $C$  people.
- $s_Z$ ,  $s_I$  and  $s_C$  are the total cure rates of  $Z$ ,  $I$  and  $C$  people.

To better understand the different transfer rates between classes, we present the diagram shown in Figure 1.

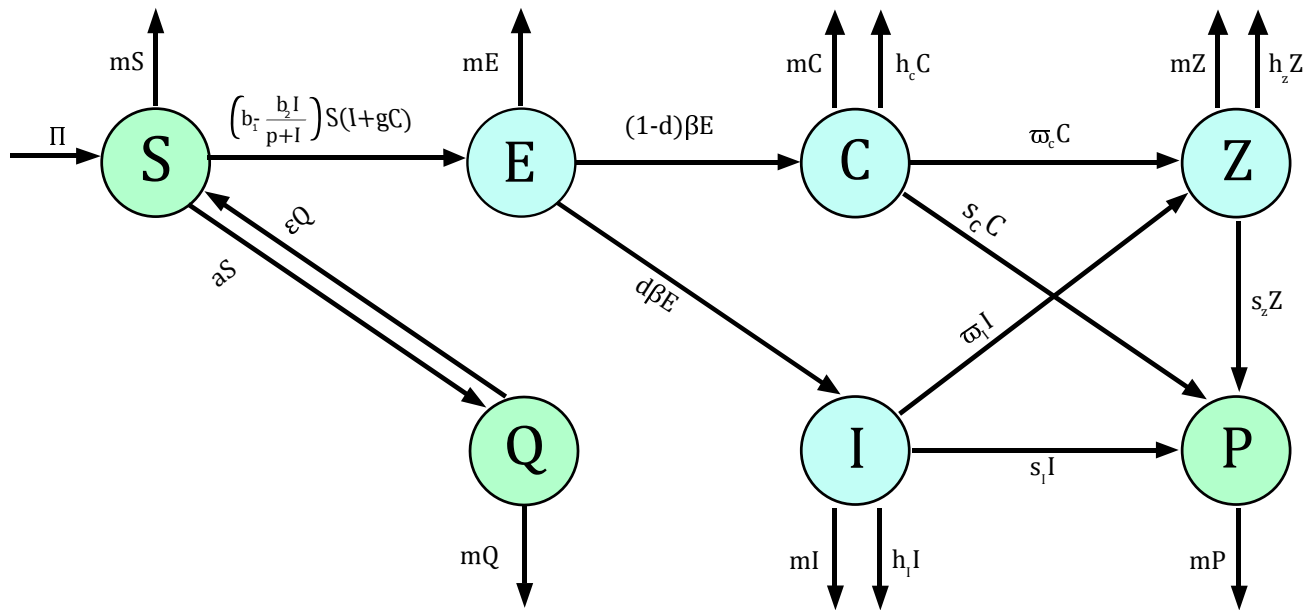


Figure 1. Illustrative diagram of SECIQZP epidemic model transfer rates

Fluctuations are a common feature of epidemic outbreaks, where the number of cases or the transmission rate can vary over time due to various factors such as changes in behavior, public health interventions, or the emergence of new variants of the pathogen [18]. The magnitude and frequency of fluctuations in an epidemic outbreak can depend on a variety of factors, including the mode of transmission, the population demographics, and the effectiveness of control measures. For example, in an outbreak of a highly infectious disease with a short incubation period, fluctuations may be more pronounced due to the rapid spread of the pathogen [19]. To account for fluctuations in epidemic outbreaks, mathematical models are often used to simulate the spread of the disease over time and evaluate the impact of different control measures. These models can help public health officials make informed decisions about when to implement or relax interventions to achieve the optimal balance between controlling the outbreak and minimizing the economic and social costs of control measures [20].

Random jumps are a type of stochastic process where the magnitude of changes in a variable occurs randomly over time [21]. In the context of an epidemic situation, random jumps could refer to sudden and significant increases in the number of cases or spread of the disease that occur unpredictably [22]. In epidemiology, random jumps have been used to model the spread of infectious diseases in populations with complex social structures or mobility patterns, where outbreaks can occur in unpredictable locations or at unpredictable times. Random jumps can also capture the behavior of disease outbreaks that exhibit sudden bursts of activity due to super-spreader events or other factors [23].

The novelty of this study is to probe the impact of jumps on the dynamics of system (1). The pivotal objective of this article is to provide sufficient criteria for asymptotic extinction and persistence. The global threshold is difficult to derive in this model due to its complexity, but we will do our best to offer precise conditions and this is the strength of our study. By considering the standard Lévy jumps associated with the compensated Poisson measure defined on a probabilistic basis

$(\Omega, \mathcal{F}, \{\mathcal{F}_t\}_{t \geq 0}, \mathbb{P})$ , our model takes the following general form:

$$\begin{aligned}
 dS(t) &= \left( \Pi - (\mathfrak{m} + \mathfrak{a})S(t) - S(t) \left( I(t) + gC(t) \right) \left( \mathfrak{b}_1 - \frac{\mathfrak{b}_2 I(t)}{p + I(t)} \right) + \varepsilon Q(t) \right) dt + d\mathbf{L}_1(t), \\
 dE(t) &= \left( S(t) \left( I(t) + gC(t) \right) \left( \mathfrak{b}_1 - \frac{\mathfrak{b}_2 I(t)}{p + I(t)} \right) - (\mathfrak{m} + \beta)E(t) \right) dt + d\mathbf{L}_2(t), \\
 dC(t) &= \left( (1 - \mathfrak{d}) \beta E(t) - (\mathfrak{m} + \omega_C + \mathfrak{s}_C + \mathfrak{h}_C) C(t) \right) dt + d\mathbf{L}_3(t), \\
 dI(t) &= \left( \beta \mathfrak{d} E(t) - (\mathfrak{m} + \omega_I + \mathfrak{s}_I + \mathfrak{h}_I) I(t) \right) dt + d\mathbf{L}_4(t), \\
 dQ(t) &= \left( \mathfrak{a} S(t) - (\mathfrak{m} + \varepsilon) Q(t) \right) dt + d\mathbf{L}_5(t), \\
 dZ(t) &= \left( \omega_I I(t) + \omega_C C(t) - (\mathfrak{m} + \mathfrak{h}_Z + \mathfrak{s}_Z) Z(t) \right) dt + d\mathbf{L}_6(t), \\
 dP(t) &= \left( \mathfrak{s}_Z Z(t) + \mathfrak{s}_I I(t) + \mathfrak{s}_C C(t) - \mathfrak{m} P(t) \right) dt + d\mathbf{L}_7(t),
 \end{aligned} \tag{2}$$

where

$$\begin{aligned}
 d\mathbf{L}_1(t) &= \beta_1 S(t) d\mathbb{X}_1(t) + \int_{\mathcal{Z}} \gamma_1(z) S(t_-) \mathbb{Y}_-(ds, dz), \\
 d\mathbf{L}_2(t) &= \beta_2 E(t) d\mathbb{X}_2(t) + \int_{\mathcal{Z}} \gamma_2(z) E(t_-) \mathbb{Y}_-(ds, dz), \\
 d\mathbf{L}_3(t) &= \beta_3 C(t) d\mathbb{X}_3(t) + \int_{\mathcal{Z}} \gamma_3(z) C(t_-) \mathbb{Y}_-(ds, dz), \\
 d\mathbf{L}_4(t) &= \beta_4 I(t) d\mathbb{X}_4(t) + \int_{\mathcal{Z}} \gamma_4(z) I(t_-) \mathbb{Y}_-(ds, dz), \\
 d\mathbf{L}_5(t) &= \beta_5 Q(t) d\mathbb{X}_5(t) + \int_{\mathcal{Z}} \gamma_5(z) Q(t_-) \mathbb{Y}_-(ds, dz), \\
 d\mathbf{L}_6(t) &= \beta_6 Z(t) d\mathbb{X}_6(t) + \int_{\mathcal{Z}} \gamma_6(z) Z(t_-) \mathbb{Y}_-(ds, dz), \\
 d\mathbf{L}_7(t) &= \beta_7 P(t) d\mathbb{X}_7(t) + \int_{\mathcal{Z}} \gamma_7(z) P(t_-) \mathbb{Y}_-(ds, dz).
 \end{aligned}$$

In this setting,  $\mathbb{X}_\ell$  ( $\ell = 1, \dots, 7$ ), are Wiener processes with positive amplitudes  $\beta_\ell$  ( $i = 1, \dots, 7$ ) respectively.  $\mathbb{Y}_-$  is the compensated Poisson measure associated with a Lévy measure  $\Lambda_+$  defined on  $(\mathbb{R}^7 \setminus \{0\}, \mathcal{B}(\mathbb{R}^7 \setminus \{0\}))$ .  $\gamma_\ell : \mathcal{Z} \subset \mathbb{R}^7 \setminus \{0\} \rightarrow \mathbb{R}$  are measurable functions and  $\gamma_\ell(z) > -1$ .

The organization of the remaining parts is as follows: In Section 2, we present the probabilistic analysis of a perturbed SECIQZP model (2) by offering the associated hypothetical framework and giving the condition of said properties. In Section 3, we numerically check our obtained results. In Section 4, we summarize the main results of our study.

## 2 Stochastic analysis of a perturbed SECIQZP model

### Hypothetical framework

The first step of this section is to clearly define the hypothetical framework of our analysis. This includes the specification of the well-posedness of our perturbed system, the necessary assumptions and the useful techniques. Regarding the underlying assumption, we assume the following:

(A) The quantities  $\int_{\mathcal{Z}} \gamma_k^2(z) \Lambda_+(dz)$  and  $\int_{\mathcal{Z}} \left( \gamma_k(z) - \ln(1 + \gamma_k(z)) \right) \Lambda_+(dz)$  are finite for all  $k \in$

$\{1, \dots, 7\}$ .

Under (A), system (2) is mathematically well-defined and has a unique positive solution [24]. In other words, it is a model that provides a reliable and accurate representation of the biological disease being studied. To derive some large-time estimates of the solution, we need to add a second assumption:

(B) Suppose that for a given  $s > 2$ , we have

$$m - 0.5(s - 1) \left( \beta_1^2 \vee \beta_2^2 \vee \beta_3^2 \vee \beta_4^2 \vee \beta_5^2 \vee \beta_6^2 \vee \beta_7^2 \right) - s^{-1} \mathbf{I}_s(z) > 0,$$

where

$$\begin{aligned} \mathbf{I}_s(z) = \int_{\mathcal{Z}} & \left( \left( 1 + \overbrace{\gamma_1(z) \vee \gamma_2(z) \vee \gamma_3(z) \vee \gamma_4(z) \vee \gamma_5(z) \vee \gamma_6(z) \vee \gamma_7(z)}^{\gamma^*(z)} \right)^s - 1 \right. \\ & \left. - s \left( \underbrace{\gamma_1(z) \wedge \gamma_2(z) \wedge \gamma_3(z) \wedge \gamma_4(z) \wedge \gamma_5(z) \wedge \gamma_6(z) \wedge \gamma_7(z)}_{\gamma_*(z)} \right) \right) \Lambda_+(dz). \end{aligned}$$

**Lemma 1.** Under (B), we have the following properties:

- (a)  $\lim_{t \rightarrow \infty} \frac{y_\ell(t)}{t} = 0 \quad a.s. \quad \forall \ell \in \{1, \dots, 7\}$ .
- (b)  $\lim_{t \rightarrow \infty} \frac{1}{t} \int_0^t y_\ell(s) d\mathbb{X}_\ell(s) = 0 \quad a.s. \quad \forall \ell \in \{1, \dots, 7\}$ .
- (c)  $\lim_{t \rightarrow \infty} \frac{1}{t} \int_0^t \int_{\mathcal{Z}} \gamma_\ell(z) y_\ell(s_-) \mathbb{Y}_-(ds, dz) = 0 \quad a.s. \quad \forall \ell \in \{1, \dots, 7\}$ .

The proof of the above lemma is similar to a previously proven result in [25], it is better to omit the proof in order to avoid redundancy and to streamline the presentation of the argument.

### Asymptotic extinction

Asymptotic extinction refers to the extinction of a species or population due to random, unpredictable events that occur in the environment, rather than gradual, predictable changes. These events may include natural disasters, epidemics, or fluctuations in the availability of resources. It can be difficult to predict or prevent, as it is often influenced by factors beyond human control. However, conservation efforts can help mitigate the effects of stochasticity by protecting habitat and promoting genetic diversity within populations. Theoretically, we can provide sufficient conditions for disease extinction which are provided in the following theorem.

**Theorem 1.** Assume that (A) and (B) hold. Then, we have the following inequality:

$$\limsup_{t \rightarrow \infty} \frac{1}{t} \ln \left( E(t) + C(t) + I(t) \right) \leq b_1 \mathbf{S}^\bullet - m - \frac{1}{6} \left( \beta_2^2 \wedge \beta_3^2 \wedge \beta_4^2 \right) - \tilde{\chi} = Cte \quad a.s.,$$

where  $\mathbf{S}^\bullet = \frac{\Pi}{m} \times \frac{m + \varepsilon}{a + m + \varepsilon}$  and

$$\tilde{\chi} = \int_{\mathcal{Z}} \left\{ \left( \ln(1 + \gamma^*(z)) - \gamma^*(z) \right) \mathbb{1}_{\{\gamma^*(z) \leq 0\}} + \left( \ln(1 + \gamma_*(z)) - \gamma_*(z) \right) \mathbb{1}_{\{\gamma^*(z) > 0\}} \right\} \Lambda_+(dz).$$

More precisely, the asymptotic extinction of a virus occurs when  $Cte < 0$ .

**Proof** By employing the stochastic Itô's formula, we get

$$\begin{aligned} & d \ln (E(t) + C(t) + I(t)) \\ &= \left\{ \frac{1}{E(t) + C(t) + I(t)} \left( S(t) (I(t) + gC(t)) \left( b_1 - b_2 \frac{I(t)}{p + I(t)} \right) \right. \right. \\ &\quad \left. \left. - (\omega_C + s_C + h_C) C(t) - (\omega_I + s_I + h_I) I(t) \right) - m - \frac{\beta_2^2 E^2(t) + \beta_3^2 C^2(t) + \beta_4^2 I^2(t)}{2 (E(t) + C(t) + I(t))^2} \right. \\ &\quad \left. + \int_{\mathcal{Z}} \left\{ \ln \left( 1 + \frac{\gamma_2(z)E(t) + \gamma_3(z)C(t) + \gamma_4(z)I(t)}{E(t) + C(t) + I(t)} \right) - \frac{\gamma_2(z)E(t) + \gamma_3(z)C(t) + \gamma_4(z)I(t)}{E(t) + C(t) + I(t)} \right\} \Lambda_+(dz) \right\} dt \\ &\quad + \frac{1}{E(t) + C(t) + I(t)} \left( \beta_2 E(t) d\mathbb{X}_2(t) + \beta_3 C(t) d\mathbb{X}_3(t) + \beta_4 I(t) d\mathbb{X}_4(t) \right) \\ &\quad + \int_{\mathcal{Z}} \ln \left( 1 + \frac{\gamma_2(z)E(t_-) + \gamma_3(z)C(t_-) + \gamma_4(z)I(t_-)}{E(t_-) + C(t_-) + I(t_-)} \right) \mathbb{Y}_-(dt, dz). \end{aligned}$$

Thanks to the positivity of the solution, we get

$$\begin{aligned} & d \ln (E(t) + C(t) + I(t)) \\ &\leq \left\{ S(t) \left( b_1 - b_2 \frac{I(t)}{p + I(t)} \right) - m - 0.5(\beta_2^2 \wedge \beta_3^2 \wedge \beta_4^2) \times \frac{E^2(t) + C^2(t) + I^2(t)}{(E(t) + C(t) + I(t))^2} \right\} dt \\ &\quad + \int_{\mathcal{Z}} \left\{ \ln \left( 1 + \frac{\gamma_2(z)E(t) + \gamma_3(z)C(t) + \gamma_4(z)I(t)}{E(t) + C(t) + I(t)} \right) - \frac{\gamma_2(z)E(t) + \gamma_3(z)C(t) + \gamma_4(z)I(t)}{E(t) + C(t) + I(t)} \right\} \Lambda_+(dz) dt \\ &\quad + \frac{\beta_2 E(t)}{E(t) + C(t) + I(t)} d\mathbb{X}_2(t) + \beta_4 \frac{C(t)}{E(t) + C(t) + I(t)} d\mathbb{X}_3(t) + \beta_5 \frac{I(t)}{E(t) + C(t) + I(t)} d\mathbb{X}_4(t) \\ &\quad + \int_{\mathcal{Z}} \ln \left( 1 + \frac{\gamma_2(z)E(t_-) + \gamma_3(z)C(t_-) + \gamma_4(z)I(t_-)}{E(t_-) + C(t_-) + I(t_-)} \right) \mathbb{Y}_-(dt, dz). \end{aligned}$$

By employing Cauchy-Schwartz inequality, we get  $E^2(t) + C^2(t) + I^2(t) \geq \frac{1}{3} (E(t) + C(t) + I(t))^2$ .

Furthermore, we can easily check that

$$\int_{\mathcal{Z}} \left\{ \ln \left( 1 + \frac{\gamma_2(z)E(t) + \gamma_3(z)C(t) + \gamma_4(z)I(t)}{E(t) + C(t) + I(t)} \right) - \frac{\gamma_2(z)E(t) + \gamma_3(z)C(t) + \gamma_4(z)I(t)}{E(t) + C(t) + I(t)} \right\} \Lambda_+(dz) \leq -\tilde{\chi}.$$

Consequently,

$$\begin{aligned} d \ln (E(t) + C(t) + I(t)) &\leq \left\{ b_1 S(t) - m - \frac{(\beta_2^2 \wedge \beta_3^2 \wedge \beta_4^2)}{6} - \tilde{\chi} \right\} dt + \frac{\beta_2 E(t)}{E(t) + C(t) + I(t)} d\mathbb{X}_2(t) \\ &\quad + \frac{\beta_3 C(t)}{E(t) + C(t) + I(t)} d\mathbb{X}_3(t) + \frac{\beta_4 I(t)}{E(t) + C(t) + I(t)} d\mathbb{X}_4(t) \quad (3) \\ &\quad + \int_{\mathcal{Z}} \ln \left( 1 + (\gamma_2(z) \vee \gamma_3(z) \vee \gamma_4(z)) \right) \mathbb{Y}_-(dt, dz). \end{aligned}$$

We integrate (3) from 0 to  $t$ , and we divide by  $t$  on both sides, we obtain

$$\begin{aligned}
 \frac{\ln(E(t) + C(t) + I(t))}{t} &\leq \frac{\mathfrak{b}_1}{t} \int_0^t S(s) ds - \mathfrak{m} - \frac{1}{6} (\beta_2^2 \wedge \beta_3^2 \wedge \beta_4^2) - \tilde{\chi} \\
 &+ \frac{\beta_2}{t} \int_0^t \frac{E(s)}{E(s) + C(s) + I(s)} d\mathbb{X}_2(s) + \frac{\beta_3}{t} \int_0^t \frac{C(s)}{E(s) + C(s) + I(s)} dB_3(s) \\
 &+ \frac{\beta_4}{t} \int_0^t \frac{I(s)}{E(s) + C(s) + I(s)} d\mathbb{X}_4(s) + \frac{\ln(E(0) + C(0) + I(0))}{t} \\
 &+ \frac{1}{t} \int_0^t \int_{\mathcal{Z}} \ln(1 + (\gamma_2(z) \vee \gamma_3(z) \vee \gamma_4(z))) \mathbb{Y}_-(ds, dz). \tag{4}
 \end{aligned}$$

Now, we need to estimate  $\frac{1}{t} \int_0^t S(s) ds$ . From (2), we remark that

$$\begin{aligned}
 S(t) &= \Pi t - (\mathfrak{m} + \mathfrak{a}) \int_0^t S(s) ds - \int_0^t S(s) (I(s) + gC(s)) \left( \mathfrak{b}_1 - \frac{\mathfrak{b}_2 I(s)}{p + I(s)} \right) ds + \varepsilon \int_0^t Q(s) ds \\
 &+ \beta_1 \int_0^t S(s) d\mathbb{X}_1(s) + \int_0^t \int_{\mathcal{Z}} \gamma_1(z) S(s_-) \mathbb{Y}_-(ds, dz) + S(0) \\
 &\leq \Pi t - (\mathfrak{m} + \mathfrak{a}) \int_0^t S(s) ds + \varepsilon \int_0^t Q(s) ds + \beta_1 \int_0^t S(s) d\mathbb{X}_1(s) \\
 &+ \int_0^t \int_{\mathcal{Z}} \gamma_1(z) S(s_-) \mathbb{Y}_-(ds, dz) + S(0).
 \end{aligned}$$

Then

$$\begin{aligned}
 \frac{1}{t} \int_0^t S(s) ds &\leq \frac{1}{\mathfrak{m} + \mathfrak{a}} \left( \Pi + \frac{\varepsilon}{t} \int_0^t Q(s) ds + \frac{\beta_1}{t} \int_0^t S(s) d\mathbb{X}_1(s) \right. \\
 &\left. + \frac{1}{t} \int_0^t \int_{\mathcal{Z}} \gamma_1(z) S(s_-) \mathbb{Y}_-(ds, dz) + \frac{S(0)}{t} - \frac{S(t)}{t} \right). \tag{5}
 \end{aligned}$$

Again, we need to estimate  $\frac{1}{t} \int_0^t Q(s) ds$ . From system (2), we have

$$Q(t) = \mathfrak{a} \int_0^t S(s) ds - (\mathfrak{m} + \varepsilon) \int_0^t Q ds + \beta_2 \int_0^t Q(s) d\mathbb{X}_5(s) + \int_0^t \int_{\mathcal{Z}} \gamma_1(z) Q(s_-) \mathbb{Y}_-(ds, dz) + Q(0),$$

which implies that

$$\frac{1}{t} \int_0^t Q(s) ds = \frac{1}{\mathfrak{m} + \varepsilon} \left( \mathfrak{a} \int_0^t S(s) ds + \frac{\beta_5}{t} \int_0^t Q(s) d\mathbb{X}_5(s) + \frac{1}{t} \int_0^t \int_{\mathcal{Z}} \gamma_5(z) Q(s_-) \mathbb{Y}_-(ds, dz) + \frac{Q(0) - Q(t)}{t} \right). \tag{6}$$

Combining (5) with (6) yields

$$\begin{aligned} \frac{1}{t} \int_0^t S(s) \, ds &\leq \frac{1}{m+a} \left\{ \Pi + \varepsilon \left( \frac{a}{(m+\varepsilon)t} \int_0^t S(s) \, ds + \frac{\beta_5}{(m+\varepsilon)t} \int_0^t Q(s) \, d\mathbb{X}_5(s) \right. \right. \\ &\quad \left. \left. + \frac{1}{(m+\varepsilon)t} \int_0^t \int_{\mathcal{Z}} \gamma_5(z) Q(s_-) \mathbb{Y}_-(ds, dz) + \frac{Q(0)}{(m+\varepsilon)t} \right) \right. \\ &\quad \left. + \frac{\beta_1}{t} \int_0^t S(s) \, d\mathbb{X}_1(s) + \frac{1}{t} \int_0^t \int_{\mathcal{Z}} \gamma_1(z) S(s_-) \mathbb{Y}_-(ds, dz) + \frac{S(0)}{t} \right\}. \end{aligned}$$

Thus,

$$\begin{aligned} \frac{1}{t} \int_0^t S(s) \, ds &\leq \frac{\Pi(m+\varepsilon)}{m(a+m+\varepsilon)} + \frac{\varepsilon\beta_2}{m(a+m+\varepsilon)t} \int_0^t Q(s) \, d\mathbb{X}_5(s) + \frac{(m+\varepsilon)\beta_1}{m(m+a+\varepsilon)t} \int_0^t S(s) \, d\mathbb{X}_1(s) \\ &\quad + \frac{\varepsilon}{m(a+m+\varepsilon)t} \int_0^t \int_{\mathcal{Z}} \gamma_5(z) Q(s_-) \mathbb{Y}_-(ds, dz) \\ &\quad + \frac{(m+\varepsilon)}{m(m+a+\varepsilon)t} \int_0^t \int_{\mathcal{Z}} \gamma_1(z) S(s_-) \mathbb{Y}_-(ds, dz) \\ &\quad + \frac{\varepsilon Q(0)}{m(m+a+\varepsilon)t} + \frac{(m+\varepsilon)S(0)}{m(m+a+\varepsilon)t}. \end{aligned} \quad (7)$$

From Lemma 1, we obtain

$$\lim_{t \rightarrow \infty} \frac{1}{t} \int_0^t S(s) \, ds \leq \frac{\Pi}{m} \times \frac{m+\varepsilon}{a+m+\varepsilon} = \mathbf{S}^\bullet. \quad (8)$$

An application direct of the strong law of large numbers for local martingales gives

$$\begin{cases} \lim_{t \rightarrow \infty} \frac{1}{t} \int_0^t \int_{\mathcal{Z}} \ln \left( 1 + (\gamma_2(z) \vee \gamma_3(z) \vee \gamma_4(z)) \right) \mathbb{Y}_-(ds, dz) = 0 \quad \text{a.s.} \\ \lim_{t \rightarrow \infty} \frac{\beta_2}{t} \int_0^t \frac{E(s)}{E(s) + C(s) + I(s)} \, d\mathbb{X}_2(s) = 0 \quad \text{a.s.}, \\ \lim_{t \rightarrow \infty} \frac{\beta_3}{t} \int_0^t \frac{A(s)}{E(s) + C(s) + I(s)} \, d\mathbb{X}_3(s) = 0 \quad \text{a.s.}, \\ \lim_{t \rightarrow \infty} \frac{\beta_4}{t} \int_0^t \frac{I(s)}{E(s) + C(s) + I(s)} \, d\mathbb{X}_4(s) = 0 \quad \text{a.s.} \end{cases} \quad (9)$$

Finally and from results (4), (8) and (9), we conclude that

$$\limsup_{t \rightarrow \infty} \frac{1}{t} \ln \left( E(t) + C(t) + I(t) \right) \leq \mathbf{b}_1 \mathbf{S}^\bullet - m - \frac{1}{6} \left( \beta_2^2 \wedge \beta_3^2 \wedge \beta_4^2 \right) - \tilde{\chi} \quad \text{a.s.}$$

If  $\underline{Cte} < 0$ , then asymptotic extinction will occur fine. ■

**Remark 1.** The positivity of the solution allows us to affirm that  $\lim_{t \rightarrow \infty} E(t) = 0$ ,  $\lim_{t \rightarrow \infty} C(t) = 0$  and  $\lim_{t \rightarrow \infty} I(t) = 0$  a.s. Here the total extinction of the virus is mentioned.

**Corollary 1.** According to the hypothesis and the context of Theorem 1, we get

$$\lim_{t \rightarrow \infty} \frac{1}{t} \int_0^t S(s) ds = \mathbf{S}^\bullet \text{ a.s.}, \quad \lim_{t \rightarrow \infty} \frac{1}{t} \int_0^t Q(s) ds = \mathbf{Q}^\bullet \text{ a.s.}$$

**Proof** From system (2), we obtain

$$\begin{aligned} d(S(t) + E(t)) &= \left\{ \Pi - (\mathbf{m} + \mathbf{a}) S(t) + \varepsilon Q(t) - (\mathbf{m} + \beta) E(t) \right\} dt \\ &\quad + \beta_1 S(t) d\mathbf{X}_1(t) + \int_{\mathcal{Z}} \gamma_1(z) S(t_-) \mathbf{Y}_-(dt, dz) \\ &\quad + \beta_2 E(t) d\mathbf{X}_2(t) + \int_{\mathcal{Z}} \gamma_2(z) E(t_-) \mathbf{Y}_-(dt, dz). \end{aligned} \quad (10)$$

We integrate (10) from 0 to  $t$ , and we divide by  $t$  on both sides, we get

$$\begin{aligned} \frac{1}{t} (S(t) + E(t)) &= \Pi - \frac{(\mathbf{m} + \mathbf{a})}{t} \int_0^t S(s) ds + \frac{\varepsilon}{t} \int_0^t Q(s) ds - \frac{(\mathbf{m} + \beta)}{t} \int_0^t E(s) ds \\ &\quad + \frac{S(0) + E(0)}{t} + \beta_1 \int_0^t S(s) d\mathbf{X}_1(s) + \int_0^t \int_{\mathcal{Z}} \gamma_1(z) S(s_-) \mathbf{Y}_-(ds, dz) \\ &\quad + \beta_2 \int_0^t E(s) d\mathbf{X}_2(s) + \int_0^t \int_{\mathcal{Z}} \gamma_2(z) E(s_-) \mathbf{Y}_-(ds, dz). \end{aligned}$$

From the expression (6), we have

$$\begin{aligned} \frac{1}{t} (S(t) + E(t)) &= \Pi - \frac{(\mathbf{m} + \mathbf{a})}{t} \int_0^t S(s) ds + \frac{\varepsilon}{(\varepsilon + \mathbf{m})t} \left( \mathbf{a} \int_0^t S(s) ds - \frac{Q(t) - Q(0)}{t} \right. \\ &\quad \left. + \frac{\beta_5}{t} \int_0^t Q(s) d\mathbf{X}_5(s) + \int_0^t \int_{\mathcal{Z}} \gamma_5(z) Q(s_-) \mathbf{Y}_-(ds, dz) \right) - \frac{(\mathbf{m} + \beta)}{t} \int_0^t E(s) ds \\ &\quad + \frac{S(0) + E(0)}{t} + \beta_1 \int_0^t S(s) d\mathbf{X}_1(s) + \int_0^t \int_{\mathcal{Z}} \gamma_1(z) S(s_-) \mathbf{Y}_-(ds, dz) \\ &\quad + \beta_2 \int_0^t E(s) d\mathbf{X}_2(s) + \int_0^t \int_{\mathcal{Z}} \gamma_2(z) E(s_-) \mathbf{Y}_-(ds, dz). \end{aligned}$$

Then

$$\begin{aligned} \frac{1}{t} \left( -\frac{\varepsilon \mathbf{a}}{\varepsilon + \mathbf{m}} + \mathbf{m} + \mathbf{a} \right) \int_0^t S(s) ds &= \Pi + \frac{\varepsilon}{\mathbf{m} + \varepsilon} \frac{Q(0) - Q(t)}{t} - \frac{S(t) + E(t)}{t} - \frac{(\mathbf{m} + \beta)}{t} \int_0^t E(s) ds \\ &\quad + \frac{\varepsilon \beta_5}{(\mathbf{m} + \varepsilon)t} \int_0^t Q(s) d\mathbf{X}_5(s) + \frac{\varepsilon}{(\mathbf{m} + \varepsilon)t} \int_0^t \int_{\mathcal{Z}} \gamma_5(z) Q(s_-) \mathbf{Y}_-(ds, dz) \\ &\quad + \frac{S(0) + E(0)}{t} + \frac{\beta_1}{t} \int_0^t S(s) d\mathbf{X}_1(s) + \frac{1}{t} \int_0^t \int_{\mathcal{Z}} \gamma_1(z) S(s_-) \mathbf{Y}_-(ds, dz) \\ &\quad + \frac{\beta_2}{t} \int_0^t E(s) d\mathbf{X}_2(s) + \frac{1}{t} \int_0^t \int_{\mathcal{Z}} \gamma_2(z) E(s_-) \mathbf{Y}_-(ds, dz). \end{aligned}$$

By using Lemma 1, we directly obtain that

$$\lim_{t \rightarrow \infty} \frac{1}{t} \left( -\frac{\varepsilon \alpha}{\varepsilon + m} + m + \alpha \right) \int_0^t S(s) \, ds = \Pi - \lim_{t \rightarrow \infty} \frac{(m + \beta)}{t} \int_0^t E(s) \, ds \quad \text{a.s.},$$

From Remark 1, we indicated that  $\lim_{t \rightarrow \infty} E(t) = 0$  a.s., which implies that  $\lim_{t \rightarrow \infty} \frac{1}{t} \int_0^t E(s) \, ds = 0$  a.s. So

$$\lim_{t \rightarrow \infty} \frac{1}{t} \int_0^t S(s) \, ds = \Pi \left( -\frac{\varepsilon \alpha}{\varepsilon + m} + m + \alpha \right)^{-1} = \frac{\Pi}{m} \times \frac{m + \varepsilon}{\alpha + m + \varepsilon} = \mathbf{S}^\bullet,$$

and

$$\lim_{t \rightarrow \infty} \frac{1}{t} \int_0^t Q(s) \, ds = \frac{q}{(\Pi + m)t} \int_0^t S(s) \, ds - \frac{Q(t)}{(\Pi + m)t} + \frac{Q(0)}{(\Pi + m)t} + \frac{\beta_2}{\Pi + m} \times \frac{1}{t} \int_0^t Q(s) \, dB_2(s).$$

Therefore,

$$\lim_{t \rightarrow \infty} \frac{1}{t} \int_0^t Q(s) \, ds = \frac{\alpha \mathbf{S}^\bullet}{\varepsilon + m} = \mathbf{Q}^\bullet.$$

■

**Remark 2.** From the above results, we can directly infer that

$$\lim_{t \rightarrow \infty} \frac{1}{t} \int_0^t Z(s) \, ds = 0 \text{ a.s.}, \quad \text{and} \quad \lim_{t \rightarrow \infty} \frac{1}{t} \int_0^t P(s) \, ds = 0 \text{ a.s.}$$

### Asymptotic persistence

Asymptotic persistence of a virus refers to the scenario where the infection becomes endemic in a population, meaning that it becomes present at a relatively constant level within that population over time. This can occur when the virus has a low but steady transmission rate, allowing it to continue spreading even when there are no major outbreaks. In this subsection, we give an optimal condition for the continuation of the virus which is presented in the following theorem.

**Theorem 2.** Assume that (A) and (B) hold. If  $f_1(\hat{u}) > f_2 + f_3$ , then we have the following inequality

$$\liminf_{t \rightarrow \infty} \frac{1}{t} \int_0^t (I(s) + C(s)) \, ds \geq \frac{1}{b_1} (f_1(\hat{u}) - f_2 - f_3) = \underline{Cte} \quad \text{a.s.},$$

where

- $f_1(u) = 3 \left( \sqrt[3]{g(1-d)u} + \sqrt[3]{d \times (1-u)} \right) \sqrt[3]{\Pi(b_1 - b_2)} \beta, \quad \forall u \in (0, 1),$
- $f_2 = 7m + \beta + (\omega_C + s_C + h_C) + (\omega_I + s_I + h_I) + (h_Z + s_Z) + |\Pi - \alpha|,$
- $f_3 = \frac{1}{2} \sum_{i=1}^7 \beta_i^2 + \sum_{i=1}^7 \int_{\mathcal{Z}} \left( \gamma_i(z) - \ln(1 + \gamma_i(z)) \right) \Lambda_+(dz),$
- $\hat{u} = \sqrt{g(1-d)} \left( \sqrt{g(1-d)} + \sqrt{d} \right)^{-1}, \quad (0 < \hat{u} < 1).$

More precisely, the asymptotic persistence of a virus occurs when  $\underline{Cte} > 0$ .

**Proof** We define the function  $\widehat{\mathcal{F}}(y) = \sum_{\ell=1}^7 \ln(y_\ell)$ . Direct use of Itô's formula gives

$$\begin{aligned} d\widehat{\mathcal{F}}(y(t)) = & \left\{ \left( \frac{\Pi}{S(t)} - (m + a) - (I(t) + gC(t)) \left( b_1 - \frac{b_2 I(t)}{\vartheta + I(t)} \right) + \frac{\varepsilon Q(t)}{S(t)} \right) \right. \\ & + \left( \frac{S(t)}{E(t)} (I(t) + gC(t)) \left( b_1 - \frac{b_2 I(t)}{\vartheta + I(t)} \right) - (m + \beta) \right) \\ & + \left( (1 - \vartheta) \beta \frac{E(t)}{C(t)} - (m + \omega_C + s_C + h_C) \right) \\ & + \left( \beta \vartheta \frac{E(t)}{I(t)} - (m + \omega_I + s_I + h_I) \right) + \left( a \frac{S(t)}{Q(t)} - (m + \varepsilon) \right) \\ & + \left( \omega_I \frac{I(t)}{Z(t)} + \omega_C \frac{C(t)}{Z(t)} - (m + h_Z + s_Z) \right) + \left( s_Z \frac{Z(t)}{P(t)} + s_I \frac{I(t)}{P(t)} + s_C \frac{C(t)}{P(t)} - m \right) \\ & - 0.5 \sum_{i=1}^7 \beta_i^2 - \sum_{i=1}^7 \int_{\mathcal{Z}} (\gamma_i(z) - \ln(1 + \gamma_i(z))) \Lambda_+(dz) \Big\} dt \\ & + \sum_{i=1}^7 \beta_i dX_i(t) + \sum_{i=1}^7 \int_{\mathcal{Z}} \ln(1 + \gamma_i(z)) Y_-(dt, dz). \end{aligned}$$

Then

$$\begin{aligned} d\widehat{\mathcal{F}}(y(t)) \geq & \left\{ \frac{\Pi}{S(t)} - b_1(I(t) + gC(t)) + (\varepsilon \wedge a) \left( \frac{Q(t)}{S(t)} + \frac{S(t)}{Q(t)} \right) + \frac{S(t)}{E(t)} (b_1 - b_2) (I(t) + gC(t)) \right. \\ & + (1 - \vartheta) \beta \frac{E(t)}{C(t)} + \beta \vartheta \frac{E(t)}{I(t)} - \sum_{i=1}^7 \int_{\mathcal{Z}} (\gamma_i(z) - \ln(1 + \gamma_i(z))) \Lambda_+(dz) \\ & - \left[ 7m + \Pi + a + \beta + (\omega_C + s_C + h_C) + (\omega_I + s_I + h_I) + (h_Z + s_Z) + 0.5 \sum_{i=1}^7 \beta_i^2 \right] \Big\} dt \\ & + \sum_{i=1}^7 \beta_i dX_i(t) + \sum_{i=1}^7 \int_{\mathcal{Z}} \ln(1 + \gamma_i(z)) Y_-(dt, dz). \end{aligned}$$

By remarking that  $2(\Pi \wedge a) = \Pi + a - |\Pi - a|$ ; and  $(S^2(t) + Q^2(t)) \geq 2S(t)Q(t)$ , we get

$$\begin{aligned} d\widehat{\mathcal{F}}(X(t)) \geq & \left( \left[ \frac{(1 - \widehat{u})\Pi}{S(t)} + (b_1 - b_2) \frac{S(t)I(t)}{E(t)} + \beta \vartheta \frac{E(t)}{I(t)} \right] \right. \\ & + \left[ \frac{\widehat{u}\Pi}{S(t)} + g(b_1 - b_2) \frac{S(t)C(t)}{E(t)} + (1 - \vartheta) \beta \frac{E(t)}{C(t)} \right] \\ & \left. - b_1(I + gC(t)) - f_2 - f_3 \right) dt + \sum_{i=1}^7 \beta_i dX_i(t) + \sum_{i=1}^7 \int_{\mathcal{Z}} \ln(1 + \gamma_i(z)) Y_-(dt, dz). \end{aligned}$$

By employing the arithmetic-geometric inequality, we directly obtain

$$\begin{aligned}
 d\widehat{\mathcal{F}}(X(t)) &\geq \left( 3\sqrt[3]{(1-\widehat{u})\Pi(b_1-b_2)\beta\delta} + 3\sqrt[3]{\widehat{u}\Pi(b_1-b_2)g\beta(1-\delta)} - b_1(I+gC(t)) - f_2 - f_3 \right) dt \\
 &\quad + \sum_{i=1}^7 \beta_i d\mathbb{X}_i(t) + \sum_{i=1}^7 \int_{\mathcal{Z}} \ln(1+\gamma_i(z)) \mathbb{Y}_-(dt, dz) \\
 &\geq \left( (f_1(\widehat{u}) - f_2 - f_3) - b_1(I+gC(t)) \right) dt \\
 &\quad + \sum_{i=1}^7 \beta_i d\mathbb{X}_i(t) + \sum_{i=1}^7 \int_{\mathcal{Z}} \ln(1+\gamma_i(z)) \mathbb{Y}_-(dt, dz).
 \end{aligned} \tag{11}$$

An integration from 0 to  $t$  on both sides of (11) leads to

$$\begin{aligned}
 \frac{1}{t} \left( \widehat{\mathcal{F}}(y(t)) - \widehat{\mathcal{F}}(y(0)) \right) &\geq (f_1(\widehat{u}) - f_2 - f_3) - \frac{b_1}{t} \int_0^t (I(s) + gC(s)) ds \\
 &\quad + \frac{1}{t} \sum_{i=1}^7 \beta_i \mathbb{X}_i(t) + \frac{1}{t} \sum_{i=1}^7 \int_0^t \int_{\mathcal{Z}} \ln(1+\gamma_i(z)) \mathbb{Y}_-(dt, dz).
 \end{aligned}$$

Hence,

$$\begin{aligned}
 \frac{1}{t} \int_0^t (I(s) + C(s)) ds &\geq \int_0^t (I(s) + gC(s)) ds \geq \frac{1}{b_1} \left( \frac{\widehat{\mathcal{F}}(X(0)) - \widehat{\mathcal{F}}(X(t))}{t} + (f_1(\widehat{u}) - f_2 - f_3) \right) \\
 &\quad + \frac{1}{t} \sum_{i=1}^7 \int_0^t \int_{\mathcal{Z}} \ln(1+\gamma_i(z)) \mathbb{Y}_-(dt, dz).
 \end{aligned}$$

Thanks to the strong law of large numbers for local martingales and Lemma 1, we finally get

$$\liminf_{t \rightarrow \infty} \frac{1}{t} \int_0^t (I(s) + C(s)) ds \geq \frac{1}{b_1} (f_1(\widehat{u}) - f_2 - f_3) = \underline{Cte} \quad \text{a.s.}$$

If  $Cte > 0$ , then asymptotic persistence will occur almost surely. That is to say that all classes of the population persist in the mean. ■

**Remark 3.** *In the context of a disease, persistence in the mean refers to the tendency of the disease incidence or prevalence to revert back to its long-term average over time. This means that if the incidence or prevalence of a disease is higher (or lower) than its long-term average in one period, it is likely to be closer to the average in the next period.*

### 3 Numerical verification

A numerical verification of theoretical results involves using computational methods to simulate a mathematical model or theory and comparing the simulation results to the analytical predictions. This process helps to validate the theoretical results and to gain a better understanding of the underlying phenomena. For this reason, we present the following two examples in order to validate the outcomes of Theorems 1 and 2.

### Example 1: Asymptotic extinction

We consider the following initial data:

$$(S(0), E(0), C(0), I(0), Q(0), Z(0), P(t)) = (3, 1.6, 1.2, 1.3, 1.8, 0, 5, 0.2).$$

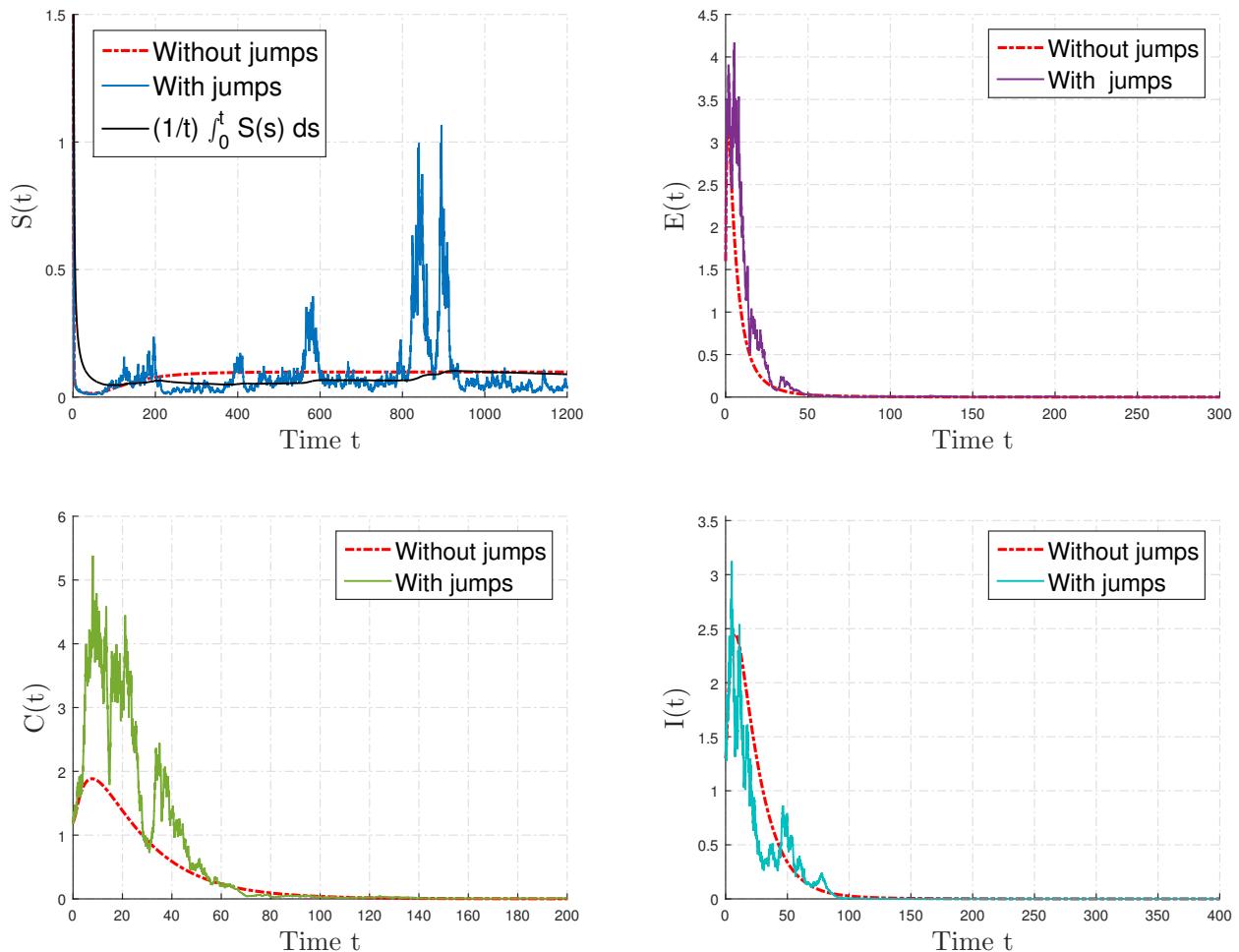
For deterministic parameters, we select  $\Pi = 0.01$ ,  $m = 0.014$ ,  $h_C = 0.0005$ ,  $h_I = 0.0008$ ,  $h_Z = 0.004$ ,  $\alpha = 0.1003$ ,  $\epsilon = 0.071$ ,  $b_1 = 1.2$ ,  $b_2 = 0.1$ ,  $p = 0.71$ ,  $g = 0.0594$ ,  $\beta = 0.6201$ ,  $\nu = 0.2$ ,  $\omega_I = 0.033$ ,  $\omega_C = 0.024$ ,  $s_Z = 0.02$ ,  $s_I = 0.0183$  and  $s_C = 0.0139$ . For stochastic parameters, we select  $\beta_\ell = 0.25$  and  $\gamma_\ell = 0.12$ . Then

$$m - 0.5(s - 1) (\beta_1^2 \vee \beta_2^2 \vee \beta_3^2 \vee \beta_4^2 \vee \beta_5^2 \vee \beta_6^2 \vee \beta_7^2) - s^{-1} \mathbf{I}_s(z) = 0.00145 > 0,$$

and

$$\limsup_{t \rightarrow \infty} \frac{1}{t} \ln (E(t) + C(t) + I(t)) \leq b_1 \mathbf{S}^\bullet - m - \frac{1}{6} (\beta_2^2 \wedge \beta_3^2 \wedge \beta_4^2) - \tilde{\chi} = -0.0075 < 0.$$

Consequently, the conditions of Theorem 1 are verified and the infection will asymptotically extinct (see Figure 2).



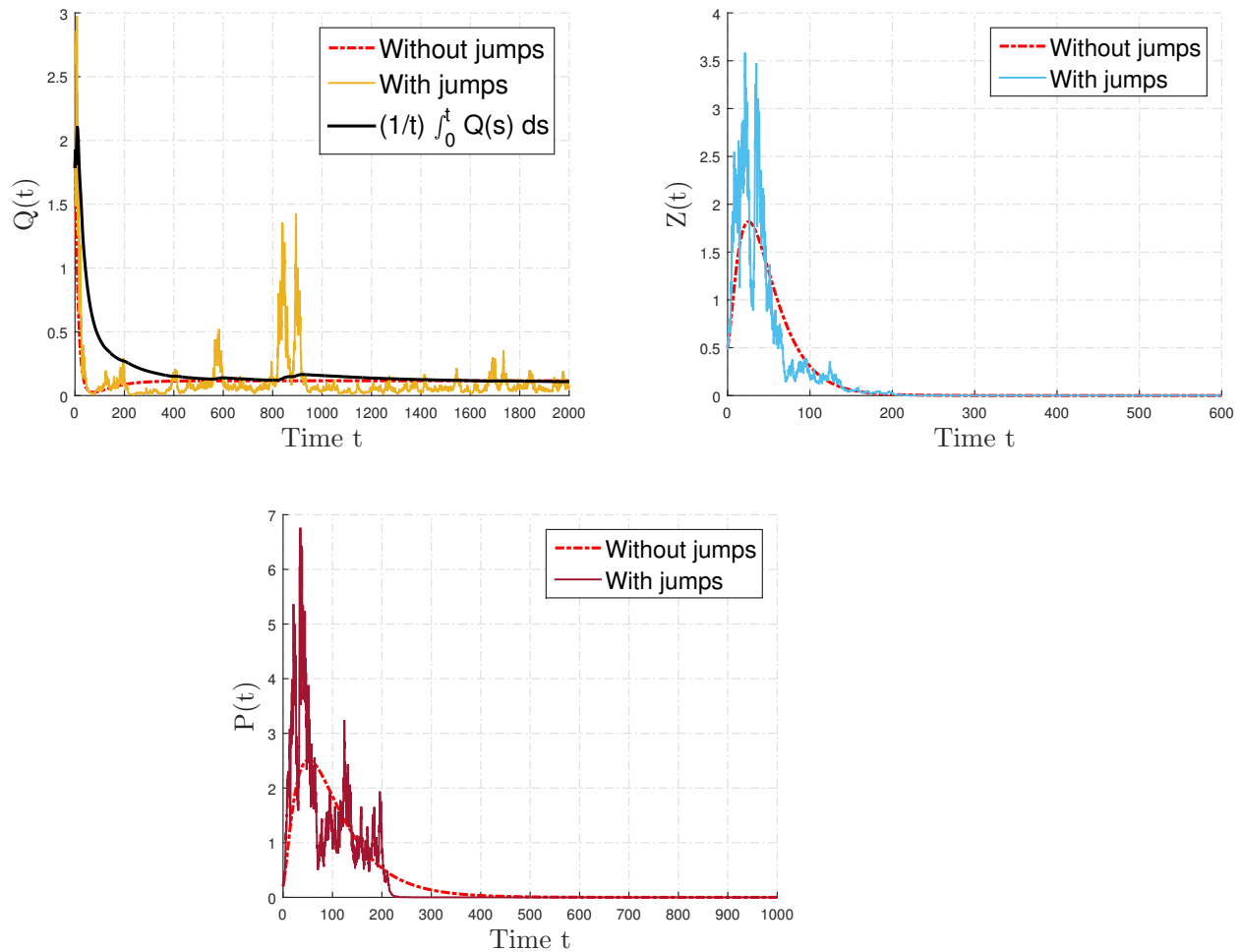


Figure 2. Random paths of perturbed model (2) in the case of asymptotic extinction

### Example 2: Asymptotic persistence

We consider the following initial data:

$$\left( S(0), E(0), C(0), I(0), Q(0), Z(0), P(t) \right) = \left( 3, 1.6, 1.2, 1.3, 1.8, 0, 5, 0.2 \right).$$

For deterministic parameters, we select  $\Pi = 0.04$ ,  $m = 0.014$ ,  $h_C = 0.0005$ ,  $h_I = 0.0008$ ,  $h_Z = 0.004$ ,  $\alpha = 0.1003$ ,  $\varepsilon = 0.071$ ,  $b_1 = 1.2$ ,  $b_2 = 0.1$ ,  $p = 0.71$ ,  $g = 0.0594$ ,  $\beta = 0.6201$ ,  $\nu = 0.2$ ,  $\omega_I = 0.033$ ,  $\omega_C = 0.024$ ,  $s_Z = 0.02$ ,  $s_I = 0.0183$  and  $s_C = 0.0139$ . For stochastic parameters, we select  $\beta_\ell = 0.15$  and  $\gamma_\ell = 0.08$ . Then  $f_1(\hat{u}) = 0.145 > f_2 + f_3 = 0.0378$ , and

$$\liminf_{t \rightarrow \infty} \frac{1}{t} \int_0^t \left( I(s) + C(s) \right) ds \geq \frac{1}{b_1} (f_1(\hat{u}) - f_2 - f_3) = 0.0893 > 0.$$

From Figure 4, we confirm the result of Theorem 1. Therefore, all model classes persist almost surely, which are shown in Figures 3 and 4.

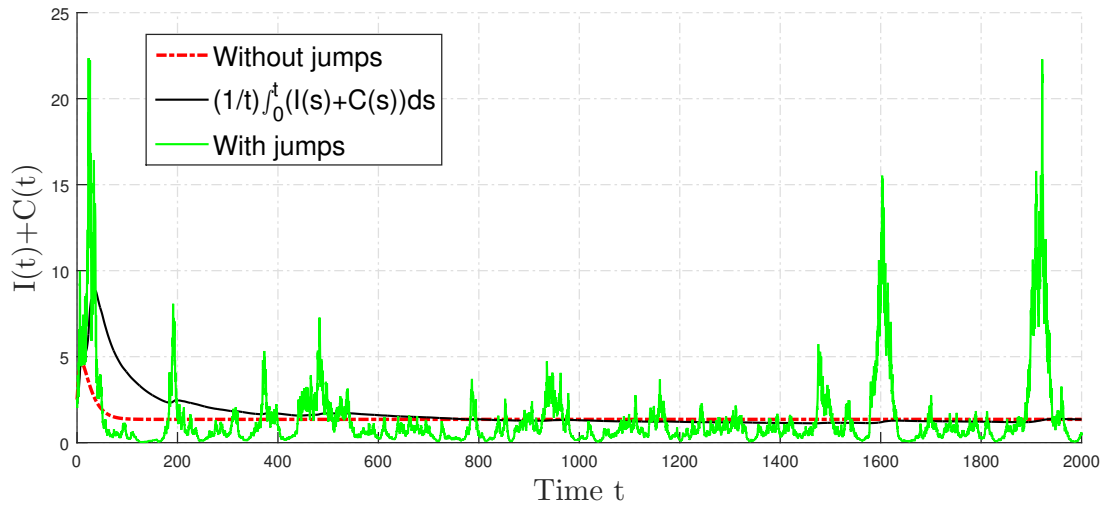
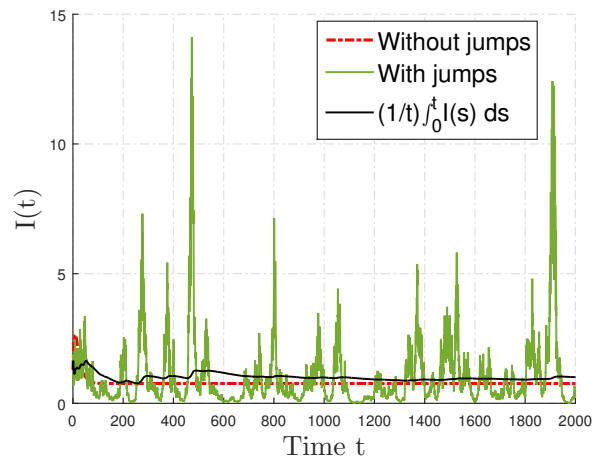
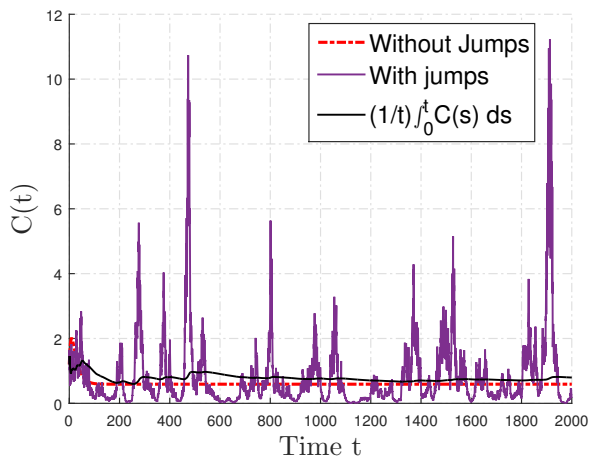
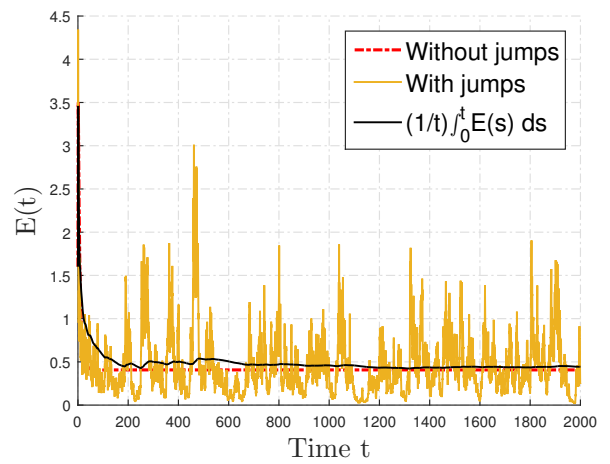
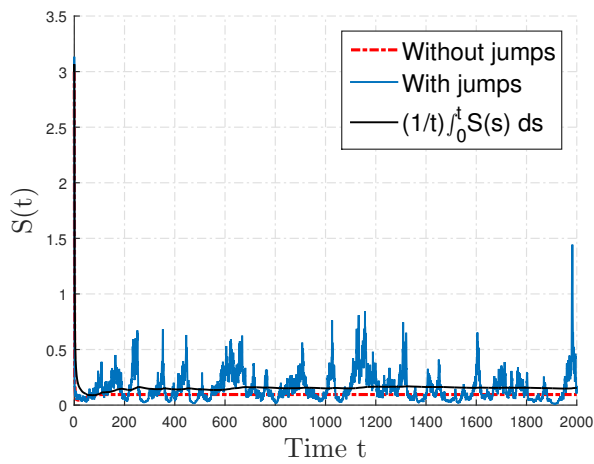
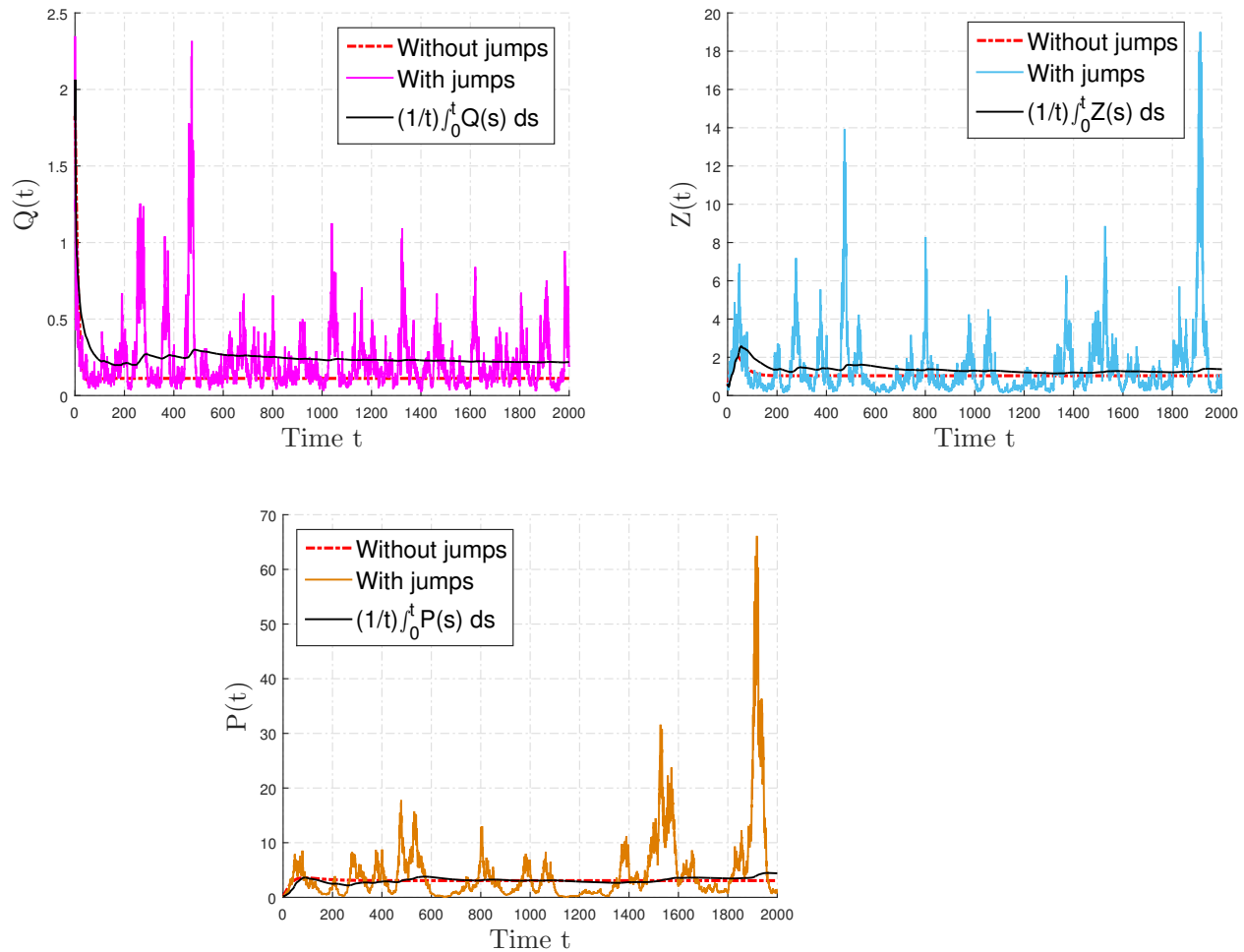


Figure 3. Random paths of the solution  $I(t) + C(t)$  in the case of asymptotic persistence





**Figure 4.** Random paths of perturbed model (2) in the case of asymptotic persistence

#### 4 Concluding remarks

Intervention measures are strategies implemented in epidemiology to prevent or control the spread of infectious diseases. These measures can be classified into primary, secondary, and tertiary prevention. In this article, we have proposed a general epidemic model that takes into consideration various measurement interventions such as media, isolation, and therapy. Our model is extended to a more general and real context by considering the effect of discontinuities. Epidemiological leaps refer to sudden increases in the number of cases of a particular disease within a population or geographic area. These jumps can occur for a variety of reasons, including changes in the environment, behaviors, or characteristics of the pathogen. It is important to understand these factors to develop effective strategies to control and manage the spread of the disease. For this reason, we have provided the conditions for the extinction and persistence of the infection. Finally, we performed some numerical experiments to validate our study.

In general, we point out that this study generalizes many previous works to the case of standard Lévy jumps. Furthermore, this study offers a few new insights for understanding the transmission of the disease with complex real-world assumptions. In other words, the techniques and models investigated in this work open up several research opportunities for future studies.

## Declarations

### Ethical approval

Not applicable.

### Consent for publication

Not applicable.

### Conflicts of interest

The author declares that he has no conflict of interest.

### Funding

Not applicable.

### Author's contributions

The author confirmed the results and contributed to the final manuscript.

### Acknowledgements

Not applicable.

## References

- [1] Brauer, F. and Castillo-Chavez, C. *Mathematical Models in Population Biology and Epidemiology* (Vol. 40). Springer: New York, (2012).
- [2] Capasso, V. *Mathematical Structures of Epidemic Systems* (Vol. 97). Springer, (2008).
- [3] Safarishahrbiari, A., Lawrence, T., Lomotey, R., Liu, J., Waldner, C. and Osgood, N. Particle filtering in a SEIRV simulation model of H1N1 influenza. In *2015 Winter Simulation Conference (WSC)*, pp. 1240-1251, Huntington Beach, CA, USA, (2015, December). [[CrossRef](#)]
- [4] Brauer, F. Compartmental models in epidemiology. In *Mathematical Epidemiology* (pp. 19-79). Berlin, Heidelberg: Springer, (2008). [[CrossRef](#)]
- [5] Ming, W.K., Huang, J. and Zhang, C.J. Breaking down of healthcare system: Mathematical modelling for controlling the novel coronavirus (2019-nCoV) outbreak in Wuhan, China. *BioRxiv*, (2020). [[CrossRef](#)]
- [6] Nesteruk, I. Statistics-based predictions of coronavirus epidemic spreading in mainland China, Igor Sikorsky Kyiv Polytechnic Institute, MedRxiv, (2020).
- [7] Li, R., Pei, S., Chen, B., Song, Y., Zhang, T., Yang, W. and Shaman, J. Substantial undocumented infection facilitates the rapid dissemination of novel coronavirus (SARS-CoV-2). *Science*, 368(6490), 489-493, (2020). [[CrossRef](#)]
- [8] Russell, T.W., Hellewell, J., Abbott, S., Golding, N., Gibbs, H., Jarvis, C.I., et al. Using a delay-adjusted case fatality ratio to estimate under-reporting. *Centre for Mathematical Modeling of Infectious Diseases Repository*, 22, (2020).
- [9] Pal, D., Ghosh, D., Santra, P.K. and Mahapatra, G.S. Mathematical analysis of a COVID-19 epidemic model by using data-driven epidemiological parameters of diseases spread in India. *Biophysics*, 67(2), 231-244, (2022). [[CrossRef](#)]
- [10] Hu, Z., Cui, Q., Han, J., Wang, X., Wei, E.I. and Teng, Z. Evaluation and prediction of the COVID-19 variations at different input population and quarantine strategies, a case study

- in Guangdong province, China. *International Journal of Infectious Diseases*, 95, 231-240, (2020). [[CrossRef](#)]
- [11] Darnell, M.E., Subbarao, K., Feinstone, S.M. and Taylor, D.R. Inactivation of the coronavirus that induces severe acute respiratory syndrome, SARS-CoV. *Journal of Virological Methods*, 121(1), 85-91, (2004). [[CrossRef](#)]
- [12] Wu, J., Tang, B., Bragazzi, N.L., Nah, K. and McCarthy, Z. Quantifying the role of social distancing, personal protection and case detection in mitigating COVID-19 outbreak in Ontario, Canada. *Journal of Mathematics in Industry*, 10, 1-12, (2020). [[CrossRef](#)]
- [13] Mohsen, A.A., Al-Husseiny, H.F., Zhou, X. and Hattaf, K. Global stability of COVID-19 model involving the quarantine strategy and media coverage effects. *AIMS Public Health*, 7(3), 587, (2020). [[CrossRef](#)]
- [14] Ivorra, B., Ferrández, M.R., Vela-Pérez, M. and Ramos, A.M. Mathematical modeling of the spread of the coronavirus disease 2019 (COVID-19) taking into account the undetected infections. *The Case of China. Communications in Nonlinear Science and Numerical Simulation*, 88, 105303, (2020). [[CrossRef](#)]
- [15] Karimi-Zarchi, M., Neamatzadeh, H., Dastgheib, S.A., Abbasi, H., Mirjalili, S.R., Behforouz, A., Ferdosian F. and Bahrami, R. Vertical transmission of coronavirus disease 19 (COVID-19) from infected pregnant mothers to neonates: a review. *Fetal and Pediatric Pathology*, 39(3), 246-250, (2020). [[CrossRef](#)]
- [16] Lu, D., Sang, L., Du, S., Li, T., Chang, Y. and Yang, X.A. Asymptomatic COVID-19 infection in late pregnancy indicated no vertical transmission. *Journal of Medical Virology*, 92(9), 1660-1664, (2020). [[CrossRef](#)]
- [17] Schwartz, D.A. and Dhaliwal, A. Infections in pregnancy with COVID-19 and other respiratory RNA virus diseases are rarely, if ever, transmitted to the fetus: experiences with coronaviruses, parainfluenza, metapneumovirus respiratory syncytial virus, and influenza. *Archives of Pathology & Laboratory Medicine*, 144(8), 920-928, (2020). [[CrossRef](#)]
- [18] Naim, M., Sabbar, Y. and Zeb, A. Stability characterization of a fractional-order viral system with the non-cytolytic immune assumption. *Mathematical Modelling and Numerical Simulation with Applications*, 2(3), 164-176, (2022). [[CrossRef](#)]
- [19] Kiouach, D. and Sabbar, Y. The threshold of a stochastic SIQR epidemic model with Levy jumps. In *Trends in Biomathematics: Mathematical Modeling for Health, Harvesting, and Population Dynamics* (pp. 87-105). Cham: Springer, (2019). [[CrossRef](#)]
- [20] Zhang, X.B., Huo, H.F., Xiang, H., Shi, Q. and Li, D. The threshold of a stochastic SIQS epidemic model. *Physica A: Statistical Mechanics and Its Applications*, 482, 362-374, (2017). [[CrossRef](#)]
- [21] Liu, Q. and Jiang, D. The dynamics of a stochastic vaccinated tuberculosis model with treatment. *Physica A: Statistical Mechanics and its Applications*, 527, 121274, (2019). [[CrossRef](#)]
- [22] Cai, Y., Kang, Y. and Wang, W. A stochastic sirs epidemic model with nonlinear incidence rate. *Applied Mathematics and Computation*, 305, 221-240, (2017). [[CrossRef](#)]
- [23] Kiouach, D. and Sabbar, Y. Threshold analysis of the stochastic Hepatitis B epidemic model with successful vaccination and Levy jumps. In *IEEE 2019 4th World Conference on Complex Systems (WCCS)*, pp. 1-6, Ouarzazate, Morocco, (2019, April). [[CrossRef](#)]
- [24] Sabbar, Y., Din, A. and Kiouach, D. Influence of fractal–fractional differentiation and independent quadratic Lévy jumps on the dynamics of a general epidemic model with vaccination

strategy. *Chaos, Solitons & Fractals*, 171, 113434, (2023). [[CrossRef](#)]

[25] Zhao, Y. and Jiang, D. The threshold of a stochastic SIS epidemic model with vaccination. *Applied Mathematics and Computation*, 243, 718-727, (2014). [[CrossRef](#)]

Bulletin of Biomathematics (BBM)  
(<https://bulletinbiomath.org>)



**Copyright:** © 2023 by the authors. This work is licensed under a Creative Commons Attribution 4.0 (CC BY) International License. The authors retain ownership of the copyright for their article, but they allow anyone to download, reuse, reprint, modify, distribute, and/or copy articles in *BBM*, so long as the original authors and source are credited. To see the complete license contents, please visit (<http://creativecommons.org/licenses/by/4.0/>).

**How to cite this article:** Sabbar, Y. (2023). Asymptotic extinction and persistence of a perturbed epidemic model with different intervention measures and standard Lévy jumps. *Bulletin of Biomathematics*, 1(1), 58-77. <https://doi.org/10.59292/bulletinbiomath.2023004>



RESEARCH PAPER

## A fractional order vaccination model for COVID-19 incorporating environmental transmission: a case study using Nigerian data

Anne Ojoma Atede <sup>1,\*</sup>, Andrew Omame <sup>1,2,†</sup> and Simeon Chioma Inyama <sup>1,‡</sup>

<sup>1</sup>Department of Mathematics, Federal University of Technology, Owerri, Nigeria, <sup>2</sup>Abdus Salam School of Mathematical Sciences, Government College University Katchery Road, Lahore 54000, Pakistan

\* Corresponding Author

‡ anoja4god@gmail.com (Anne Ojoma Atede); andrew.omame@futo.edu.ng (Andrew Omame); scinyamam2011@yahoo.com (Simeon Chioma Inyama)

### Abstract

In this work, a fractional-order vaccination model for the novel Coronavirus 2019 (COVID-19) incorporating environmental transmission is considered and analyzed using tools of fractional calculus. The Laplace transform technique and the fixed point theorem lay out the model solutions' existence and uniqueness. The solutions' positivity and boundedness are also demonstrated. Additionally, the stability of the model's equilibrium points is discussed using the fractional-order system stability theory. The model is fitted using the data sets for the Pfizer vaccination program in Nigeria from April 1, 2021, to June 10, 2021. In conclusion, simulation results for various fractional parameter values are presented. It has been observed that increasing fractional-order values has distinct effects on the various model compartments, for  $\mathcal{R}_0 < 1$  and  $\mathcal{R}_0 > 1$ , respectively.

**Keywords:** Fractional derivative; stability; COVID-19; environmental transmission; numerical simulation

**AMS 2020 Classification:** 34C60; 92C42; 92D30; 92D25

### 1 Introduction

In 1965, scientists found a human coronavirus in the passageway that separates the upper and lower parts of the human body to let in and let out the air. [1] was the first discovered in an adult with a common cold. Humans can become infected with seven different kinds of coronavirus. In 2002, the sort liable for the serious intense respiratory condition (SARS) arose in South China. For a brief period, it impacted 28 different nations, giving an all-out number of around 8000

additional infected individuals bringing about 774 passings by July 2003, with a little increase in 2004 having just four additional cases, [2]. Experts believe that bats are the source of the coronavirus (SARS-COV2), which also gave rise to the middle east respiratory syndrome (MERS) and severe acute respiratory syndrome (SARS) [3]. It is one of a group of viruses that can cause a variety of symptoms, including fever, pneumonia, difficulty breathing, and a lung infection. In China, Wuhan Hubei province, an outbreak of a respiratory illness occurred in December 2019. The WHO declared Coronavirus disease (COVID-19) a global public health emergency due to the virus's rapid spread and as the leading cause of this illness. According to WHO, it affected roughly 19 countries by the end of January 2020, with 11791 confirmed cases and 213 deaths. The common symptoms are dry cough, exhaustion, fever (although some older people may not experience these symptoms), aches and pains, nasal congestion, a runny nose, sore throat, or diarrhea [4]. Droplets from the infected person's mouth or nose can spread the virus between people who are within two meters away from each other. It can likewise be spread in ineffectively ventilated indoor settings where individuals stay for a more broadened period, [4]. Reports show that transmission in children between the ages of 10-14 and teenagers have lower vulnerability than grown-ups, [5], [6]. Millions of people around the world, including in China, Canada, the United States, France, and Germany, have contracted COVID-19 since its discovery. According to the National Centers for Disease Control and Prevention (NCDC), as of June 25, 2021, approximately 167430 individuals in Nigeria had been identified as carrying the virus, 163937 individuals had been discharged, and approximately 2119 deaths had been recorded [7].

Mathematical models have become excellent tools for comprehending the behavior of infectious diseases [8, 9]. There have been a variety of approaches taken to investigate the means by which the disease is transmitted from person to person, the ways in which it can be avoided, and the possibilities for infectious disease control. Mathematical models have been an essential device or tool in completing this task. Numerous models have been developed by numerous individuals, including mathematicians and biologists, since the COVID-19 outbreak to explain the virus's spread from person to person. Mathematical modeling of COVID-19 transmission was taken into consideration by Sarita et al. [10]. They considered the roles of different intervention strategies such as lockdown, quarantine, and isolation of symptomatic individuals. They concluded in the model's numerical simulation and sensitivity analysis that disease could be prevented or controlled by minimizing close association, increasing the effectiveness of confined and quarantined individuals with symptoms. Enahoro et al. [11] examined the COVID-19 pandemic in Nigeria through mathematical modeling and analysis. They examined the model by applying the data gotten from the Nigeria Center for disease control (NCDC). Okuonghae and co-authors [12] analyzed Lagos' COVID-19 population dynamics using a mathematical model and concluded that the virus's prevalence would significantly decrease if regular social isolation, mask use, and other preventative measures were maintained. Bashir et al. [13] fostered an ideal optimal control model for the Coronavirus (COVID-19) pandemic. Their findings demonstrated that the control effect of increasing the number of susceptible individuals decreases the number of infectious individuals. Mohammed and others [14] looked into a fractional-order mathematical model for the dynamics of COVID-19 that included quarantine, isolation, and the viral load in the environment. The model's numerical simulation demonstrated that a 50% increase in the isolation rate of exposed individuals will significantly reduce the number of infected cases. It would likewise be diminished if the asymptomatic infected individual could take precautionary measures and quit working uninhibitedly in a susceptible population. Omame et al. [9] developed a fractional-order model for COVID-19 and tuberculosis co-infection utilizing the Atangana-Baleanu derivative. According to their simulations, reducing the risk of COVID-19 infection among people with inactive tuberculosis also reduces the spread of the virus and the two diseases simultaneously

affecting a population. Using the Caputo-Fabrizio derivative and the homotopy analysis transform, Baleanu et al. examined a fractional-order model for COVID-19 transmission in their research. A convergent series solution was provided for the model [16]. Rezapour and others [15] also considered a Caputo derivative-based SIR model; using reliable data and an approximate fractional Euler solution, their model predicts the transmission of COVID-19 from one infected person to another in Iran and around the world.

Fractional differential equations have gained wider applications in the modelling of physical and biological processes in recent years [17–20]. It has demonstrated its importance due to its capacity to capture the memory, hereditary, and also properties that are not local [21]. Fractional derivatives and integrals are crucial for epidemiological modeling as they store relevant information for recollection, which will assist with spreading disease. A lot of models to control disease circulation have been extensively analyzed using fractional derivatives [22–26].

With the help of the Caputo fractional-order derivative, the primary goal of this study will be to develop a novel vaccination model for COVID-19 that incorporates environmental transmission and is tailored to actual Nigerian data. This study will significantly contribute to understanding the effective transmission of Coronavirus in our immediate environment. The main motivation for using the Caputo fractional derivative is that it has a unique way of dealing with pressing issues that affect people, like an epidemic, and also allows the conventional, initial, and boundary conditions to be taken into account [27, 28].

## 2 Preliminaries

Some relevant definitions and methodologies required in this paper are now highlighted in this subsection.

**Definition 1** [29] *Fractional integral of order  $\psi > 0$ ,  $\psi \in \mathbb{R}^+$  reads*

$$J_t^\psi f(t) = \frac{1}{\Gamma(\psi)} \int_0^t (t-\zeta)^{\psi-1} f(\zeta) d\zeta, \quad t > 0,$$

with the symbol  $\Gamma$  as the Gamma function given as

$$\Gamma(\psi) = \int_0^\infty \exp(-\zeta) \zeta^{\psi-1} d\zeta, \quad \Gamma(\psi+1) = \psi \Gamma(\psi), \quad \text{Re}\{\psi\} > 0,$$

where  $f(t) = 1$ , the fractional integral of order  $\psi > 0$  reads

$$J_t^\psi(1) = \frac{1}{\Gamma(\psi)} \int_0^t (t-\zeta)^{\psi-1} (1) d\zeta = \frac{t^\psi}{\Gamma(\psi+1)}.$$

**Definition 2** [29] *Caputo fractional derivative of order  $\psi > 0$ ,  $\psi \in \mathbb{R}^+$  reads*

$$D_t^\psi f(t) = J_t^{n-\psi} D^n f(t) = \frac{1}{\Gamma(n-\psi)} \int_0^t (t-\zeta)^{n-\psi-1} f^{(n)}(\zeta) d\zeta,$$

having  $n$  as a non-negative integer giving as  $n - 1 < \psi \leq n$ , and  $0 < \psi \leq 1$ , the definition above reduces to

$$D_t^\psi f(t) = \frac{1}{\Gamma(1-\psi)} \int_0^t (t-\zeta)^{-\psi} f'(\zeta) d\zeta. \quad (1)$$

**Definition 3 ([29])** Caputo fractional derivatives can simply be defined as

$$D_t^\psi (t-t_0)^q = \frac{\Gamma(q+1)(t-t_0)^{q-\psi}}{\Gamma(q-\psi+1)},$$

with  $0 < \psi \leq 1$ ,  $q > -1$ .

**Definition 4** Series expansion of the Mittag-Leffler of two-parameter  $\alpha_1, \alpha_2$  type function is given as

$$E_{\alpha_1, \alpha_2}(z) = \sum_{r=0}^{\infty} \frac{z^r}{\Gamma(\alpha_1 r + \alpha_2)}, \quad \alpha_1 > 0, \quad \alpha_2 > 0, \quad z \in \mathbb{C}. \quad (2)$$

It follows from (2) that

$$E_{1,1}(z) = \sum_{r=0}^{\infty} \frac{z^r}{\Gamma(r+1)} = \sum_{r=0}^{\infty} \frac{z^r}{r!} = e^z,$$

The renowned exponential function. Further

$$E_{1,2}(z) = \sum_{r=0}^{\infty} \frac{z^r}{\Gamma(r+2)} = \sum_{r=0}^{\infty} \frac{z^r}{(r+1)!} = \frac{1}{z} \sum_{r=0}^{\infty} \frac{z^{r+1}}{(r+1)!} = \frac{e^z - 1}{z},$$

Generally

$$E_{1,n}(z) = \frac{1}{z^{n-1}} \times \left( e^z - \sum_{r=0}^{n-2} \frac{z^r}{\Gamma(r+1)} \right).$$

**Definition 5 [29]** Laplace transform of Caputo fractional derivative (1) is given as

$$\mathcal{L} \{ D_t^\psi f(t) \} = s^\psi \tilde{f}(s) - s^{\psi-1} f(0), \quad 0 < \psi \leq 1, \quad (3)$$

with  $\mathcal{L}$  as the Laplace transform operator, and  $\tilde{f}(s) = \mathcal{L}\{f(t)\}$ .

**Lemma 1 [30]** Given  $\psi \in \mathbb{R}^+$ ,  $\theta_1(t)$  and  $\theta_2(t)$  stand for the non-negative functions and  $\theta_3(t)$  stands for both the non-negative together with the increasing function for  $0 \leq t \leq S$ ,  $S > 0$ ,  $\theta_3(t) \leq N$ , with  $N$  as a

constant. Supposing

$$\theta_1 \leq \theta_2 + \theta_3(t) \int_0^t (t - \zeta)^{\psi-1} \theta_1(\zeta) d\zeta,$$

then

$$\theta_1 \leq \theta_2 E_\psi \left( \theta_3(t) \frac{\pi}{\Gamma(1 - \psi) \sin(\pi\psi)} S^\psi \right).$$

### 3 Model formulation

At a certain time  $t$ , we represent the entire population of humans with  $N_H(t)$ , which we divide into the states of being such that the occurrence of any one implies the non-occurrence of all the others (mutually exclusive) subdivision of a population of unvaccinated susceptible individuals ( $S_c(t)$ ), individuals vaccinated with the *Pfizer* vaccine ( $V_c(t)$ ), asymptomatic infectious individuals ( $A_c(t)$ ), unvaccinated symptomatic infectious individuals ( $J_u(t)$ ), vaccinated symptomatic infectious individuals ( $J_v(t)$ ) and recovered individuals ( $R(t)$ ). Hence,  $N_H(t) = S_c + V_c + A_c + J_u + J_v + R$ .

How do we get the population of unvaccinated susceptible individuals,  $S_c$ , created by bringing in new individuals at the rate  $\Omega$ . Contacts with an infected environment cause individuals to be infected with COVID-19 and therefore reduce an entire population at the rate  $\vartheta C_{EV}$  and contacts with infected individuals at the rate:  $\frac{\beta(\omega A_c + I_u + q_v J_v)}{N_H}$ . The modification parameter  $0 < \theta < 1$ , accounts for reduced probability of transmission by asymptomatic infectious individuals. The parameter  $q_v$  ( $q_v < 1$ ) is a modification term accounting for the reduced infectiousness of vaccinated infectious individuals.  $\beta$  is the effective contact rate for transmitting COVID-19 infection from humans.  $\vartheta$  is the effective contact rate for the transmission of COVID-19 infection from the infected environment.  $C_{EV}$  is the concentration of COVID-19 in the environment. We can define the active changing mode by which the fractional order model for COVID-19 is being transmitted in a population by the system of non-linear fractional differential equations in Eq. (4) below, alongside the Table 1 depicting the connected state variables and parameters in the model (4).

$$\begin{aligned} D_t^\psi S_c &= \Omega - \delta S_c - \left( \frac{\beta(\omega A_c + J_u + q_v J_v)}{N_H} \right) S_c - \vartheta C_{EV} S_c - \mu S_c, \\ D_t^\psi V_c &= \delta S_c - (1 - \xi) \left( \frac{\beta(\omega A_c + J_u + q_v J_v)}{N_H} + \vartheta C_{EV} \right) V_c - \mu V_c, \\ D_t^\psi A_c &= p \left( \frac{\beta(\omega A_c + J_u + q_v J_v)}{N_H} + \vartheta C_{EV} \right) S_c + f(1 - \xi) \left( \frac{\beta(\omega A_c + J_u + q_v J_v)}{N_H} + \vartheta C_{EV} \right) V_c \\ &\quad - (\gamma_A + \mu) A_c, \\ D_t^\psi J_u &= (1 - p) \left( \frac{\beta(\omega A_c + J_u + q_v J_v)}{N_H} + \vartheta C_{EV} \right) S_c - (\gamma_{JU} + d_{JU} + \mu) J_u, \\ D_t^\psi J_v &= (1 - f)(1 - \xi) \left( \frac{\beta(\omega A_c + J_u + q_v J_v)}{N_H} + \vartheta C_{EV} \right) V_c - (\gamma_{JV} + d_{JV} + \mu) J_v, \\ D_t^\psi R &= \gamma_A A_c + \gamma_{JU} J_u + \gamma_{JV} J_v - \mu R, \\ D_t^\psi C_{EV} &= \chi_1 A_c + \chi_2 J_u + \chi_3 J_v - \mu_{EV} C_{EV}, \end{aligned} \tag{4}$$

with the corresponding initial conditions

$$S_c(0) \geq 0, V_c(0) \geq 0, A_c(0) \geq 0, J_u(0) \geq 0, J_v(0) \geq 0, R(0) \geq 0, C_{ev}(0) \geq 0. \quad (5)$$

**Table 1.** Representation of the variables in the model (4)

Variable	Interpretation
$S_c$	unvaccinated susceptible individuals
$V_c$	Vaccinated with vaccine ( <i>Pfizer</i> )
$A_c$	Asymptomatic individuals (vaccinated and unvaccinated)
$J_u$	unvaccinated symptomatic individuals
$J_v$	Vaccinated symptomatic individuals
$R$	Recovered humans
$C_{ev}$	COVID-19 concentration in the environment

**Table 2.** Representation of parameters in the model (4)

Parameter	Interpretation	Baseline Value	Reference
$\Omega$	Recruitment rate	$\frac{206139587}{54.69 \times 365} \text{day}^{-1}$	[31]
$\beta$	Effective transmission rate of COVID-19	0.00016708	Fitted
$\delta$	COVID-19 vaccination rate	$0.0059 \text{day}^{-1}$	Fitted
$\mu$	Natural death rate	$\frac{1}{54.69 \times 365} \text{day}^{-1}$	[31]
$\xi$	COVID-19 vaccine efficacy	0.95	[32]
$p$	Fraction of unvaccinated susceptible that move to asymptomatic class	0.5	Assumed
$f$	Fraction of vaccinated susceptible that move to asymptomatic class	0.5	Assumed
$\omega$	Modification parameter that accounts for reduced infectiousness of humans in $J_u$ class in comparison with humans in $J_v$ class	0.7	[12]
$\gamma_a, \gamma_{ju}, \gamma_{jv}$	Recovery rates for individuals in the $A_c, J_u,$ and $J_v$ classes, respectively	$0.13978 \text{day}^{-1}$	[12]
$\mu_{ev}$	COVID-19 removal rate from the environment	$0.03 \text{day}^{-1}$	Assumed
$d_{ju}, d_{jv}$	Disease induced death rates for individuals in the $J_u,$ and $J_v$ classes, respectively	0.015	[12]
$\chi_1, \chi_2, \chi_3$	Virus shedding rates from infected humans	$0.0005 \text{day}^{-1}$	Assumed

## Fundamentals of the model

The boundedness and positivity of the solutions prove that equations (4)-(5) are mathematically and biologically presented.

**Invariant domain**

**Theorem 1** Assume  $S_c(t), V_c(t), A_c(t), J_u(t), J_v(t), R(t), C_{EV}(t)$ , are solutions to the equations (4)-(5), then

i. the set  $\nabla = \nabla_H \cup \nabla_{EV}$ , where,

$$\nabla_H = \left\{ (S_c(t), V_c(t), A_c(t), J_u(t), J_v(t), R(t)) \in \mathbb{R}_+^7 : S_c + V_c + A_c + J_u + J_v + R, \leq \frac{\Omega}{\mu} \right\},$$

$$\nabla_{EV} = \left\{ C_{EV} : C_{EV} \leq \frac{(\chi_1 + \chi_2 + \chi_3)\beta}{\mu_{EV}} \right\},$$

is positively invariant with regard to the governing model,

ii. each solution to the equations (4)-(5) beginning from the initial point  $S_0, E_0, I_0, R_0$  and  $P_0$  remain positive at every value of  $t \geq 0$ .

**Proof** Let us closely observe the expression below for time  $t$

$$N_H = S_c + V_c + A_c + J_u + J_v + R. \quad (6)$$

summing up the equations corresponding to the human compartments of the model generates

$$\begin{aligned} D_t^\psi N_H(t) &= D_t^\psi S_c(t) + D_t^\psi V_c(t) + D_t^\psi A_c(t) + D_t^\psi J_u(t) + D_t^\psi J_v + D_t^\psi R \\ &= \Omega - (S_c + V_c + A_c + J_u + J_v + R) \mu \\ &\leq \Omega - \mu N_H. \end{aligned}$$

Hence, by using Laplace transform, the inequality becomes

$$s^\psi \tilde{N}_H(s) - s^{\psi-1} N_H(0) \leq \frac{\Omega}{s} - \mu \tilde{N}_H(s),$$

from which

$$\tilde{N}_H(s) \leq \frac{\Omega}{s(s^\psi + \mu)} + N_H(0) \frac{s^{\psi-1}}{s^\psi + \mu}.$$

By partial fraction, the above expression can be re-written as

$$\begin{aligned} \tilde{N}_H(s) &\leq \frac{\Omega}{\mu} \left( \frac{1}{s} - \frac{s^{\psi-1}}{\mu \left( \frac{s^\psi}{\mu} + 1 \right)} \right) + N_H(0) \frac{s^{\psi-1}}{s^\psi + \mu} \\ &= \frac{\Omega}{\mu} \left( \frac{1}{s} \right) - \left( \frac{\Omega}{\mu} - N_H(0) \right) \frac{1}{s} \left( 1 + \frac{\mu}{s^\psi} \right)^{-1}, \\ \tilde{N}_H(s) &\leq \frac{\Omega}{\mu} \left( \frac{1}{s} \right) - \left( \frac{\Omega}{\mu} - N_H(0) \right) \sum_{r=0}^{\infty} \frac{(-\mu)^r}{s^{\psi r + 1}}. \end{aligned}$$

The inverse Laplace transform with the help of (2) gives

$$\begin{aligned} N_H(t) &\leq \frac{\Omega}{\mu} - \left( \frac{\Omega}{\mu} - N_H(0) \right) \sum_{r=0}^{\infty} \frac{(-\mu t^\psi)^r}{\Gamma(\psi r + 1)} \\ &\leq \frac{\Omega}{\mu} - \left( \frac{\Omega}{\mu} - N_H(0) \right) E_\psi(-\mu t^\psi). \end{aligned}$$

It follows that as  $t \rightarrow \infty$

$$0 \leq N_H \leq \frac{\Omega}{\mu}, \quad (7)$$

of which the requirements that make equations (4)-(5) bounded and also indicate that there is an achievable possible region. ■

### Positivity

Suppose that by contradiction, the third equation of the model is not true.

Let  $t_1 = \min\{t : S_c(t)V_c(t)A_c(t)J_u(t)J_v(t)R(t)C_{ev}(t) = 0\}$ . Suppose  $A_c(t_1) = 0$ , it suggest that  $S_c(t) > 0, V_c(t) > 0, A_c(t) > 0, J_u(t) > 0, J_v(t) > 0, R(t) > 0, C_{ev}(t) > 0$ , for all  $[0, t_1]$ , suppose by assumption, the expression below exists,

$$\Theta_1 = \min_{0 \leq t \leq t_1} \left\{ P \left( \frac{\beta(\omega A_c + J_u + \varrho_v J_v) + \vartheta C_{ev}}{A_c} \right) S_c + f(1 - \xi) \left( \frac{\beta(\omega A_c + J_u + \varrho_v J_v) + \vartheta C_{ev}}{A_c} \right) V_c - (\gamma_A + \mu) \right\}.$$

It follows that

$$D_t^\psi A_c(t) - \Theta_1 A_c(t) > 0. \quad (8)$$

We state (without proof) that continuous function  $\Phi_1$  can be established in a way that the equation below is discovered

$$D_t^\psi A_c(t) - \Theta_1 A_c(t) = -\Phi_1(t).$$

With the Laplace transform, the last equality becomes

$$s^\psi \tilde{A}_c(s) - s^{\psi-1} A_c(0) - \Theta_1 \tilde{A}_c(s) = -\tilde{\Phi}_1(s),$$

from which

$$\begin{aligned} \tilde{A}_c(s) &= A_c(0) \frac{s^{\psi-1}}{s^\psi - \Theta_1} - \frac{\tilde{\Phi}_1(s)}{s^\psi - \Theta_1} = \frac{A_c(0)}{s} \left( 1 - \frac{\Theta_1}{s^\psi} \right)^{-1} - \frac{\tilde{\Phi}_1(s)}{s^\psi} \left( 1 - \frac{\Theta_1}{s^\psi} \right)^{-1} \\ &= A_c(0) \sum_{r=0}^{\infty} \frac{\Theta_1^r}{s^{\psi r + 1}} - \tilde{\Phi}_1(s) \sum_{r=0}^{\infty} \frac{\Theta_1^r}{s^{\psi r + \psi}}. \end{aligned}$$

The inverse Laplace transform using the Mittag-Leffler function and forgetting the non-positive term produces a solution to the above terms in (8) that meets the expression below.

$$A_c(t) > A_c(0) \sum_{r=0}^{\infty} \frac{(\Theta_1 t^\psi)^r}{\Gamma(\psi r + 1)} = A_c(0) E_\psi (\Theta_1 t^\psi).$$

Hence, the positivity of the solution  $A_c$  is as follows:

$$A_c(t) > A_c(0) E_\psi (\Theta_1 t^\psi) > 0,$$

which contradicts  $A_c(t_1) = 0$ . Similarly, suppose  $J_u(t_1) = 0$  which implies that  $S_c(t) > 0$ ,  $V_c(t) > 0$ ,  $A_c(t) > 0$ ,  $J_v(t) > 0$ ,  $R(t) > 0$ ,  $C_{ev} > 0$ , for all  $0 \leq t \leq t_1$ . Assume the expression is true

$$\Theta_2 = \min_{0 \leq t \leq t_1} \left\{ (1-p) \left( \frac{\beta(\omega A_c + J_u + \varrho_v J_v) + \vartheta C_v}{J_u} \right) S_c - (\gamma_{ju} + d_{ju} + \mu) \right\},$$

then

$$D_t^\psi J_u(t) > \Theta_2 J_u(t). \quad (9)$$

It follows that a continuous function  $\Phi_2(t)$  may be established in a way that the equation below is discovered

$$D_t^\psi J_u(t) - \Theta_2 J_u(t) = -\Phi_2(t).$$

With the Laplace transform, the equation becomes

$$s^\psi \tilde{J}_u(s) - s^{\psi-1} J_u(0) - \Theta_2 \tilde{J}_u(s) = -\tilde{\Phi}_2(s),$$

from which

$$\tilde{J}_u(s) = J_u(0) \frac{s^{\psi-1}}{s^\psi - \Theta_2} - \frac{\tilde{\Phi}_2(s)}{s^\psi - \Theta_2} = J_u(0) \sum_{r=0}^{\infty} \frac{\Theta_2^r}{s^{\psi r + 1}} - \tilde{\Phi}_2(s) \sum_{r=0}^{\infty} \frac{\Theta_2^r}{s^{\psi r + \psi}}.$$

Using the inverse Laplace transform, applying the Mittag-Leffler function, and forgetting the non-positive term, the solution to the equation (9) meets that of the quantity below

$$J_u(t) > J_u(0) \sum_{r=0}^{\infty} \frac{(\Theta_2 t^\psi)^r}{\Gamma(\psi r + 1)} = J_u(0) E_\psi (\Theta_2 t^\psi).$$

Hence, the positivity of the solution  $I_u$  is as follows

$$J_u(t) > J_u(0) E_\psi (\Theta_2 t^\psi) > 0,$$

which contradicts  $J_u(t_1) = 0$ . Applying the similar method of solution to the question above, we assume  $J_v(t_1) = 0$  which suggests that  $S_c(t) > 0$ ,  $V_c(t) > 0$ ,  $A_c(t) > 0$ ,  $J_u, R(t) > 0$ ,  $C_{ev}(t) > 0$  for

all  $0 \leq t \leq t_1$ . Suppose the expression below is true

$$\Theta_3 = \min_{0 \leq t \leq t_1} \left\{ (1-f)(1-\xi) \left( \frac{\beta(\omega A_c + J_u + \varrho_v J_v)}{J_v} + \vartheta C_{EV} \right) V_c - (\gamma_{JV} + d_{JV} + \mu) \right\}.$$

So that

$$D_t^\psi J_v(t) > \Theta_3 J_v(t). \quad (10)$$

It follows that a continuous function  $\Phi_3(t)$  can be established in a way that the equation below is discovered

$$D_t^\psi J_v(t) - \Theta_3 J_v(t) = -\Phi_3(t).$$

By using the Laplace transform, the above inequality becomes

$$s^\psi \tilde{J}_v(s) - s^{\psi-1} J_v(0) - \Theta_3 \tilde{J}_v(s) = -\tilde{\Phi}_3(s),$$

from which

$$\tilde{J}_v(s) = J_v(0) \sum_{r=0}^{\infty} \frac{\Theta_3^r}{s^{\psi r + 1}} - \Phi_3(s) \sum_{r=0}^{\infty} \frac{\Theta_3^r}{s^{\psi r + \psi}}.$$

Applying the inverse Laplace transform using the Mittag-Leffler function and forgetting the non-positive term, the solution to the equation (10) meets that of the expression below.

$$J_v(t) > J_v(0) \sum_{r=0}^{\infty} \frac{(\Theta_3 t^\psi)^r}{\Gamma(\psi r + 1)} = J_v(0) E_\psi(\Theta_3 t^\psi). \quad (11)$$

Hence, the positivity of the solution  $J_v$  is as follows

$$J_v(t) > J_v(0) E_\psi(\Theta_3 t^\psi) > 0,$$

which is not in agreement with the fact that  $J_v(t_1) = 0$ . Likewise, assuming  $C_{EV}(t_1) = 0$  which suggest that  $S_c(t) > 0$ ,  $V_c(t) > 0$ ,  $A_c(t) > 0$ ,  $J_v(t) > 0$ ,  $R(t) > 0$ ,  $C_{EV} > 0$ , for all  $0 \leq t \leq t_1$ . Supposing the expression below is true

$$\Theta_4 = \min_{0 \leq t \leq t_1} \left\{ \left( \frac{\chi_1 A_c + \chi_2 J_u + \chi_3 J_v}{C_{EV}} - \mu_{EV} \right) \right\},$$

then

$$D_t^\psi C_{EV}(t) > \Theta_4 C_{EV}(t). \quad (12)$$

It follows that a continuous function  $\Phi_4(t)$  can be established in a way the equation below is discovered

$$D_t^\psi C_{EV}(t) - \Theta_4 C_{EV}(t) = -\Phi_4(t).$$

By using the Laplace transform, the inequality becomes

$$s^\psi \tilde{C}_{EV}(s) - s^{\psi-1} C_{EV}(0) - \Theta_4 \tilde{C}_{EV}(s) = -\tilde{\Phi}_4(s),$$

from which

$$\tilde{C}_{EV}(s) = C_{EV}(0) \frac{s^{\psi-1}}{s^\psi - \Theta_4} - \frac{\tilde{\Phi}_4(s)}{s^\psi - \Theta_4} = C_{EV}(0) \sum_{r=0}^{\infty} \frac{\Theta_4^r}{s^{\psi r + 1}} - \tilde{\Phi}_4(s) \sum_{r=0}^{\infty} \frac{\Theta_4^r}{s^{\psi r + \psi}}.$$

Applying the inverse Laplace transform using the Mittag-Leffler function and forgetting the non-positive term, the solution to equation (12) meets that of the quantity below.

$$C_{EV}(t) > C_{EV}(0) \sum_{r=0}^{\infty} \frac{(\Theta_4 t^\psi)^r}{\Gamma(\psi r + 1)} = C_{EV}(0) E_\psi(\Theta_4 t^\psi).$$

Hence, the positivity of the solution  $J_U$  is as follows

$$C_{EV}(t) > C_{EV}(0) E_\psi(\Theta_4 t^\psi) > 0,$$

which contradicts  $C_{EV}(t_1) = 0$ . Furthermore, the same method of solution will prove that the positivity of the solutions  $S_c, V_c, R$  and  $C_{EV}$  are as follows

$$S_c(t) > S_c(0) E_\psi(\Theta_5 t^\psi) > 0, \quad V_c(t) > V_c(0) E_\psi(\Theta_6 t^\psi) > 0,$$

$$R(t) > R(0) E_\psi(\Theta_7 t^\psi) > 0, \quad C_{EV}(t) > C_{EV}(0) E_\psi(\Theta_8 t^\psi) > 0.$$

### Existence and uniqueness of the solution

This section shows the proof of existence and uniqueness of the solution of fractional model (4)-(5). The same solution method in [33] is employed here using the theorem of Banach fixed point and Picard's operator. Furthermore, for existence, Schauder's fixed point theorem will be applied in which the boundedness of the solution shall be proven, too.

The use of fractional integral together with the Caputo fractional derivative model (4) of order  $\psi > 0$  alongside its corresponding initial conditions (5) present the Volterra-integral equations of

the second kind below as well as a solution to the fractional model.

$$\begin{aligned}
 S_c(t) - S_c(0) &= \frac{1}{\Gamma(\psi)} \int_0^t (t-\zeta)^{\psi-1} L(\zeta, S_c(\zeta)) d\zeta, \\
 V_c(t) - V_c(0) &= \frac{1}{\Gamma(\psi)} \int_0^t (t-\zeta)^{\psi-1} M(\zeta, V_c(\zeta)) d\zeta, \\
 A_c(t) - A_c(0) &= \frac{1}{\Gamma(\psi)} \int_0^t (t-\zeta)^{\psi-1} N(\zeta, A_c(\zeta)) d\zeta, \\
 J_u(t) - J_u(0) &= \frac{1}{\Gamma(\psi)} \int_0^t (t-\zeta)^{\psi-1} O(\zeta, J_u(\zeta)) d\zeta, \\
 J_v(t) - J_v(0) &= \frac{1}{\Gamma(\psi)} \int_0^t (t-\zeta)^{\psi-1} P(\zeta, J_v(\zeta)) d\zeta, \\
 R(t) - R(0) &= \frac{1}{\Gamma(\psi)} \int_0^t (t-\zeta)^{\psi-1} V(\zeta, R(\zeta)) d\zeta, \\
 C_{EV}(t) - C_{EV}(0) &= \frac{1}{\Gamma(\psi)} \int_0^t (t-\zeta)^{\psi-1} Z(\zeta, C_{EV}(\zeta)) d\zeta.
 \end{aligned} \tag{13}$$

The functions  $(L, M, N, O, P, V, Z) : [0, b] \rightarrow \mathbb{R} \times \mathbb{R}$  without proof are presumed to be continuous in such a way that the Banach space, as well as the space of all the continuous functions, are  $(\mathbb{R}, \|\cdot\|)$  and  $\mathbb{H}^1([0, b])$  respectively which is defined in  $[0, b] \rightarrow \mathbb{R}$  formed alongside Chebyshev norm.

The next thing we want to do is to show if the continuous functions  $L, M, N, O, P, V,$  and  $Z$  meet the Lipschitz conditions provided

$$\sup_{0 < t \leq S} \left\| \frac{A_c}{N_H} \right\| \leq \varphi_1, \quad \sup_{0 < t \leq S} \left\| \frac{J_u}{N_H} \right\| \leq \varphi_2, \quad \sup_{0 < t \leq S} \left\| \frac{J_v}{N_H} \right\| \leq \varphi_3, \quad \sup_{0 < t \leq S} \left\| \frac{C_{EV}}{N_H} \right\| \leq \varphi_4.$$

Thus, firstly we get

$$\begin{aligned}
 \|L(S_{c1}) - L(S_{c2})\| &= \left\| \Omega - \left( \delta + \frac{\beta(\omega A_c + J_u + q_v J_v)}{\vartheta} C_{EV} + \mu \right) S_{c1} \right. \\
 &\quad \left. - \left( \Omega - \left( \delta + \frac{\beta(\omega A_c + J_u + q_v J_v)}{N_H} + \vartheta C_{EV} + \mu \right) S_{c2} \right) \right\| \\
 &= \left\| -\frac{\beta\omega A_c}{N_H} (S_{c1} - S_{c2}) - \frac{\beta J_u}{N_H} (S_{c1} - S_{c2}) - \frac{\beta q_v J_v}{N_H} (S_{c1} - S_{c2}) - \vartheta C_{EV} (S_{c1} - S_{c2}) \right. \\
 &\quad \left. - \mu (S_{c1} - S_{c2}) \right\| \\
 &\leq \beta\omega \sup_{0 \leq t \leq S} \left\| \frac{A_c}{N_H} \right\| \|S_{c1} - S_{c2}\| + \beta \sup_{0 \leq t \leq S} \left\| \frac{J_u}{N_H} \right\| \|S_{c1} - S_{c2}\| \\
 &\quad + \vartheta \sup_{0 \leq t \leq S} \|C_{EV}\| \|S_{c1} - S_{c2}\| + \mu \|S_{c1} - S_{c2}\| + \beta q_v \sup_{0 \leq t \leq S} \left\| \frac{J_v}{N_H} \right\| \|S_{c1} - S_{c2}\| \\
 &\leq L_L \|S_{c1} - S_{c2}\|,
 \end{aligned} \tag{14}$$

where

$$L_L = (\beta\omega\varphi_1 + \beta\varphi_2 + \beta q_v \varphi_3 + \vartheta C_{EV} + \mu) > 0.$$

Secondly,

$$\begin{aligned}
\|M(V_1) - M(V_2)\| &= \left\| \delta S_c - (1 - \xi) \left( \frac{\beta(\omega A_c + J_u + \varrho_v J_v)}{N_H} + \vartheta C_{EV} \right) V_{c1} \right. \\
&\quad \left. - \left( \delta S_c - (1 - \xi) \left( \frac{\beta(\omega A_c + J_u + \varrho_v J_v)}{N_H} + \vartheta C_{EV} + \mu \right) V_{c2} \right) \right\| \\
&= - \left( \delta S_c + (1 - \xi) \left( \frac{\beta(\omega A_c + J_u + \varrho_v J_v)}{N_H} + \vartheta C_{EV} + \mu \right) \right) \|V_{c1} - V_{c2}\| \\
&= \left( (1 - \xi) \beta \omega \sup_{0 \leq t \leq S} \left\| \frac{A_c}{N_H} \right\| + (1 - \xi) \beta \sup_{0 \leq t \leq S} \left\| \frac{J_u}{N_u} \right\| \right. \\
&\quad \left. + (1 - \xi) \beta \varrho_v \sup_{0 \leq t \leq S} \left\| \frac{J_v}{N_H} \right\| + \delta S_c + \vartheta C_{EV} + \mu \right) \|V_{c1} - V_{c2}\| \\
&\leq L_M \|V_{c1} - V_{c2}\|,
\end{aligned} \tag{15}$$

where

$$L_M = ((1 - \xi) \beta \omega \varphi_5 + (1 - \xi) \beta \varphi_3 + (1 - \xi) \beta \varrho_v \varphi_4 + \delta S + \vartheta C_{EV} + \mu) > 0.$$

Applying the same method below, we get

$$\begin{aligned}
\|N(A_{c1}) - N(A_{c2})\| &= \left\| \left( -(\gamma_A + \mu) A_c + P \left( \frac{\beta(\omega A_c + J_u + \varrho_v J_v)}{N_H} + \vartheta_{EV} \right) S_c \right) \right\| \\
&\quad + \left\| f(1 - \xi) \left( \left( \frac{\beta(\omega A_c + J_u + \varrho_v J_v)}{N_H} + \vartheta C_{EV} \right) A_{c1} \right) \right\| \\
&\quad - \left\| \left( -(\gamma_A + \mu) A_c + P \left( \frac{\beta(\omega A_c + J_u + \varrho_v J_v)}{N_H} + \vartheta C_{EV} \right) S_c \right) \right\| \\
&\quad + \left\| f(1 - \xi) \left( \left( \frac{\beta(\omega A_c + J_u + \varrho_v J_v)}{N_H} + \vartheta C_{EV} \right) A_{c2} \right) \right\| \\
&= (\gamma_A + \mu) \|A_{c1} - A_{c2}\| \\
&\leq L_N \|A_{c1} - A_{c2}\|,
\end{aligned} \tag{16}$$

where

$$L_N = (\gamma_A \varphi_5 + \mu \varphi_3) > 0.$$

$$\begin{aligned}
\|O(J_{u1}) - O(J_{u2})\| &= \left\| (1 - P) \left( \frac{\beta(\omega A_c + J_u + \varrho_v J_v)}{N_H} + \vartheta C_{EV} \right) S_c - ((\gamma_{JU} + d_{JU} + \mu)) J_{u1} \right. \\
&\quad \left. - (1 - P) \left( \frac{\beta(\omega A_c + J_u + \varrho_v J_v)}{N_H} + \vartheta C_{EV} \right) S_c - ((\gamma_{JU} + d_{JU} + \mu)) J_{u2} \right\| \\
&\leq L_O \|J_{u1} - J_{u2}\|,
\end{aligned} \tag{17}$$

where

$$L_O = (\gamma_{JU} \varphi_1 + d_{JU} \varphi_2 + \mu) > 0.$$

$$\begin{aligned}
\|P(J_{v1}) - P(J_{v2})\| &= \left\| (1-f)(1-\xi) \left( \frac{\beta(\omega A_c + J_u + \varrho_v J_v)}{N_H} + \vartheta C_{EV} \right) S_c - (\gamma_{JV} + d_{JV} + \mu) J_{v1} \right. \\
&\quad \left. - (1-f)(1-\xi) \left( \frac{\beta(\omega A_c + J_u + \varrho_v J_v)}{N_H} + \vartheta C_{EV} \right) S_c - ((\gamma_{JV} + d_{JV} + \mu) J_{v2}) \right\| \\
&\leq L_P \|J_{v1} - J_{v2}\|, \tag{18}
\end{aligned}$$

where

$$L_P = (\gamma_{JV} \varphi_2 + d_{JV} \varphi_3 + \mu) > 0.$$

$$\begin{aligned}
\|V(R_1) - V(R_2)\| &= \|\gamma_A A + \gamma_U J_U + \gamma_V J_V - (\mu) R_1 - (\gamma_A A + \gamma_U J_U + \gamma_V J_V - (\mu) R_2)\| \\
&\leq L_V \|R_1 - R_2\|, \tag{19}
\end{aligned}$$

where

$$L_V = (\mu) > 0.$$

$$\begin{aligned}
\|Z(C_{EV1}) - Z(C_{EV2})\| &= \|\chi_1 A_c + \chi_2 J_u + \chi_3 J_v - (\mu_{EV}) C_{EV1} - (\chi_1 A_c + \chi_2 J_u + \chi_3 J_v - (\mu_{EV})) C_{EV2}\| \\
&\leq L_Z \|C_{EV1} - C_{EV2}\|. \tag{20}
\end{aligned}$$

where

$$L_Z = (\mu_{EV}) > 0.$$

**Theorem 2** If  $(L_L, L_M, L_N, L_O, L_P, L_V, L_Z) \frac{\Gamma(1-\psi) \sin(\pi\psi) \Gamma^\psi}{\psi\pi} < 1$ , it follows that the fractional model (4)- (5) has a unique solution on  $[0, b]$  where  $(L, M, N, O, P, V, Z) : [0, b] \times \mathbb{R} \rightarrow \mathbb{R}$  are presumed to be continuous meeting the Lipschitz condition.

**Proof** Observe the mapping below  $\eta : \mathbb{H}^1([0, b], \mathbb{R}) \rightarrow \mathbb{H}^1([0, b], \mathbb{R})$ , with a well defined  $\eta$  in  $(L, M, N, O, P, V, Z) : [0, b] \times \mathbb{R} \rightarrow \mathbb{R}$ . Using (15)-(20) and for all  $((S_{c1}, S_{c2}), (V_{c1}, V_{c2}), (A_{c1}, A_{c2}), (J_{u1}, J_{u2}), (J_{v1}, J_{v2}), (R_1, R_2), (C_{EV1}, C_{EV2}), \in \mathbb{H}^1([0, b], \mathbb{R})$  and  $0 \leq t \leq S$  we get

$$\begin{aligned}
\|\eta(S_{c1}(t)) - \eta(S_{c2}(t))\| &= \left\| S_c(0) + \frac{1}{\Gamma(\psi)} \int_0^t (t-\zeta)^{\psi-1} L(\zeta, S_{c1}(\zeta)) d\zeta \right\| \\
&\quad - \left\| \left( S_c(0) + \frac{1}{\Gamma(\psi)} \int_0^t (t-\zeta)^{\psi-1} L(\zeta, S_{c2}(\zeta)) d\zeta \right) \right\| \tag{21} \\
&\leq \frac{1}{\Gamma(\psi)} \int_0^t (t-\zeta)^{\psi-1} \|L(\zeta, S_{c1}(\zeta)) - L(\zeta, S_{c2}(\zeta))\| d\zeta \\
&\leq \frac{L_L}{\Gamma(\psi)} \int_0^t (t-\zeta)^{\psi-1} \|S_{c1}(\zeta) - S_{c2}(\zeta)\| d\zeta \\
&\leq L_L \left( \frac{\Gamma(1-\psi) \sin(\pi\psi) S^\psi}{\psi\pi} \right) \|S_{c1} - S_{c2}\|_{\mathbb{H}^1}.
\end{aligned}$$

Similar process yields

$$\begin{aligned}
 \|\eta(V_{c1}(t)) - \eta(V_{c2}(t))\| &\leq L_M \left( \frac{\Gamma(1-\psi) \sin(\pi\psi) S^\psi}{\psi\pi} \right) \|V_{c1} - V_{c2}\|_{\mathbb{H}^1}, \\
 \|\eta(A_{c1}(t)) - \eta(A_{c2}(t))\| &\leq L_N \left( \frac{\Gamma(1-\psi) \sin(\pi\psi) S^\psi}{\psi\pi} \right) \|A_{c1} - A_{c2}\|_{\mathbb{H}^1}, \\
 \|\eta(J_{u1}(t)) - \eta(J_{u2}(t))\| &\leq L_O \left( \frac{\Gamma(1-\psi) \sin(\pi\psi) S^\psi}{\psi\pi} \right) \|J_{u1} - J_{u2}\|_{\mathbb{H}^1}, \\
 \|\eta(J_{v1}(t)) - \eta(J_{v2}(t))\| &\leq L_P \left( \frac{\Gamma(1-\psi) \sin(\pi\psi) S^\psi}{\psi\pi} \right) \|J_{v1} - J_{v2}\|_{\mathbb{H}^1}, \\
 \|\eta(R_1(t)) - \eta(R_2(t))\| &\leq L_V \left( \frac{\Gamma(1-\psi) \sin(\pi\psi) S^\psi}{\psi\pi} \right) \|R_1 - R_2\|_{\mathbb{H}^1}, \\
 \|\eta(C_{EV1}(t)) - \eta(C_{EV2}(t))\| &\leq L_Z \left( \frac{\Gamma(1-\psi) \sin(\pi\psi) S^\psi}{\psi\pi} \right) \|C_{EV1} - C_{EV2}\|_{\mathbb{H}^1}.
 \end{aligned} \tag{22}$$

The condition clearly shows that  $(L_L, L_M, L_N, L_O, L_P, L_V, L_Z) \frac{\Gamma(1-\psi) \sin(\pi\psi) S^\psi}{\psi\pi} < 1$ , the parameter  $\eta$  is a contraction mapping and application of the Banach contraction mapping principle, signifying that the parameter  $\eta$  has a unique fixed point in  $0 \leq t \leq S$ . ■

Using the theorems of Schauder's fixed point, the existence of solutions of fractional model (4)- (5) shall be considered.

**Theorem 3** Assuming that  $(L, M, N, O, P, V, Z) : [0, b] \times \mathbb{R} \rightarrow \mathbb{R}$  are continuous and that there is a constants  $(L_{F1}, L_{G1}, L_{H1}, L_{K1}, L_{Q1}, L_{U1}, L_{W1}) > 0$

so that

$\|F(t, S_c)\| \leq L_{F1} (d + \|S_c\|)$ ,  $\|G(t, V_c)\| \leq L_{G1} (d + \|V_c\|)$ ,  $\|H(t, A_c)\| \leq L_{H1} (d + \|A_c\|)$ ,  
 $\|K(t, J_u)\| \leq L_{K1} (d + \|J_u\|)$ ,  $\|Q(t, J_v)\| \leq L_{Q1} (d + \|J_v\|)$ ,  $\|U(t, R)\| \leq L_{U1} (d + \|R\|)$ ,  
 $\|W(t, C_{EV})\| \leq L_{W1} (d + \|C_{EV}\|)$ , with  $0 < d \leq 1$  as an arbitrary number, it follows that (4)- (5) possesses a minimum of one solution.

**Proof** From (22), it is clear that the operator  $\eta$  is continuous. Thus let  $\{S_c^{n+1}\}_\infty, \{V_c^{n+1}\}_\infty, \{A_c^{n+1}\}_\infty, \{J_u^{n+1}\}_\infty, \{J_v^{n+1}\}_\infty, \{R^{n+1}\}_\infty, \{C_{EV}^{n+1}\}_\infty$ , be sequences so that  $S_c^{n+1} \rightarrow S_c^n, V_c^{n+1} \rightarrow V_c^n, A_c^{n+1} \rightarrow A_c^n, J_u^{n+1} \rightarrow J_u^n, J_v^{n+1} \rightarrow J_v^n, R^{n+1} \rightarrow R^n, C_{EV}^{n+1} \rightarrow C_{EV}^n$  in  $\mathbb{H}^1([0, b], \mathbb{R})$ . Then for every  $0 \leq t \leq S$  we get

$$\begin{aligned}
 \|\eta S_c^{n+1}(t) - \eta S_c^n(t)\| &= \frac{1}{\Gamma(\psi)} \left\| \int_0^t (t-\zeta)^{\psi-1} F(\zeta, S_c^{n+1}(\zeta)) d\zeta - \int_0^t (t-\zeta)^{\psi-1} F(\zeta, S_c^n(\zeta)) d\zeta \right\|, \\
 &\leq \frac{1}{\Gamma(\psi)} \int_0^h (t-\zeta)^{\psi-1} \|F(\zeta, S_c^{n+1}(\zeta)) - F(\zeta, S_c^n(\zeta))\| d\zeta, \\
 &\leq \frac{L_{F1} S^\psi}{\Gamma(\psi+1)} \|S_c^{n+1} - S_c^n\|, \\
 &\leq L_{F1} \left( \frac{\Gamma(1-\psi) \sin(\pi\psi) S^\psi}{\psi\pi} \right) \|S_c^{n+1} - S_c^n\|_{\mathbb{H}^1},
 \end{aligned} \tag{23}$$

where  $\|S_c^{n+1} - S_c^n\|_{\mathbb{H}^1} \rightarrow 0$  as  $n \rightarrow \infty$ .

Following the method of solution, we have

$$\begin{aligned} \|\eta V_c^{n+1}(t) - \eta V_c^n(t)\| &\leq L_{G1} \left( \frac{\Gamma(1-\psi) \sin(\pi\psi) S^\psi}{\psi\pi} \right) \|V_c^{n+1} - V_c^n\|_{\mathbb{H}^1}, \\ \|\eta A_c^{n+1}(t) - \eta A_c^n(t)\| &\leq L_{H1} \left( \frac{\Gamma(1-\psi) \sin(\pi\psi) S^\psi}{\psi\pi} \right) \|A_c^{n+1} - A_c^n\|_{\mathbb{H}^1}, \\ \|\eta J_u^{n+1}(t) - \eta J_u^n(t)\| &\leq L_{K1} \left( \frac{\Gamma(1-\psi) \sin(\pi\psi) T^\psi}{\psi\pi} \right) \|J_u^{n+1} - J_u^n\|_{\mathbb{H}^1}, \\ \|\eta J_v^{n+1}(t) - \eta J_v^n(t)\| &\leq L_{Q1} \left( \frac{\Gamma(1-\psi) \sin(\pi\psi) S^\psi}{\psi\pi} \right) \|J_v^{n+1} - J_v^n\|_{\mathbb{H}^1}, \\ \|\eta R^{n+1}(t) - \eta R^n(t)\| &\leq L_{U1} \left( \frac{\Gamma(1-\psi) \sin(\pi\psi) S^\psi}{\psi\pi} \right) \|R^{n+1} - R^n\|_{\mathbb{H}^1}, \\ \|\eta C_{ev}^{n+1}(t) - \eta C_{ev}^n(t)\| &\leq L_{W1} \left( \frac{\Gamma(1-\psi) \sin(\pi\psi) S^\psi}{\psi\pi} \right) \|C_{ev}^{n+1} - C_{ev}^n\|_{\mathbb{H}^1}, \end{aligned}$$

where  $\|V_c^{n+1} - V_c^n\|_{\mathbb{H}^1} \rightarrow 0$ ,  $\|A_c^{n+1} - A_c^n\|_{\mathbb{H}^1} \rightarrow 0$ ,  $\|J_u^{n+1} - J_u^n\|_{\mathbb{H}^1} \rightarrow 0$ ,  $\|J_v^{n+1} - J_v^n\|_{\mathbb{H}^1} \rightarrow 0$ ,  $\|R^{n+1} - R^n\|_{\mathbb{H}^1} \rightarrow 0$ ,  $\|C_{ev}^{n+1} - C_{ev}^n\|_{\mathbb{H}^1} \rightarrow 0$ , Hence, the operator  $\eta$  is continuous. ■

Next we show that the operator  $\eta$  is a one-to-one bounded set of  $\mathbb{H}^1([0, b], \mathbb{R})$ . Therefore, for every  $S_c \in M_{S_c}$ ,  $V_c \in M_{V_c}$ ,  $A_c \in M_{A_c}$ ,  $J_u \in M_{J_u}$ ,  $J_v \in M_{J_v}$ ,  $R \in M_R$ ,  $C_{ev} \in M_{C_{ev}}$ , also for  $y > 0$ , there is a corresponding value  $z > 0$  where  $\|\eta S_c\| \leq z$ ,  $\|\eta A_c\| \leq z$ ,  $\|\eta V_c\| \leq z$ ,  $\|\eta J_u\| \leq z$ ,  $\|\eta J_v\| \leq z$ ,  $\|\eta R\| \leq z$ ,  $\|\eta C_{ev}\| \leq z$ . The subset of Banach space of all continuous functions on the interval  $0 \leq t \leq S$  are given as follows

$$B_S = \{S_c \in \mathbb{H}^1([0, b], \mathbb{R}) : \|S_c\| \leq y\}, \quad M_{V_c} = \{V \in \mathbb{H}^1([0, b], \mathbb{R}) : \|V_c\| \leq y\},$$

$$M_{A_c} = \{A_c \in \mathbb{H}^1([0, b], \mathbb{R}) : \|A_c\| \leq y\}, \quad M_{J_u} = \{J_u \in \mathbb{H}^1([0, b], \mathbb{R}) : \|J_u\| \leq y\},$$

$$M_{J_v} = \{J_v \in \mathbb{H}^1([0, b], \mathbb{R}) : \|J_v\| \leq y\}, \quad M_R = \{R \in \mathbb{H}^1([0, b], \mathbb{R}) : \|R\| \leq y\},$$

$$B_{C_{ev}} = \{C_{ev} \in \mathbb{H}^1([0, b], \mathbb{R}) : \|C_{ev}\| \leq y\}.$$

Thus for any  $0 \leq t \leq S$ ,

$$\begin{aligned} \|\eta S_c\| &\leq \|S_c(0)\| + \frac{1}{\Gamma(\psi)} \int_0^t (t-\zeta)^{\psi-1} \|F(\zeta, S_c(\zeta))\| d\zeta \\ &\leq \|S(0)\| + \frac{\|F(\zeta, S_c(\zeta))\|}{\Gamma(\psi)} \int_0^t (t-\zeta)^{\psi-1} d\zeta \\ &\leq \|S(0)\| + L_{F1} (d + \|S_b\|) \left( \frac{\Gamma(1-\psi) \sin(\pi\psi) S^\psi}{\psi\pi} \right) \\ &\leq \|S(0)\| + L_{F1} (d + y) \left( \frac{\Gamma(1-\psi) \sin(\pi\psi) S^\psi}{\psi\pi} \right) = z. \end{aligned}$$

Applying the same method of solution, we have the following set of solutions.

$$\begin{aligned}\|\eta V_c\| &\leq \|V(0)\| + L_{G1} (d + y) \left( \frac{\Gamma(1 - \psi) \sin(\pi\psi) S^\psi}{\psi\pi} \right), \\ \|\eta A_c\| &\leq \|A(0)\| + L_{H1} (d + y) \left( \frac{\Gamma(1 - \psi) \sin(\pi\psi) S^\psi}{\psi\pi} \right), \\ \|\eta J_u\| &\leq \|J_u(0)\| + L_{K1} (d + y) \left( \frac{\Gamma(1 - \psi) \sin(\pi\psi) S^\psi}{\psi\pi} \right), \\ \|\eta J_v\| &\leq \|J_v(0)\| + L_{Q1} (d + y) \left( \frac{\Gamma(1 - \psi) \sin(\pi\psi) S^\psi}{\psi\pi} \right), \\ \|\eta R\| &\leq \|R(0)\| + L_{U1} (d + y) \left( \frac{\Gamma(1 - \psi) \sin(\pi\psi) S^\psi}{\psi\pi} \right), \\ \|\eta C_{ev}\| &\leq \|C_{ev}(0)\| + L_{W1} (d + y) \left( \frac{\Gamma(1 - \psi) \sin(\pi\psi) S^\psi}{\psi\pi} \right).\end{aligned}$$

Let  $\Phi$  maps bounded set together with equal continuous sets in  $\mathbb{H}^1([0, b], \mathbb{R})$ . Assuming that  $0 \leq t_1 \leq t_2 \leq S$ ,  $S_c \in M_{S_c}$ ,  $V_c \in M_{V_c}$ ,  $A_c \in M_{A_c}$ ,  $J_u \in M_{J_u}$ ,  $J_v \in M_{J_v}$ ,  $R \in M_R$ ,  $C_{ev} \in M_{C_{ev}}$ , with  $t_1, t_2 \in [0, b]$ , it follows that

$$\begin{aligned}\|\eta S_c(t_1) - \eta S_c(t_2)\| &= \frac{1}{\Gamma(\psi)} \left\| \int_0^{t_1} (t_1 - \zeta)^{\psi-1} F(\zeta, S_c(\zeta)) - \int_0^{t_2} (t_2 - \zeta)^{\psi-1} F(\zeta, S_c(\zeta)) \right\| d\zeta \\ &\leq \frac{1}{\Gamma(\psi)} \left\| \int_0^{t_1} \left( (t_1 - \zeta)^{\psi-1} - (t_2 - \zeta)^{\psi-1} \right) F(\zeta, S_c(\zeta)) d\zeta \right\| \\ &\quad + \frac{1}{\Gamma(\psi)} \left\| \int_{t_1}^{t_2} (t_2 - \zeta)^{\psi-1} F(\zeta, S_c(\zeta)) d\zeta \right\| \\ &\leq \frac{L_{F1} (d + y)}{\Gamma(\psi)} \left\| \int_0^{t_1} \left( (t_1 - \zeta)^{\psi-1} - (t_2 - \zeta)^{\psi-1} \right) d\zeta + \int_{t_1}^{t_2} (t_2 - \zeta)^{\psi-1} d\zeta \right\| \\ &\leq \left( \frac{L_{F1} (d + y) \Gamma(1 - \psi) \sin(\pi\psi)}{\psi\pi} \right) (t_1^\psi - t_2^\psi + 2(t_2 - t_1)^\psi).\end{aligned}$$

Applying the same method of solution, we have the following

$$\begin{aligned}\|\eta V_c(t_1) - \eta V_c(t_2)\| &\leq \left( \frac{L_{G1} (d + y) \Gamma(1 - \psi) \sin(\pi\psi)}{\psi\pi} \right) (t_1^\psi - t_2^\psi + 2(t_2 - t_1)^\psi), \\ \|\eta A_c(t_1) - \eta A_c(t_2)\| &\leq \left( \frac{L_{H1} (d + y) \Gamma(1 - \psi) \sin(\pi\psi)}{\psi\pi} \right) (t_1^\psi - t_2^\psi + 2(t_2 - t_1)^\psi), \\ \|\eta J_u(t_1) - \eta J_u(t_2)\| &\leq \left( \frac{L_{K1} (d + y) \Gamma(1 - \psi) \sin(\pi\psi)}{\psi\pi} \right) (t_1^\psi - t_2^\psi + 2(t_2 - t_1)^\psi), \\ \|\eta J_v(t_1) - \eta J_v(t_2)\| &\leq \left( \frac{L_{Q1} (d + y) \Gamma(1 - \psi) \sin(\pi\psi)}{\psi\pi} \right) (t_1^\psi - t_2^\psi + 2(t_2 - t_1)^\psi), \\ \|\eta R(t_1) - \eta R(t_2)\| &\leq \left( \frac{L_{U1} (d + y) \Gamma(1 - \psi) \sin(\pi\psi)}{\psi\pi} \right) (t_1^\psi - t_2^\psi + 2(t_2 - t_1)^\psi), \\ \|\eta C_{ev}(t_1) - \eta C_{ev}(t_2)\| &\leq \left( \frac{L_{W1} (d + y) \Gamma(1 - \psi) \sin(\pi\psi)}{\psi\pi} \right) (t_1^\psi - t_2^\psi + 2(t_2 - t_1)^\psi).\end{aligned}$$

As  $t_1$  approaches  $t_2$ , the right-hand side of the inequalities approaches zero. The operator  $\eta$  is proven to be a continuous function using the Arzola-Ascoli theorem. Hitherto, the fact that  $\eta$  maps bounded sets together with another set has been shown. In addition to that, the operator is also continuous. Lastly, we would prove that  $R(\eta) = \{(S_c, V_c, A_c, J_u, J_v, R, C_{ev}) \in \mathbb{H}^1([0, b], \mathbb{R}) : (S_c, V_c, A_c, J_u, J_v, R, C_{ev}) = \Lambda(S_c, V_c, A_c, J_u, J_v, R, C_{ev})\}$  is bounded for some  $\Lambda \in (0, 1)$  using Lemma (1). Assuming that  $(S_c, V_c, A_c, J_u, J_v, R, C_{ev}) \in R(\eta)$ , so that  $(S_c, V_c, A_c, J_u, J_v, R, C_{ev}) = \Lambda\eta(S_c, V_c, A_c, J_u, J_v, R, C_{ev})$ , it follows that for every  $t \in [0, b]$  gives

$$\begin{aligned} \|S_c(t)\| &\leq S_c(0) + \frac{1}{\Gamma(\psi)} \int_0^t (t-\zeta)^{\psi-1} \|F(\zeta, S_c(\zeta))\| d\zeta \\ &\leq S_c(0) + \frac{L_{F1}}{\Gamma(\psi)} \int_0^t (t-\zeta)^{\psi-1} (d + \|S_c(\zeta)\|) d\zeta \\ &\leq S_c(0) + \frac{cL_{F1}}{\Gamma(\psi)} \int_0^t (t-\zeta)^{\psi-1} d\zeta + \frac{L_{F1}}{\Gamma(\psi)} \int_0^t (t-\zeta)^{\psi-1} \|S_c(\zeta)\| d\zeta \\ &\leq S_c(0) + \left( L_{F1} \frac{\Gamma(1-\psi) \sin(\pi\psi) S^\psi}{\psi\pi} \right) + \left( \frac{L_{F1}\Gamma(1-\psi) \sin(\pi\psi)}{\pi} \right) \int_0^t (t-\zeta)^{\psi-1} \|S_c(\zeta)\| d\zeta \\ &\leq \left( S_c(0) + \frac{L_{F1}\Gamma(1-\psi) \sin(\pi\psi) S^\psi}{\psi\pi} E_\psi(L_{F1}T^\psi) \right) < \infty. \end{aligned} \quad (24)$$

As already proven,  $R(\eta)$  is bounded and using Schauder's fixed point theorem, the operator  $\eta$  has a fixed point and hence the solution of the fractional model.

### Basic reproduction number of the model

To get the disease-free equilibrium (DFE) of the model, the right-hand side of the equations of the model (4) is set to zero which is as follows,

$$\xi_0 = (S_c(0), V_c(0), A_c(0), J_u(0), J_v(0), R(0), C_{ev}(0)) = \left( \frac{\Omega}{\delta + \mu}, \frac{\delta\Omega}{\mu(\delta + \mu)}, 0, 0, 0, 0, 0 \right). \quad (25)$$

To get the linear stability of the disease-free equilibrium  $\xi_0$ , we apply the method of the next generation operator on the model (4). The matrix F (of new infection) and the matrix V (of the transfer of infections in and out of the disease compartments), respectively, are as follows

$$F = \begin{pmatrix} \frac{p\beta\omega Q_H}{N_H} & \frac{p\beta Q_H}{N_H} & \frac{p\beta q_v Q_H}{N_H} & p\theta Q_H \\ \frac{(1-p)\beta\omega S_c}{N_H} & \frac{(1-p)\beta S_c}{N_H} & \frac{(1-p)\beta q_v S_c}{N_H} & (1-p)\theta S_c \\ \frac{(1-f)(1-\xi)\beta\omega V_c}{N_H} & \frac{(1-f)(1-\xi)\beta V_c}{N_H} & \frac{(1-f)(1-\xi)\beta q_v V_c}{N_H} & (1-f)(1-\xi)\theta V_c \\ 0 & 0 & 0 & 0 \end{pmatrix},$$

with  $Q_H = S_c + f(1-\xi)V_c$ ,

$$V = \begin{pmatrix} \gamma_A + \mu & 0 & 0 & 0 \\ 0 & \gamma_{iu} + d_{iu} + \mu & 0 & 0 \\ 0 & 0 & \gamma_{iv} + d_{iv} + \mu & 0 \\ -\chi_1 & -\chi_2 & -\chi_3 & \mu_{ev} \end{pmatrix}.$$

Therefore, the basic reproduction number of the fractional order vaccination model for COVID-19 incorporating environmental transmission denoted by  $\mathcal{R}_0 = \max\{\mathcal{R}_{0H}, \mathcal{R}_{0EV}\}$ , where  $\mathcal{R}_{0H}$  is

human to human transmission, and  $\mathcal{R}_{0EV}$  is environment to human transmission, respectively. The associated reproduction numbers are given by

$$\mathcal{R}_{0H} = \frac{\beta\omega (\theta_1\eta_A Q_H + (1-p)S_c^* + V_c^*\eta_v)}{N_H^* G_1 G_2 G_3},$$

and

$$\mathcal{R}_{0EV} = \frac{\beta (\chi_1 + (1-p)S_c^*\chi_2 + V_c^*\chi_3)}{\mu_{EV}},$$

where,

$$G_1 = \gamma_A + \mu, G_2 = \gamma_{Iv} + d_{Iv} + \mu, G_3 = \gamma_{Iv} + d_{Iv} + \mu, Q_H = S_c^* + f(1-\xi)V_c^*, V_c = (1-f)(1-\xi)V_c^*.$$

### Local asymptomatic stability of the disease-free equilibrium

**Theorem 4** *The condition for the DFE,  $N_0$  of the model (4) to be locally asymptotically stable (LAS) is that the reproduction number must be less than 1, i.e  $R_c < 1$ , and unstable when the reproduction number is greater than 1, i.e  $R_c > 1$ .*

**Proof** To get the local stability of the model (4), we carried out the Jacobian matrix of the system (4) and computed it using the value gotten at the disease-free equilibrium given as follows:

$$\begin{pmatrix} -(\mu + \delta) & 0 & \frac{-\beta\omega S_c^*}{N_H^*} & \frac{-\beta S_c^*}{N_H^*} & \frac{-\beta q_v S_c^*}{N_H^*} & 0 & \theta S_c^* \\ \delta & -\mu & \frac{-(1-\xi)\beta\omega V_c^*}{N_H^*} & \frac{-(1-\xi)\beta V_c^*}{N_H^*} & \frac{-(1-\xi)\beta q_v V_c^*}{N_H^*} & 0 & (1-\xi)\theta V_c^* \\ 0 & 0 & \frac{p\beta\omega S_c^* + f(1-\xi)\beta\omega V_c^*}{N_H^*} - G_1 & \frac{p\beta S_c^* + f(1-\xi)\beta V_c^*}{N_H^*} & \frac{p\beta q_v S_c^* + f(1-\xi)\beta q_v V_c^*}{N_H^*} & 0 & p\theta S_c^* + f(1-\xi)\theta V_c^* \\ 0 & 0 & \frac{(1-p)\beta\omega S_c^*}{N_H^*} & \frac{(1-p)\beta S_c^*}{N_H^*} - G_2 & \frac{(1-p)\beta q_v S_c^*}{N_H^*} & 0 & (1-p)\theta S_c^* \\ 0 & 0 & \frac{(1-f)(1-\xi)\beta\omega V_c^*}{N_H^*} & \frac{(1-f)(1-\xi)\beta V_c^*}{N_H^*} & \frac{(1-f)(1-\xi)\beta q_v V_c^*}{N_H^*} - G_3 & 0 & (1-f)(1-\xi)\theta V_c^* \\ 0 & 0 & \gamma_A & \gamma_{Iv} & \gamma_{Iv} & -\mu & 0 \\ 0 & 0 & \chi_1 & \chi_2 & \chi_3 & 0 & -\mu_{EV} \end{pmatrix}.$$

The first four eigenvalues are  $\lambda_1 = -(\mu + \delta)$ ,  $\lambda_2 = -\mu$  (twice),  $\lambda_3 = -\mu_{EV}$ , while the remaining three eigenvalues are obtained from the solutions of the equations below

$$(N_H + (-1 + p)S_H\beta_1) - ((\lambda + G_2)V_H\beta_1\eta_v(1 - R_{0v})) - ((\lambda + G_2)(\lambda + G_3)Q_H\beta_1\eta_A\theta_1(1 - R_{0c})) = 0. \tag{26}$$

Following the method of the Routh-Hurwitz, the above equations will possess roots with negative real parts  $\iff \mathcal{R}_{0H} < 1$  and  $\mathcal{R}_{0EV} < 1$  respectively. Hence, the DFE  $J(N_0)$  is locally asymptotically stable if  $R_0 = \max\{\mathcal{R}_{0H}, \mathcal{R}_{0EV}\} < 1$ .

Epidemiologically, the above result implies that the prevalence of COVID-19 can be eradicated from the population provided  $R_0 < 1$  and if the initial sizes of the population of the model are in the region of attraction of the DFE.

### Generalized Ulam-Hyers-Rassias stability

In this section, the approach by Liu [30] shall be applied to prove that the fractional model is generalized UHR stable. Following [30], the definition below holds:

**Definition 6** *The fractional model (4)- (5) is generalized Ulam-Hyers-Rassias (UHR) stable with regards to  $Y(t) \in \mathbb{H}^1([0, b], \mathbb{R})$  provided there is a real value  $\Sigma_\psi > 0$  so that  $\epsilon > 0$  and for every solution*

$(S_c, V_c, A_c, J_u, J_v, R, C_{ev}) \in \mathbb{H}^1([0, b], \mathbb{R})$  of the inequalities below

$$\left| D_t^\psi S_c(t) - F(t, S_c(t)) \right| \leq Y(t), \quad \left| D_t^\psi V_c(t) - G(t, V_c(t)) \right| \leq Y(t), \quad \left| D_t^\psi A_c(t) - H(t, A_c(t)) \right| \leq Y(t),$$

$$\left| D_t^\psi J_u(t) - K(t, J_u(t)) \right| \leq Y(t), \quad \left| D_t^\psi J_v(t) - Q(t, J_v(t)) \right| \leq Y(t), \quad \left| D_t^\psi R(t) - U(t, R(t)) \right| \leq Y(t),$$

$$\left| D_t^\psi C_{ev}(t) - W(t, C_{ev}(t)) \right| \leq Y(t),$$

there is a solution  $(\bar{S}_c, \bar{V}_c, \bar{A}_c, \bar{J}_u, \bar{J}_v, \bar{R}, \bar{C}_{ev}) \in \mathbb{H}^1([0, b], \mathbb{R})$  of the fractional model (4)-(5) with

$$|S_c(t) - \bar{S}_c(t)| \leq \Sigma_\psi Y(t), \quad |V_c(t) - \bar{V}_c(t)| \leq \Sigma_\psi Y(t), \quad |A_c(t) - \bar{A}_c(t)| \leq \Sigma_\psi Y(t), \quad |J_u(t) - \bar{J}_u(t)| \leq \Sigma_\psi Y(t),$$

$$|J_v(t) - \bar{J}_v(t)| \leq \Sigma_\psi Y(t), \quad |R(t) - \bar{R}(t)| \leq \Sigma_\psi Y(t), \quad |C_{ev}(t) - \bar{C}_{ev}(t)| \leq \Sigma_\psi Y(t).$$

**Theorem 5** The fractional model (4)- (5) is generalized Ulam-Hyers-Rassias stable with regards to  $Y \in \mathbb{H}^1([0, b], \mathbb{R})$  if  $(L_F, L_G, L_H, L_K, L_Q, L_U, L_W) S^\psi < 1$ .

**Proof** From definition (6), let  $Y$  stand for the non-decreasing function of  $t$ , then there is  $\epsilon > 0$  so that

$$\int_0^t (t - \zeta)^{\psi-1} Y(\zeta) d\zeta \leq \epsilon Y(t),$$

for every  $t \in [0, b]$ . The functions  $F, G, H, K, Q, U, W$  according to prove is said to be continuous and

$$(L_F, L_G, L_H, L_K, L_Q, L_U, L_W) > 0$$

meets the Lipschitz condition as seen in the previous part. From Theorem (2), the fractional model (4)- (5) has the unique solution

$$\bar{S}_c(t) = S_c(0) + \frac{1}{\Gamma(\psi)} \int_0^t (t - \zeta)^{\psi-1} F(\zeta, \bar{S}_c(\zeta)) d\zeta.$$

Integrating the inequalities in definition (6) we get

$$\begin{aligned} \left| S_c(t) - S_c(0) - \frac{1}{\Gamma(\psi)} \int_0^t (t - \zeta)^{\psi-1} F(\zeta, S_c(\zeta)) d\zeta \right| &\leq \frac{1}{\Gamma(\psi)} \int_0^t (t - \zeta)^{\psi-1} Y(\zeta) d\zeta \\ &\leq \frac{\epsilon Y(t) \Gamma(1 - \psi) \sin(\pi\psi)}{\pi}. \end{aligned} \quad (27)$$

Using Lemma (1) and Eq. (27), we have the following

$$\begin{aligned}
|S_c(t) - \bar{S}_c(t)| &\leq \left| S_c(t) - \left( S_c(0) + \frac{1}{\Gamma(\psi)} \int_0^t (t-\zeta)^{\psi-1} F(\zeta, \bar{S}_c(\zeta)) d\zeta \right) \right| \\
&\leq \left| S_c(t) - S_c(0) - \left( \frac{1}{\Gamma(\psi)} \int_0^t (t-\zeta)^{\psi-1} F(\zeta, \bar{S}_c(\zeta)) d\zeta + \frac{1}{\Gamma(\psi)} \int_0^t (t-\zeta)^{\psi-1} F(\zeta, S_c(\zeta)) d\zeta \right. \right. \\
&\quad \left. \left. - \frac{1}{\Gamma(\psi)} \int_0^t (t-\zeta)^{\psi-1} F(\zeta, S_c(\zeta)) d\zeta \right) \right| \\
&\leq \left| S_c(t) - S_c(0) - \frac{1}{\Gamma(\psi)} \int_0^t (t-\zeta)^{\psi-1} F(\zeta, S_c(\zeta)) d\zeta \right| \\
&\quad + \frac{1}{\Gamma(\psi)} \int_0^t (t-\zeta)^{\psi-1} |F(\zeta, S_c(\zeta)) - F(\zeta, \bar{S}_c(\zeta))| d\zeta \\
&\leq \frac{\epsilon Y(t) \Gamma(1-\psi) \sin(\pi\psi)}{\pi} + \frac{L_F \Gamma(1-\psi) \sin(\pi\psi)}{\pi} \int_0^t (t-\zeta)^{\psi-1} |S_c(\zeta) - \bar{S}_c(\zeta)| d\zeta \\
&\leq \frac{\epsilon Y(t) \Gamma(1-\psi) \sin(\pi\psi)}{\pi} E_\psi(L_F S^\psi).
\end{aligned}$$

By setting  $\Sigma_\psi = \frac{\epsilon \Gamma(1-\psi) \sin(\pi\psi)}{\pi} E_\psi(L_F S^\psi)$  we have

$$|S_c(t) - \bar{S}_c(t)| \leq \Sigma_\psi Y(t), \quad t \in [0, b].$$

Using the method of solution, we have the following

$$|V_c(t) - \bar{V}_c(t)| \leq \Sigma_\psi Y(t), \quad |A_c(t) - \bar{A}_c(t)| \leq \Sigma_\psi Y(t), \quad |J_u(t) - \bar{J}_u(t)| \leq \Sigma_\psi Y(t),$$

$$|J_v(t) - \bar{J}_v(t)| \leq \Sigma_\psi Y(t), \quad |R(t) - \bar{R}(t)| \leq \Sigma_\psi Y(t), \quad |C_{ev}(t) - \bar{C}_{ev}(t)| \leq \Sigma_\psi Y(t),$$

for every  $t \in [0, b]$ . Therefore, it is concluded that the fractional model is generalized Ulam-Hyers-Rassias stable with regards to  $Y(t)$ . ■

#### 4 Numerical scheme and simulations

On account of the many benefits of the fractional predictor-corrector technique, it is applied in this section to numerically solve the proposed model. The numerical scheme is derived from the Adams-Bashforth linear multi-step method in the Caputo sense [34]. The numerical method's convergence was also a topic of discussion. The entire model (4)-(5) is simulated using the values of the parameters listed in our table 2 in accordance with the demographic and epidemiological data pertinent to the dynamics of COVID-19 incorporating environmental transmission in Nigeria. The total population of Nigeria is roughly 206,139,587, and the average lifespan in Nigeria is 54.69 years [31]. we have that  $\mu = \frac{1}{54.69} \approx 0.0183 \text{ year}^{-1}$  and  $\Omega = \mu \times 200,000,000 \approx 365,6976 \text{ year}^{-1}$ . The initial conditions are put as listed as:  $S_c(0) = 200,000,000, V_c(0) = 5000000, A_c(0) = 5000, J_u(0) = 2000, J_v(0) = 2000, R(0) = 2000, C_{ev}(0) = 2500$ .

Let  $t_k = kh, k = 0, 1, 2, \dots, m$  be the uniform grid points with some integer  $m$  and  $h = T/m$ , which is the grid step size. As a result, (4) reduces to the fractional version of the one-step Adam-Moulton method (Corrector formula) which is obtained by employing piece-wise interpolation with nodes and knots located at  $t_j, j = 0, 1, 2, \dots, k + 1$ ,

$$\begin{aligned}
S_c(t_{r+1}) - S_c(0) &= \frac{g^\psi}{\Gamma(\psi + 2)} \left( \sum_{i=0}^r u_{i,r+1} F(t_i, S_c(t_i)) + F(t_{r+1}, S_c^q(t_{r+1})) \right), \\
V_c(t_{r+1}) - V_c(0) &= \frac{g^\psi}{\Gamma(\psi + 2)} \left( \sum_{i=0}^r u_{i,r+1} G(t_i, V_c(t_i)) + G(t_{r+1}, V_c^q(t_{r+1})) \right), \\
A_c(t_{r+1}) - A_c(0) &= \frac{g^\psi}{\Gamma(\psi + 2)} \left( \sum_{i=0}^r u_{i,r+1} H(t_i, A_c(t_i)) + H(t_{r+1}, A_c^q(t_{r+1})) \right), \\
J_u(t_{r+1}) - J_u(0) &= \frac{g^\psi}{\Gamma(\psi + 2)} \left( \sum_{i=0}^r u_{i,r+1} K(t_i, J_u(t_i)) + K(t_{r+1}, J_u^q(t_{r+1})) \right), \\
J_v(t_{r+1}) - J_v(0) &= \frac{g^\psi}{\Gamma(\psi + 2)} \left( \sum_{i=0}^r u_{i,r+1} Q(t_i, J_v(t_i)) + Q(t_{r+1}, J_v^q(t_{r+1})) \right), \\
R(t_{r+1}) - R(0) &= \frac{g^\psi}{\Gamma(\psi + 2)} \left( \sum_{i=0}^r u_{i,r+1} U(t_i, R(t_i)) + U(t_{r+1}, R^q(t_{r+1})) \right), \\
C_{EV}(t_{r+1}) - C_{EV}(0) &= \frac{g^\psi}{\Gamma(\psi + 2)} \left( \sum_{i=0}^r u_{i,r+1} V(t_i, C_{EV}(t_i)) + W(t_{r+1}, C_{EV}^q(t_{r+1})) \right),
\end{aligned} \tag{28}$$

where the weight  $u_{i,r+1} = \begin{cases} r^{\psi+1} - (r-\psi)(r+1)^\psi, & i = 0. \\ (r-i+2)^{\psi+1} + (r-i)^{\psi+1} - 2(r-i+1)^{\psi+1}, & 1 \leq i \leq r. \\ 1, & i = r+1. \end{cases}$

The predictor formula motivated by the well-known one-step Adam-Bashforth method is given by

$$\begin{aligned}
S_c^q(t_{r+1}) - S_c(0) &= \frac{1}{\Gamma(\psi)} \sum_{i=0}^r v_{i,r+1} F(t_i, S_c(t_i)), \\
V_c^q(t_{r+1}) - V_c(0) &= \frac{1}{\Gamma(\psi)} \sum_{i=0}^r v_{i,r+1} G(t_i, V_c(t_i)), \\
A_c^q(t_{r+1}) - A_c(0) &= \frac{1}{\Gamma(\psi)} \sum_{i=0}^r v_{i,r+1} H(t_i, A_c(t_i)), \\
J_u^q(t_{r+1}) - J_u(0) &= \frac{1}{\Gamma(\psi)} \sum_{i=0}^r v_{i,r+1} K(t_i, J_u(t_i)), \\
J_v^q(t_{r+1}) - J_v(0) &= \frac{1}{\Gamma(\psi)} \sum_{i=0}^r v_{i,r+1} Q(t_i, J_v(t_i)), \\
R^q(t_{r+1}) - R(0) &= \frac{1}{\Gamma(\psi)} \sum_{i=0}^r v_{i,r+1} U(t_i, R(t_i)), \\
C_{EV}^q(t_{r+1}) - C_{EV}(0) &= \frac{1}{\Gamma(\psi)} \sum_{i=0}^r v_{i,r+1} W(t_i, C_{EV}(t_i)),
\end{aligned} \tag{29}$$

where the weight is given by

$$v_{i,r+1} = \psi^{-1} g^\psi \left( (r-i+1)^\psi - (r-i)^\psi \right).$$

### Model fitting

The genetic algorithm method was used to fit the model in accordance with [35], which specifies the values for the parameters under investigation. The above investigation was carried out using the *fmincon* function in the optimization toolbox of MATLAB. Figure 1 presents the fitting of the model 4. It was applied to the weekly total number of COVID-19 cases that had been confirmed in Nigeria between April 1, 2021, and June 10, 2021. The figure demonstrates that the model behaves very similarly to Nigeria's COVID-19 data. The table provides a rough estimate of additional fitting-derived parameters.1.

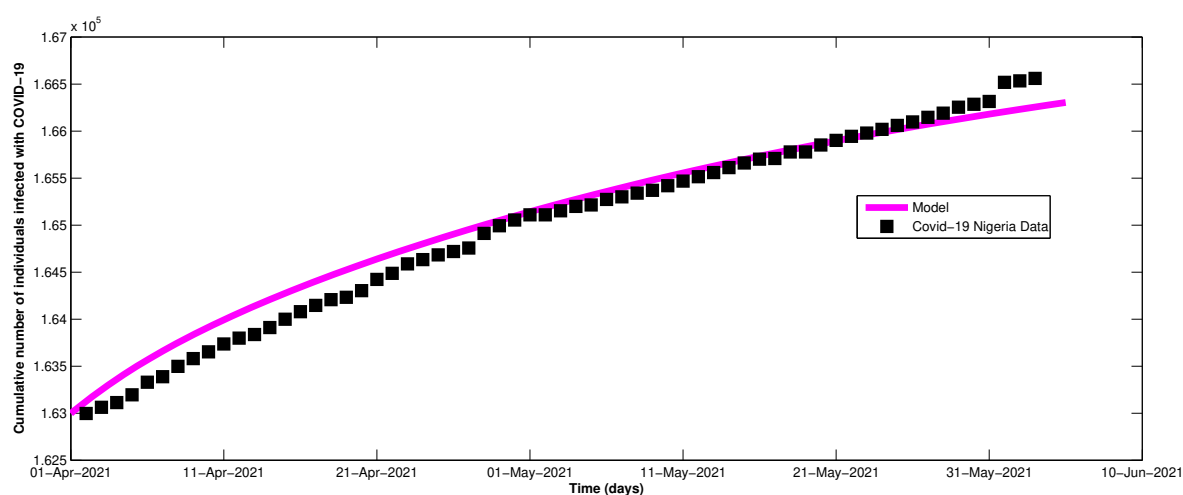


**Figure 1.** Fitting the model to the cumulative number of confirmed COVID-19 cases in Nigeria. All other parameters are as in Table 1

### Impact of different values of fractional order on the model classes

Figure 1 presents simulations of the susceptible class at various fractional orders. During the first 35 days of the simulation, it is observed that the total population grows as the fractional order decreases and that the trend reverses as the fractional order increases. The simulations of the vaccinated class at various fractional orders are shown in Figure 2. A comparative pattern is noticed; The total population rises while the fractional order decreases during the first quarter of the simulation period (35 days). As the fractional grows, the total population then shifts in the opposite direction. The simulations for the Asymptomatic class are shown in Figure 3; For the first quarter of the simulation period, it is observed that the total population does not increase or decrease when the fractional order decreases. By the by, accordingly, it increments and diminishes eventually as the fractional order diminishes. The simulations for the unvaccinated asymptomatic class are shown in Figure 4; it shows that for the initial 30 days of the simulations time frame, a decline in the fractional order value leaves the population unaltered as there was neither an increment nor a diminishing in the complete population. As the fractional order decreased, there was an increase in the total population.

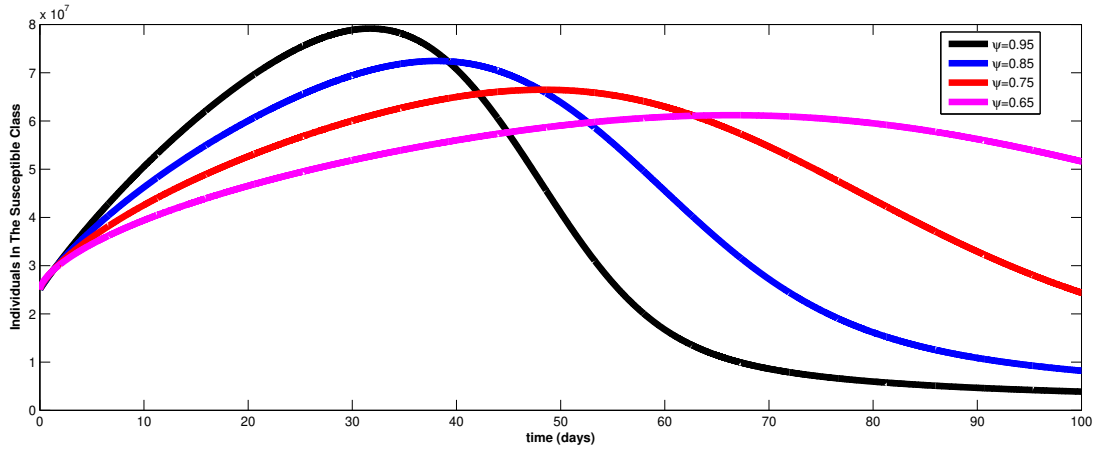


**Figure 2.** Simulations of the Susceptible individuals at different fractional order values. All other parameters as in Table 1

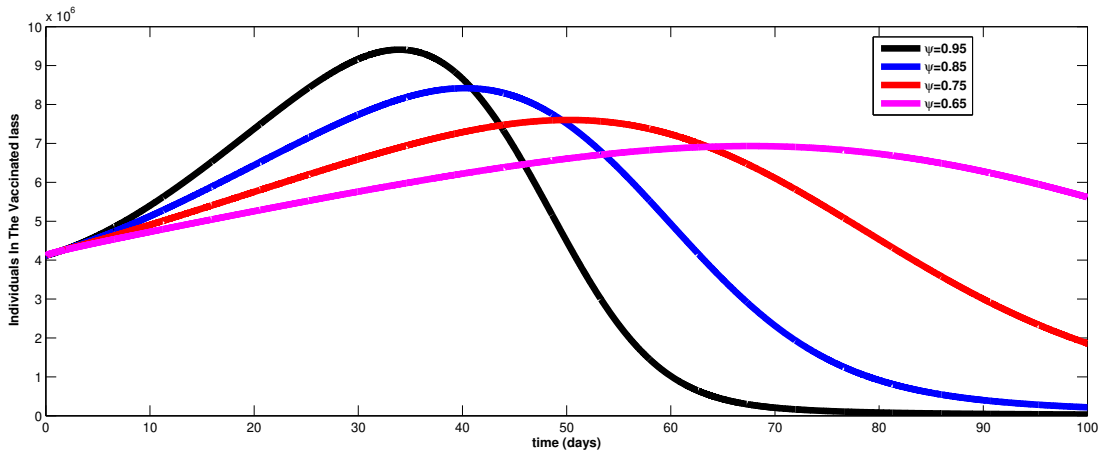


**Figure 3.** Simulations of the Vaccinated individuals at different fractional order values. Using additional parameters from Table 1

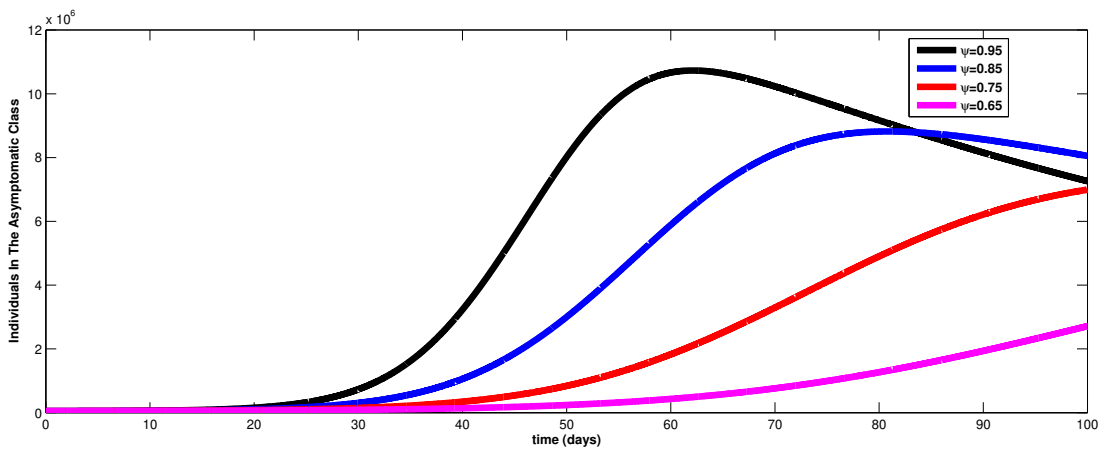


**Figure 4.** Simulations of the Asymptomatic individuals at different fractional order values. Using additional parameters from Table 1

Figure 5 presents the simulations of the vaccinated asymptomatic class; During the first forty days of the simulation, it is observed that the fractional order decreases while the total population increases slightly; After that, the fractional order decreases, resulting in a significant increase in the total population. The simulations for the Recovered class are shown in Figure 6; for the first 40 days of the simulations, it is observed that the total population does not change as the fractional order decreases; rather, it does not increase or decrease. Nonetheless, following a decline in the fractional order, there was an expansion in the complete population. The simulations of the environment's COVID-19 concentration are shown in Figure 7; the simulations demonstrate that as the fractional order decreased, neither an increase nor a decrease in the total population occurred; as a result, the total population increased as the fractional order decreased.

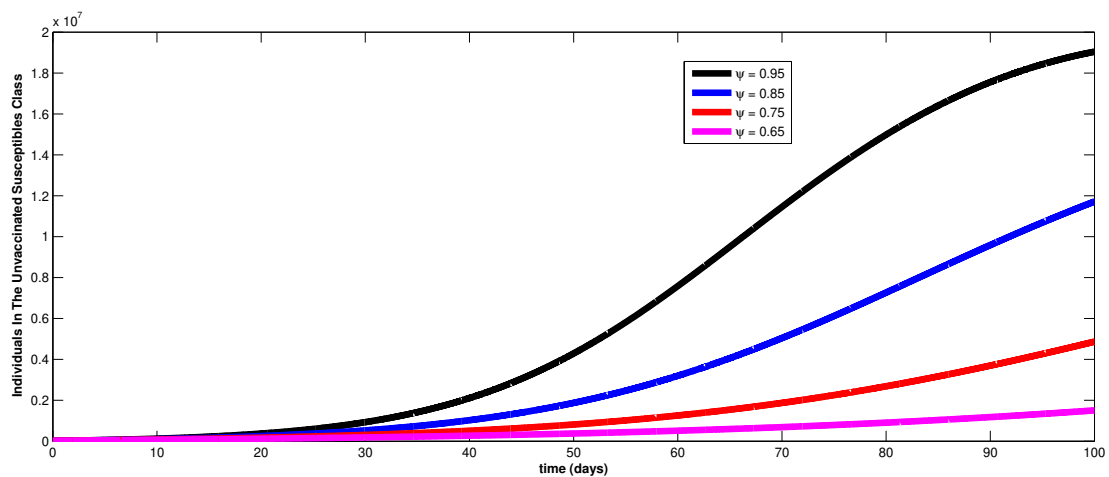


**Figure 5.** Simulations of the unvaccinated susceptible individuals at different fractional order values. Using additional parameters from Table 1

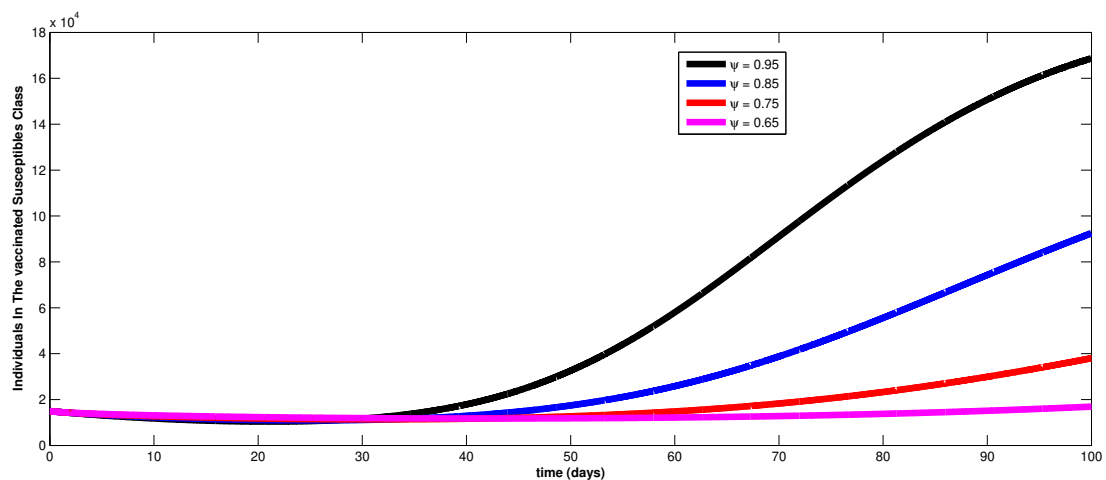


**Figure 6.** Simulations of the vaccinated susceptible individuals at different fractional order values. Using additional parameters from Table 1

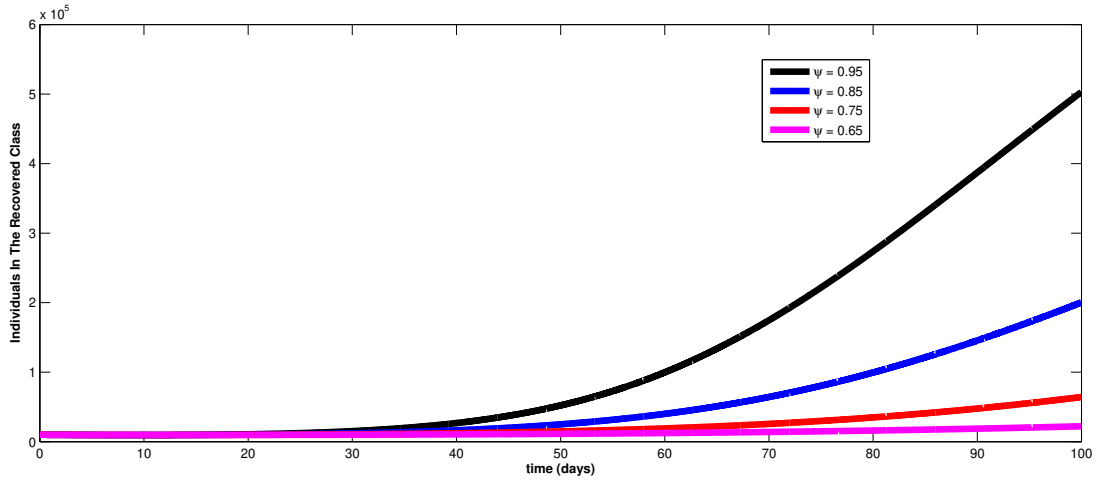


**Figure 7.** Simulations of the Recovered individuals at different fractional order values. Using additional parameters from Table 1

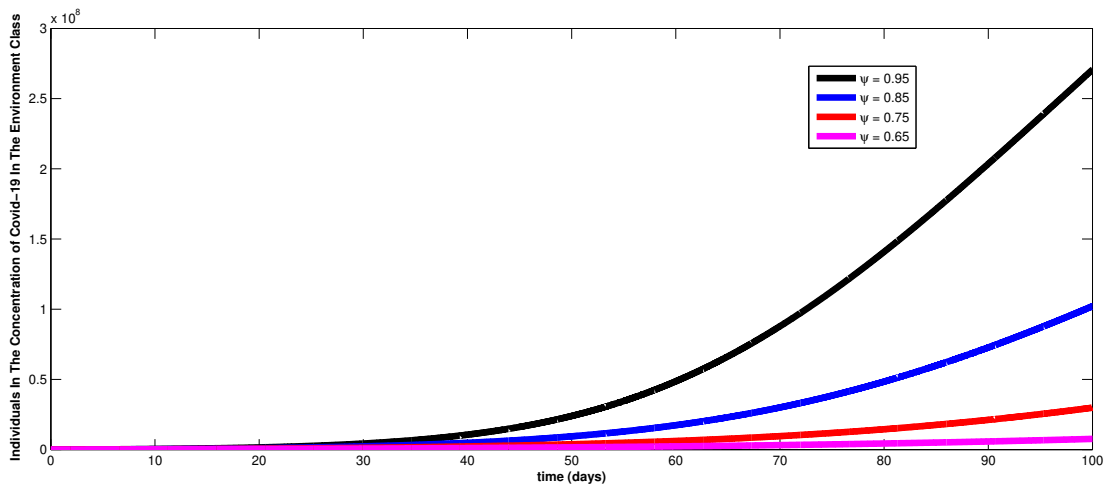


**Figure 8.** Simulations of the concentration of COVID-19 in the environment at different fractional order values. Using additional parameters from Table 1

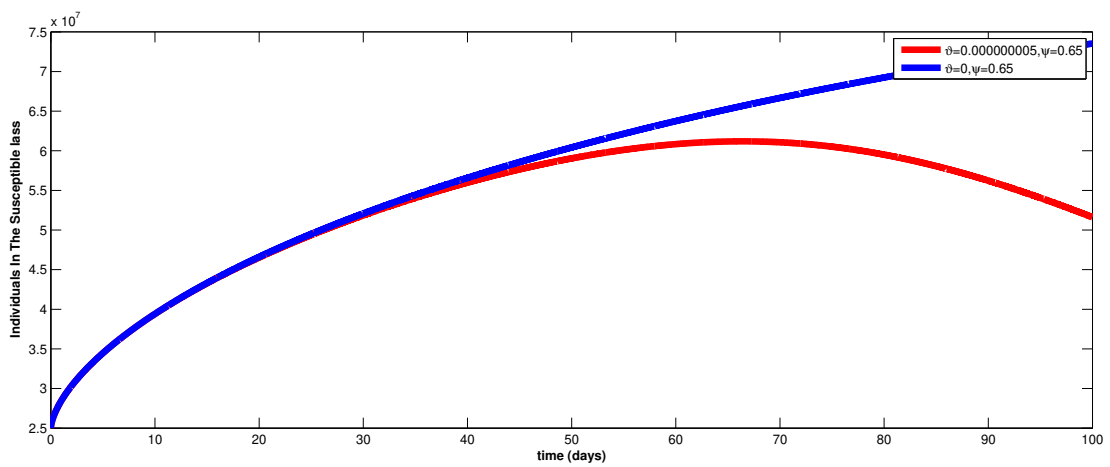


**Figure 9.** Simulation of the susceptible individual in the presence and absence of environmental transmission of COVID-19. Here,  $\psi = 0.65$ . Using additional parameters from Table 1

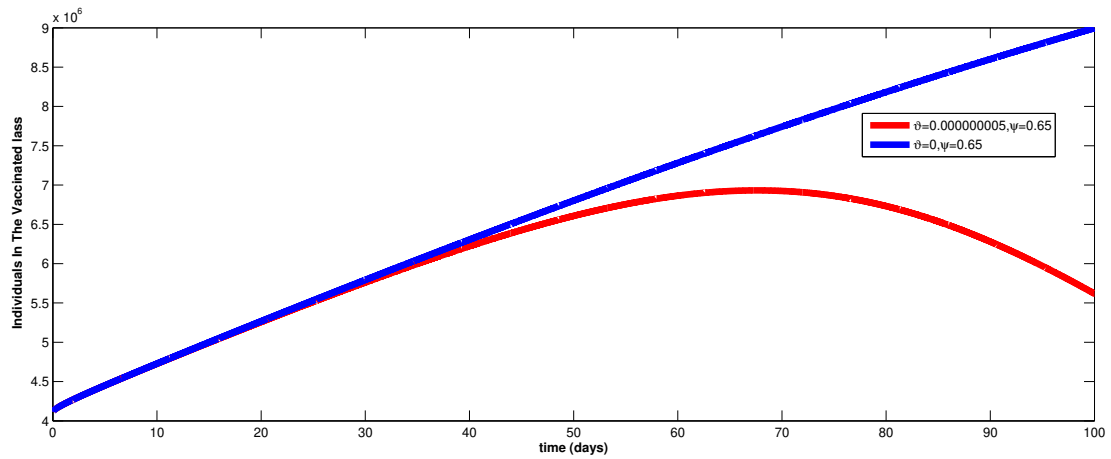


**Figure 10.** Simulation of the vaccinated individual in the presence and absence of environmental transmission of COVID-19. Here,  $\psi = 0.65$ . Using additional parameters from Table 1

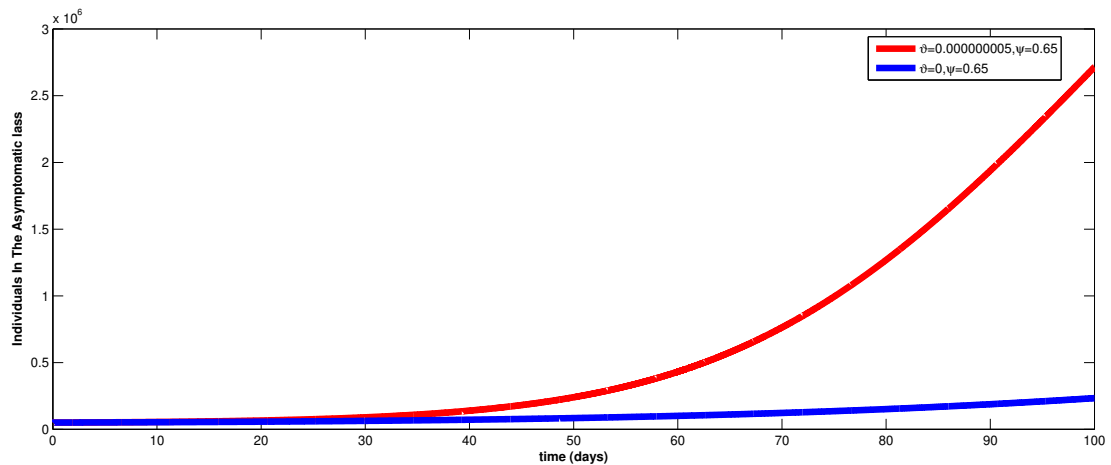


**Figure 11.** Simulation of the asymptomatic susceptible individual in the presence and absence of environmental transmission of COVID-19. Here,  $\psi = 0.65$ . Using additional parameters from table 1

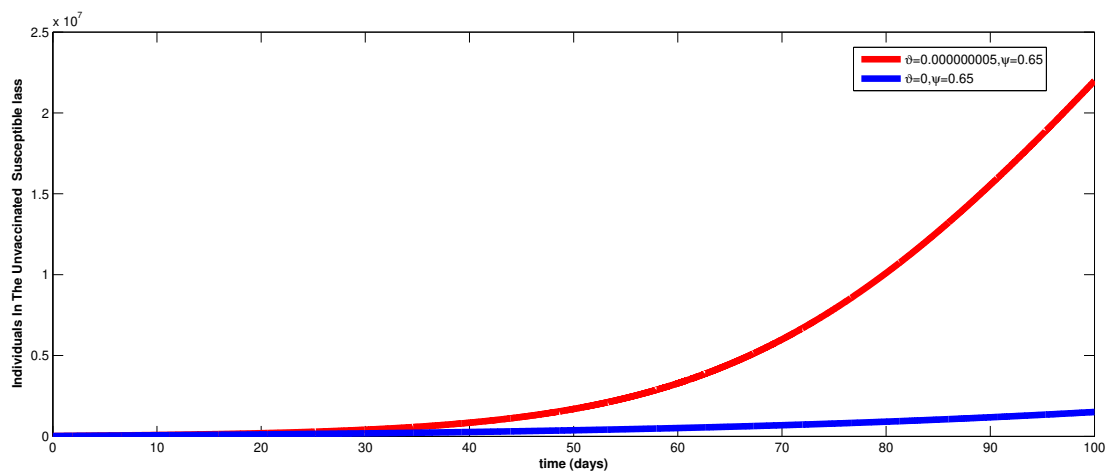


**Figure 12.** Simulation of the unvaccinated susceptible individual in the presence and absence of environmental transmission of COVID-19. Here,  $\psi = 0.65$ . Using additional parameters from Table 1

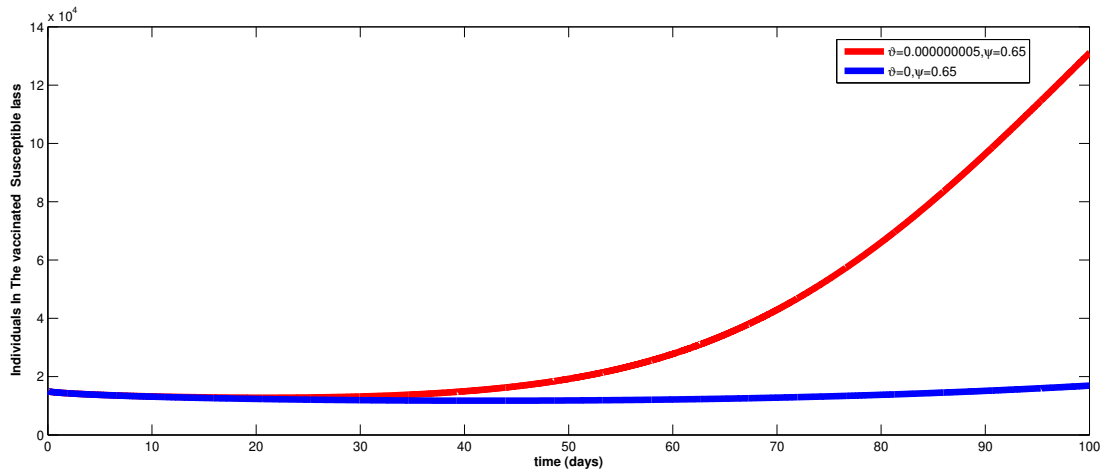


**Figure 13.** Simulation of the vaccinated susceptible individual in the presence and absence of environmental transmission of COVID-19. Here,  $\psi = 0.65$ . Using additional parameters from Table 1

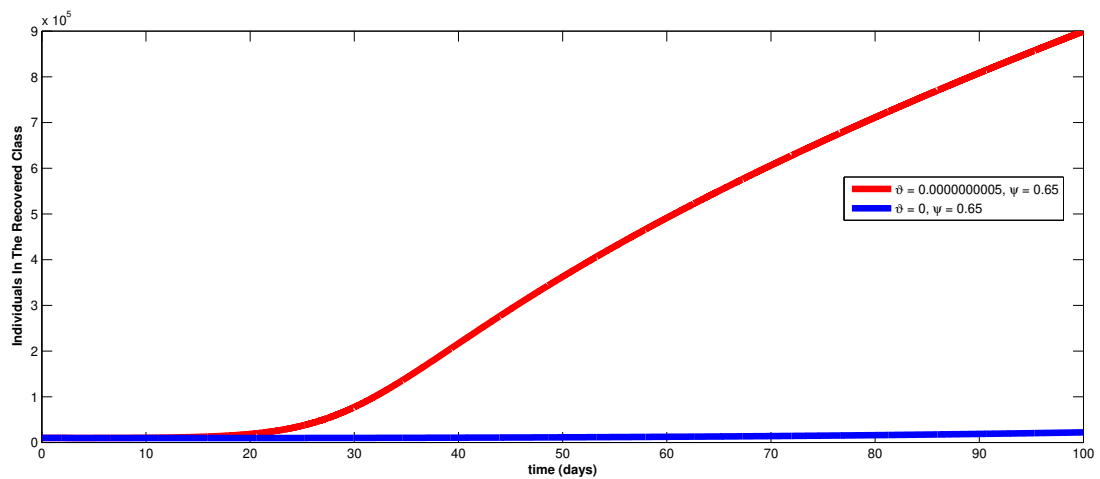


**Figure 14.** Simulation of vaccinated Recovered individual in the presence and absence of environmental transmission of COVID-19. Here,  $\psi = 0.65$ . Using additional parameters from Table 1

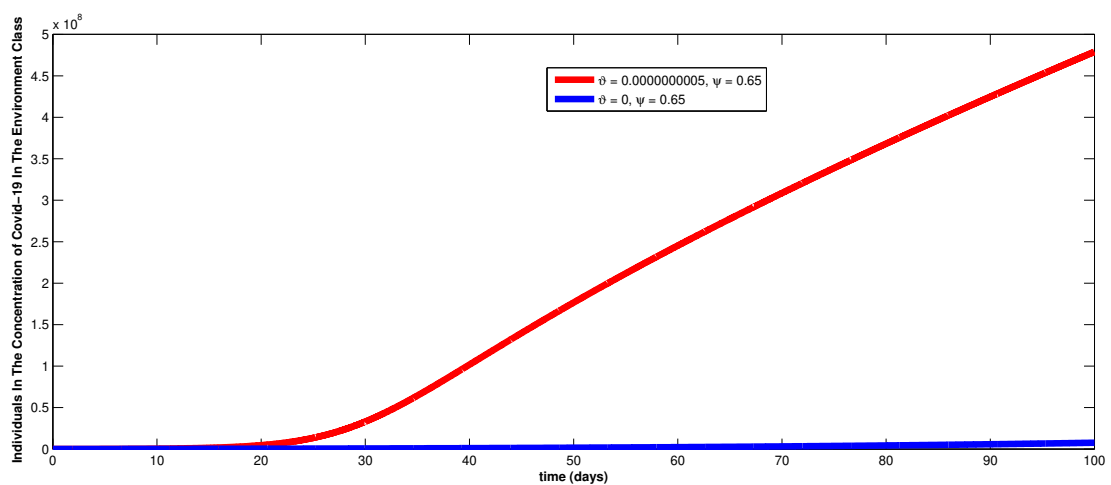


**Figure 15.** Simulation of concentration of COVID-19 in the environment in the presence and absence of environmental transmission of COVID-19. Here,  $\psi = 0.65$ . Using additional parameters from Table 1

## Impact of environmental transmission on the model classes

Figure 8 presents the simulations of the susceptible individuals in the presence and absence of environmental transmission of Coronavirus. It has been carefully observed that when there is no environmental transmission, the population grows because there are no infected people and that is because the population is made up of people who are susceptible. However, the number of asymptomatic individuals exposed to COVID-19 rises as environmental transmission decreases the population.

In Figure 9, the simulations of the vaccinated individuals in the presence and absence of environmental transmission are introduced. When there is no environmental transmission, the population as a whole grows because there is no infection. On the other hand, when there is environmental transmission, the population as a whole shrinks dramatically, leading to an increase in the number of people who are asymptomatic after coming into effective contact with the infected environment. The simulations of the asymptomatic individuals in the presence and absence of environmental transmission are shown in Figure 10.

The shortfall of environmental transmission shows no impact on the absolute population for the initial 40 days of the simulations time frame yet somewhat increments after the primary period, this is on the grounds that the class is as of now an infected class that shows no side effects. The infection grows rather than decreases as a result of environmental transmission; For the first quarter of the simulation, the presence of environmental transmission has no effect on asymptomatic individuals; however, after the first simulation period, the number of symptomatic individuals rises.

In Figure 11, the simulations of the unvaccinated asymptomatic individuals in the presence and absence of environmental transmission are introduced; at the point when there is no environmental transmission, for the principal quarter of the simulations time frame, the people in the class neither increments nor diminishes however marginally expanded after the primary period, this is on the grounds that it is now an infected class, so the shortfall of environmental transmission does not influence the class, yet when there is an environmental transmission, the class stay unaltered for the main quarter of the reproductions time frame yet increments after the primary time of the simulations.

The simulations of the vaccinated asymptomatic individuals in the presence and absence of environmental transmission are shown in Figure 12; at the point when there is no environmental transmission, it somewhat builds the quantity of the asymptomatic individual, yet when there is an environmental transmission, we have a larger number of asymptomatic people. The simulations of the Recovered individuals with and without environmental transmission are shown in Figure 13.

The absence of environmental transmission is observed to have no effect on the class. However, after 20 days of simulation, there are more asymptomatic individuals in the presence of environmental transmission. In Figure 14, the simulations of the concentration of Coronavirus in the environment are introduced. It is observed that when there is no environmental transmission, the class stay unaltered for the initial 20 days of the simulations time frame. At the point when there is environmental transmission, the quantity of the asymptomatic people fundamentally expanded following 20 days.

## 5 Conclusion

The fractional derivative was used to consider and analyze a fractional-order vaccination model for COVID-19 incorporating environmental transmission. The Mittag-Leffler function is used to demonstrate the solutions' positivity and boundedness. The existence and uniqueness of the

model solutions are additionally shown utilizing Banach and Schauder's fixed point theorem. In addition, we demonstrate the Ulam-Hyers-Rassias stability of the fractional-order model. For the locally asymptotically stable system, it was demonstrated that the reproduction number was lower than unity. Numerical simulations were likewise viewed as utilizing information pertinent to Coronavirus cases for Nigeria and fitted to the week-by-week combined number of affirmed cases from April 1, 2021, to June 10, 2021, to look at the effect of various fractional order values on the model classes and the effect of environmental transmission on the model classes.

The highlights of the simulations are as follows:

- (i) As depicted in Figure 2, the fractional-order value decreases with increasing model class population.
- (ii) There is a larger overall population when there is no environmental transmission. The number of people who are asymptomatic rises when there is environmental transmission, as shown in Figure 9.

### Declarations

#### Ethical approval

Not applicable.

#### Consent for publication

Not applicable.

#### Conflicts of interest

The authors declare that they have no conflict of interest.

#### Funding

Not applicable.

#### Author's contributions

A.O.A.: Conceptualization, Software, Formal Analysis, Validation, Visualization, Data Curation, Writing-Original draft. A.O.: Methodology, Supervision, Writing-Review and Editing. S.C.I.: Supervision, Review. All authors discussed the results and contributed to the final manuscript.

#### Acknowledgements

Not applicable.

#### References

- [1] Kahn, J.S. and McIntosh, K. History and recent advances in coronavirus discovery. *The Pediatric Infectious Disease Journal*, 24(11), S223-S227, (2005). [[CrossRef](#)]
- [2] Bhargava HD, WebMD Medical Reference, August 15, (2021).
- [3] WMCH Wuhan Municipal Health and Health Commission's Briefing on the Current Pneumonia Situation in our City, February 1, (2020).
- [4] World Health Organization (WHO), URL: <https://www.who.int/health-topics/coronavirus>, (2021). (Access Date: February 2023).
- [5] Viner, R.M., Mytton, O.T., Bonell, C., Melendez-Torres, G.J., Ward, J., et al. Susceptibility to SARS-CoV-2 infection among children and adolescents compared with adults: a systematic review and meta-analysis. *JAMA Pediatrics*, 175(2), 143-156, (2021). [[CrossRef](#)]

- [6] Koh, W.C., Naing, L., Chaw, L., Rosledzana, M.A., Alikhan, M.F., Jamaludin, S.A., et al. What do we know about SARS-CoV-2 transmission? A systematic review and meta-analysis of the secondary attack rate and associated risk factors. *PLoS one*, 15(10), e0240205, (2020). [[CrossRef](#)]
- [7] <https://www.ncdc.gov.ng/coronavirus>, (2021). (Access Date: November 2022).
- [8] Ahmed, I., Modu, G.U., Yusuf, A., Kumam, P. and Yusuf, I. A mathematical model of Coronavirus Disease (COVID-19) containing asymptomatic and symptomatic classes. *Results in Physics*, 21, 103776, (2021). [[CrossRef](#)]
- [9] Omame, A., Abbas, M. and Onyenegecha, C.P. A fractional-order model for COVID-19 and tuberculosis co-infection using Atangana–Baleanu derivative. *Chaos, Solitons & Fractals*, 153, 111486, (2021). [[CrossRef](#)]
- [10] Bugalia, S., Bajiya, V.P., Tripathi, J.P., Li, M.T. and Sun, G.Q. Mathematical modeling of COVID-19 transmission: the roles of intervention strategies and lockdown. *Mathematical Biosciences and Engineering*, 17(5), 5961-5986, (2020). [[CrossRef](#)]
- [11] Iboi, E.A., Sharomi, O., Ngonghala, C.N., & Gumel, A.B. Mathematical modeling and analysis of COVID-19 pandemic in Nigeria. *Mathematical Biosciences and Engineering*, 17(6), 7192-7220, (2020). [[CrossRef](#)]
- [12] Okuonghae, D. and Omame, A. Analysis of a mathematical model for COVID-19 population dynamics in Lagos, Nigeria. *Chaos, Solitons & Fractals*, 139, 110032, (2020). [[CrossRef](#)]
- [13] Baba, B. A. and Bilgehan, B. Optimal control of a fractional order model for the COVID–19 pandemic. *Chaos, Solitons & Fractals*, 144, 110678, (2021). [[CrossRef](#)]
- [14] Aba Oud, M.A., Ali, A., Alrabaiah, H., Ullah, S., Khan, M.A. and Islam, S. A fractional order mathematical model for COVID-19 dynamics with quarantine, isolation, and environmental viral load. *Advances in Difference Equations*, 2021, 106, (2021). [[CrossRef](#)]
- [15] Rezapour, S., Mohammadi, H. and Samei, M.E. SEIR epidemic model for COVID-19 transmission by Caputo derivative of fractional order. *Advances in Difference Equations*, 2020, 490, (2020). [[CrossRef](#)]
- [16] Baleanu, D., Mohammadi, H. and Rezapour, S. A fractional differential equation model for the COVID-19 transmission by using the Caputo-Fabrizio derivative. *Advances in Difference Equations*, 2020, 229, (2020). [[CrossRef](#)]
- [17] Huang, C., Wang, J., Chen, X. and Cao, J. Bifurcations in a fractional-order BAM neural network with four different delays. *Neural Networks*, 141, 344-354, (2021). [[CrossRef](#)]
- [18] Xu, C., Mu, D., Liu, Z., Pang, Y., Liao, M. and Aouiti, C. New insight into bifurcation of fractional-order 4D neural networks incorporating two different time delays. *Communications in Nonlinear Science and Numerical Simulation*, 118, 107043, (2023). [[CrossRef](#)]
- [19] Xu, C., Liu, Z., Li, P., Yan, J. and Yao, L. Bifurcation mechanism for fractional-order three-triangle multi-delayed neural networks. *Neural Processing Letters*, (2022). [[CrossRef](#)]
- [20] Xu, C., Zhang, W., Aouiti, C., Liu, Z. and Yao, L. Bifurcation insight for a fractional-order stage-structured predator–prey system incorporating mixed time delays. *Mathematical Methods in the Applied Sciences*, (2023). [[CrossRef](#)]
- [21] Sene, N. SIR epidemic model with Mittag-Leffer fractional derivative. *Chaos, Solitons & Fractals*, 137, 109833, (2020). [[CrossRef](#)]
- [22] Omame, A., Abbas, M. and Abdel-Aty, A.H. Assessing the impact of SARS-CoV-2 infection on the dynamics of dengue and HIV via fractional derivatives. *Chaos, Solitons & Fractals*, 162,

- 112427, (2022). [[CrossRef](#)]
- [23] Omame, A., Abbas, M. and Onyenegecha, C.P. A fractional order model for the co-interaction of COVID-19 and Hepatitis B virus. *Results in Physics*, 37, 105498, (2022). [[CrossRef](#)]
- [24] Omame, A., Okuonghae, D., Nwajeri, U.K. and Onyenegecha, C.P. A fractional-order multi-vaccination model for COVID-19 with non-singular kernel. *Alexandria Engineering Journal*, 61(8), 6089-6104, (2022). [[CrossRef](#)]
- [25] Omame, A., Nwajeri, U.K., Abbas, M. and Onyenegecha, C.P. A fractional order control model for Diabetes and COVID-19 co-dynamics with Mittag-Leffler function. *Alexandria Engineering Journal*, 61(10), 7619-7635, (2022). [[CrossRef](#)]
- [26] Omame, A., Isah, M.E., Abbas, M., Abdel-Aty, A.H. and Onyenegecha, C.P. A fractional order model for Dual Variants of COVID-19 and HIV co-infection via Atangana-Baleanu derivative. *Alexandria Engineering Journal*, 61(12), 9715-9731, (2022). [[CrossRef](#)]
- [27] Ogunrinde, R.B., Nwajeri, U.K., Fadugba, S. E., Ogunrinde, R.R. and Oshinubi, K.I. Dynamic model of COVID-19 and citizens reaction using fractional derivative. *Alexandria Engineering Journal*, 60(2), 2001-2012, (2021). [[CrossRef](#)]
- [28] Atangana, A. and Secer, A. A note on fractional order derivatives and table of fractional derivatives of some special functions. *Abstract and Applied Analysis*, 2013, 279681, (2013). [[CrossRef](#)]
- [29] Gorenflo, R., Mainardi, F. Fractional Calculus. In: Carpinteri, A., Mainardi, F. (eds) *Fractals and Fractional Calculus in Continuum Mechanics*. International Centre for Mechanical Sciences, vol 378. Springer, Vienna, (1997). [[CrossRef](#)]
- [30] Liu, K., Feckan, M. and Wang, J. Hyers–Ulam stability and existence of solutions to the generalized Liouville–Caputo fractional differential equations. *Symmetry*, 12(6), 955, (2020). [[CrossRef](#)]
- [31] <https://www.populationpyramid.net/nigeria/2021/> (Access Date: February 2023).
- [32] United States Food and Drug Administration, <https://www.fda.gov/media/144245/download>, (2021), (Access Date: January 2023).
- [33] Nwajeri, U.K., Omame, A. and Onyenegecha, C.P. Analysis of a fractional order model for HPV and CT co-infection. *Results in Physics*, 28, 104643, (2021). [[CrossRef](#)]
- [34] Diethelm, K. and Freed, A.D. The FracPECE subroutine for the numerical solution of differential equations of fractional order. *Forschung und Wissenschaftliches Rechnen*, 57-71, (1998).
- [35] McCall, J. Genetic algorithm for modeling and optimization. *Journal of Computational and Applied Mathematics*, 184(1), 205-222, (2005). [[CrossRef](#)]

Bulletin of Biomathematics (BBM)  
(<https://bulletinbiomath.org>)



**Copyright:** © 2023 by the authors. This work is licensed under a Creative Commons Attribution 4.0 (CC BY) International License. The authors retain ownership of the copyright for their article, but they allow anyone to download, reuse, reprint, modify, distribute, and/or copy articles in

*BBM*, so long as the original authors and source are credited. To see the complete license contents, please visit (<http://creativecommons.org/licenses/by/4.0/>).

**How to cite this article:** Atede, A.O., Oname, A. & Inyama, S.C. (2023). A fractional order vaccination model for COVID-19 incorporating environmental transmission: a case study using Nigerian data. *Bulletin of Biomathematics*, 1(1), 78-110. <https://doi.org/10.59292/bulletinbiomath.2023005>